UNIVERSIDAD AUTÓNOMA DE MADRID

DEPARTAMENTO DE BIOQUÍMICA

THREE DIMENSIONAL ORGANIZATION MECHANISMS AND POLARIZED PROTEIN TRAFFIC IN THYROID FOLLICULAR CELLS

DOCTORAL THESIS

PETRINA KOUMARIANOU

MADRID 2015

DEPARTAMENTO DE BIOQUÍMICA

FACULTAD DE MEDICINA

UNIVERSIDAD AUTÓNOMA DE MADRID

THREE DIMENSIONAL ORGANIZATION MECHANISMS

AND POLARIZED PROTEIN TRAFFIC IN THYROID FOLLICULAR CELLS

Memoria que presenta la licenciada en Biología, Petrina Koumarianou para optar al grado de Doctor por la Universidad Autónoma de Madrid.

Directora de tesis: Pilar Santisteban Sanz

Instituto de Investigaciones Biomédicas “Alberto Sols”

Madrid 2015

CSIC
Consejo Superior de Investigaciones Científicas

UAM
Universidad Autónoma de Madrid

MINISTERIO
DE ECONOMÍA
Y COMPETITIVIDAD

CSIC
CONSEJO SUPERIOR DE INVESTIGACIONES CIENTÍFICAS

UAM
UNIVERSIDAD AUTONOMA
DE MADRID

INSTITUTO DE INVESTIGACIONES BIOMÉDICAS
"ALBERTO SOLS", IIBM

Pilar Santisteban Sanz, Profesora de Investigación del CSIC en el instituto de Investigaciones Biomédicas "Alberto Sols", Madrid

AUTORIZA: la presentación de la tesis doctoral titulada: "*Three dimensional organization mechanisms and polarized protein traffic in thyroid follicular cells*" realizada bajo mi dirección, por la Licenciada en Biología Petrina Koumarianou.

En esta memoria de tesis doctoral se han estudiado los mecanismos que controlan la polaridad de la célula epitelial tiroidea, la formación del folículo tiroideo y el tráfico de la proteína transportadora de yodo (NIS). Los datos obtenidos han demostrado el papel decisivo del factor Pax8 en la formación del folículo tiroideo a través del control de sus dianas transcripcionales implicadas en polaridad. Asimismo se han definido los eventos que controlan tanto el transporte de NIS hacía la membrana basolateral como su internalización. El conocer estos mecanismos es imprescindible para un mejor entendimiento de la fisiopatología tiroidea.

El trabajo realizado por la doctoranda ha sido de gran calidad demostrando su responsabilidad científica, su enorme dedicación al trabajo y un juicio crítico muy necesario en la búsqueda de nuevos conocimientos científicos. Ha demostrado por tanto que tiene la formación investigadora necesaria para que este trabajo sea presentado como Tesis Doctoral en el Departamento de Bioquímica de la Facultad de Medicina de la Universidad Autónoma de Madrid

Y para que conste a efectos oportunos se expide el presente certificado en

Madrid a 16 de Diciembre de 2014

http://www.iib.uam.es

C/ ARTURO DUPERIER, Nº 4
28029 MADRID ESPAÑA
TEL.: 91 585 4400
FAX: 91 585 4401

ACKNOWLEDGEMENT

En primer lugar, agradecer a mi directora de tesis Pilar Santisteban el haberme dado la oportunidad de hacer la tesis en su laboratorio. Gracias por esa enorme confianza que siempre has tenido en mí, por apoyarme en todo y empujarme cuando mi lado negativo lo dudaba todo. Gracias a ti he crecido como científica y he descubierto el apasionante mundo de la biología celular. Tu capacidad de estar trabajando en mil cosas a la vez siempre será un ejemplo para mí. También hay que reconocer que el día a día en tu laboratorio no sería lo mismo sin esas celebraciones, los aperitivos y los vinitos acompañados por las delicias culinarias de Eduardo. Gracias Edu por cuidarnos y mimarnos con esas cocas mallorquinas y tantas otras cosas, por tu energía y tu sonrisa.

Por supuesto esta tesis no habría sido igual sin mis compañeros del laboratorio 2.9. Gracias a los que me acogieron hace 5 años, hicieron que me sintiera como en casa y me enseñaron el mundo de las células foliculares. A Marga que tanto trabajo nos ahorraba y por su paciencia. A Christian por esas charlas sobre las PCRs, el cine y el teatro y por supuesto por esos masajes que tanto echo de menos. A Pablo mi primer compi de poyata y escritorio por sus consejos y a Ana por su cariño. A Suzana por compartir las desgracias de NIS y por esas charlas filosóficas. A Garci por sus consejos y su visión clínica tan util. A Ana que tanto me enseñó, muchas gracias por tu ayuda, tu apoyo y compañía hasta tan tarde. Estoy segura que serás una gran científica. A Miguel por estar siempre dispuesto a analizar mis dudas científicas y encontrar soluciones, y por esa música tan especial que nos hacía aguantar hasta que la cogimos cariño al final. A Lara que sin ella el lado oscuro ya no es igual… Muchas gracias por tu ayuda, por tu visión tan práctica, por tu amistad y tu cariño. A León que llena el laboratorio de vida y entusiasmo. Lion, gracias por tu amistad y esos momentos tan divertidos de bailes y risas. A Aris por su apoyo y esas charlas para entender el mundo. También agradecer a toda esa gente que pasó por el labo y dejó su huella, a Sole, David, Jesus y a Javi que tanto me ayudó con los arrays, así como a los “pequeños” del labo: Alberto, Carlos, Adrián, Celia y Andrea que me sacaban de la biblio para comer. Muchas gracias a todos.

Y por supuesto a Antonio de la Vieja, el rey de NIS. Antonio, muchas gracias por introducirme en el mundo de esa proteina, por enseñarme con paciencia, por todos tus consejos y explicaciones, por estar siempre dispuesto a ayudarme con todo y por compartir tu inspiradora pasión por la ciencia.

También me gustaría agradecer a Daniela Corda y a la gente de su laboratorio en Nápoles que me acogieron y me ayudaron las dos veces que estuve allí. Especialmente a Alessandro que sin su ayuda no podría haber hecho ni la mitad de lo que hice. Por las largas horas en el confocal, por sus consejos, su paciencia y por esas pizzas y grappas de vuelta a casa. ¡Grazie per tutti Ale! Gracias también a Inma y Antonino por su ayuda y su compañía dentro y fuera del laboratorio, a Romina por su amistad y su ayuda, y al resto de la gente por el buen ambiente.

En el IIB mucha gente me apoyó y me ayudó durante estos años. Y primero, Pilar y Bárbara del 2.10. Empezamos haciendo el máster el 2009 y juntas hemos compartido el día a día durante los años de la tesis así como bodas, sobrinos y más acontecimientos... Chicas, muchísimas gracias por vuestra amistad, el apoyo y la paciencia. Sin vosotras todo habría sido más difícil y más duro. También agradecer a Daniela, Sol, Ana, Sandra, Luiscar y Eunice por todas esas comidas, los juegos de los continentes, los cumpleaños, las quedadas fuera del IIB, el apoyo y vuestra ayuda. Todo eso hace que los días sean más llevaderos cuando las cosas se complican. Gracias a Laura del 0.3 por los ratoncitos, su paciencia y el apoyo (pronto vas a ser también doctora, Laurita). Muchas gracias también a María Tiana por su cariño, su energía, su apoyo y por compartir la pasión por el swing. Agradecer a las chicas del 2.4.2 por sus ánimos y especialmente a Andréa por la compañía en cultivos y el apoyo (eres la siguiente Andrea) y a Celia por los anticuerpos y los consejos. Gracias a Esther del 1.12 por su ayuda con los pull-down y sus consejos, a Laura del 2.5.1 por las charlas en los pasillos y los ánimos y a Ilenia del CBM por su ayuda y los protocolos de los transwell. Gracias también a las personas de los servicios sin las que no habría podido terminar esta tesis. A Lola y a Ana del Sidi que hemos pasado muchas horas juntas y vosotras sabéis muy bien lo que cuesta encontrar esos boloncios, jeje, gracias por toda vuestra ayuda y compañía chicas. A Lucía y a Diego del IIB por la ayuda con el video-lapse que tanto nos costó poner a punto pero lo conseguimos al final, a Guti y a Alex que me salvaron el portátil y a mí de un colapso nervioso una semana antes de entregar la tesis, y gracias en especial a Javi por hacer esas figuras tan bonitas. A Diego y a Carlos por todos los buenos días y buenas noches, por poner la calefacción para que esté calentita la biblio cuando llegue.

Tampoco habría llevado a cabo esa tesis sin el apoyo de todos los amigos, los de Madrid y los de Grecia. Vero y Charo, gracias por esas meriendas de reponer fuerzas y los ánimos. Esther y Rocio, gracias por las tardes en la Romana, las cenas en el Piccola y vuestro cariño. Irene, gracias por estar siempre ahí, por tu amistad y el apoyo. Gracias también a mis compis de ballet, de lindy y de balboa por su interés, los ánimos y los bailes. ¿Qué haría sin esa salida de emergencia, sin la ilusión y la emoción del swing? Gracias Alba y Gas por confiar en mí y por ofrecerme ese oasis entre semana.

Αγαπημένοι μου φίλοι από Αθήνα, είναι σπάνιο και πολύτιμο να ζούμε μακρυά και να βρισκόμαστε τόσο σπάνια, αλλά παρά ταύτα κάθε φορά που συναντιόμαστε να νιώθω την ίδια εγγύτητα και την ίδια αγάπη από μέρους σας. Ευγενία, Πανδώρα και Χρίστο, Ιωάννα, Ζαχαριάδη, Μελίνα και Δημήτρη, Λίλα και Δημήτρη, Όλγα και Αντρέα, Έφη, Μαρία, Μαριέττα, Κωστή Αποστολάκη, Χριστιάννα, σας ευχαριστώ για την υποστήριξη και την φροντίδα. Μαράκι μου, να που τελειώνω επιτέλους και θα μπορούμε πια να πάμε και κανένα ταξιδάκι μαζί, χαχα. ‘Ενα μεγάλο ευχαριστώ για την ψυχική ενδυνάμωση και καθοδήγηση στον π. Σαράντη, τον π. Δημήτρη Τσιαμπαρλή και τον π. Σιλουανό.

Agradecer también a mi familia y a mi familia política que aunque viviendo lejos siempre han estado cerca, siempre han confiado en mí y me han apoyado en todo. Αγαπημένοι μου γονείς και αδέρφια, σας ευχαριστώ για την υποστήριξη που μου δείχνετε όλα αυτά τα χρόνια. Νικολή, Ελεαννούλις, Γιάννη, Φιλοθέη και Δημήτρη, η αγάπη σας και η εμπιστοσύνη σας ήταν για μένα πολύτιμη βοήθεια και μου έδινε θάρρος για να προχωρώ και φέρω εις πέρας την έρευνα. Πατέρα μου, χάρη στο δικό σου παράδειγμα, στην επιμονή και την υπομονή που χαρακτηρίζει στον τρόπο διδασκαλίας σου, έμαθα να είμαι μεθοδική κι επιμελής και να αγαπώ τις θετικές επιστήμες. Μητέρα μου, χάρη στη δική σου αφοσίωση και συνέπεια έμαθα να είμαι απαιτητική και λεπτολόγος στη δουλειά μου. Σας ευχαριστώ πολύ για όλα όσα έχετε κάνει για μένα από μικρή, σας αγαπώ πολύ και μου λείπετε!

Charo y Grego, muchas gracias por la confianza, los ánimos y vuestro apoyo durante esa tesis.

Alberto, gracias por estar a mi lado los días soleados y nublados de esa tesis, gracias por darme fuerza cuando todo parecía “senza fine”, gracias por creer en mí y por enseñarme cómo ser mejor persona.

Le vent se lève!… Il faut tenter de vivre!

Paul Valèry

SUMMARY

The structural and functional unit of the thyroid gland is the thyroid follicle that consists in a single layer of follicular cells enclosing a central lumen where thyroid hormones are synthesized and stored. Follicular cells or thyrocytes are epithelial polarized cells with the apical membrane facing the lumen and the basal membrane surrounded by the basement membrane towards the stroma. We have studied the follicle formation process in three dimensional (3D) Matrigel cultures using the rat follicular cell line FRT and mouse primary thyrocytes. Our results demonstrate that follicles originated either from single or plural cells acquire apical-basal polarity after the first cell division. Apical membrane is defined at a specific site of the cell-cell junctions where the exocytosis of apical membrane components occurs. Lumen is formed by further apical exocytosis followed by membrane separation or coalescence between apical vacuolar compartments. Mature tight junctions separate the apical from the basolateral domains and both actin filaments and acetylated microtubules exhibit a polarized apical distribution. Through microarray-based differential expression analysis we have identified regulators of 3D follicular organization. Among them, Pax8 transcription factor was discovered to play a critical role in polarity orientation and follicle formation. In the absence of Pax8 apical membrane orientation was inverted and lumen formation was impaired. The polarized distribution of cell cytoskeleton was altered due to the transcriptional inhibition of both cadherin-16 and its cytoskeleton linker, αB-crystallin. Apical transport of Rac1 through actin filaments was also blocked and thus local actin organization and apical traffic were affected. Other Pax8 transcriptional targets described to be involved in apical transport such as Rab17 and myosin Vb could also participate in follicular apical membrane formation. Thyroid function is determined by the polarized distribution of thyroid specific proteins at the apical-basal membranes and inside the lumen. NIS, the sodium/iodide symporter, is a key protein for iodide uptake and thyroid hormone synthesis, and is localized in the basolateral plasma membrane. We have identified a clathrin-mediated pathway responsible for NIS basolateral traffic, in which the clathrin adaptor complexes AP-1A and AP-1B sort NIS at the *trans*-Golgi and the recycling endosomes. More specifically, we have demonstrated that the medium subunit of AP-1B controls NIS basolateral sorting through common recycling endosomes. In its absence, NIS is apically missorted where remains functional. Besides, direct NIS basolateral transport from the *trans*-Golgi to the basolateral membrane is mediated by AP-1A through clathrin-coated vesicles that also carry the transferrin receptor. In the absence of AP-1A medium subunit, AP-1B fully compensates its function. NIS internalization pathways were also studied and preliminary results have shown that the mechanism is clathrin-independent and that NIS is finally degraded by lysosomes.

RESUMEN

La unidad estructural y funcional del tiroides es el folículo tiroideo que consiste en una capa de células foliculares posicionadas alrededor de un lumen central donde se sintetizan y se almacenan las hormonas tiroideas. Las células foliculares o tirocitos son células epiteliales polarizadas con la membrana apical hacia el lumen y la membrana basal rodeada de la lámina basal hacia el estroma. Hemos estudiado la formación del folículo en cultivos tridimensionales (3D) de Matrigel usando la línea tiroidea de rata FRT y cultivos primarios de tirocitos de ratón. Nuestros resultados demuestran que los folículos formados tanto a partir de una como de varias células, adquieren la polaridad ápico-basal tras la primera división. La formación de la membrana apical se inicia entre las uniones célula-célula en el sitio donde se exocitan los componentes de la membrana apical. El lumen se forma tras la exocitosis seguida por la separación de las membranas apicales o por coalescencia entre compartimentos apicales de vacuolas. Las uniones estrechas separan el dominio apical del dominio basolateral, y los filamentos de actina junto con los microtubulos acetilados se distribuyen apicalmente. Mediante un array de expresión hemos identificado reguladores de la organización folicular en 3D. De entre ellos el factor de transcripción Pax8 resultó tener un papel esencial en la orientación de la polaridad y en la formación del folículo. En ausencia de Pax8 la orientación de la membrana apical se invierte y se impide la formación del lumen. La distribución polarizada del citoesqueleto se altera debido a la inhibición transcripcional tanto de la cadherina-16 como de su proteína de unión al citosqueleto, la cristalina alfa B. El transporte apical de Rac1, a través de los filamentos de actina, se inhibe y como consecuencia la organización apical de actina y el tráfico están afectados. Otras dianas transcripcionales de Pax8 que están involucradas en el transporte apical, como las proteínas Rab17 y myosina Vb, podrían estar también participando en la formación de la membrana apical. La función tiroidea depende de la localización polarizada de proteínas específicas de tiroides en la membrana ápico-basolateral y dentro del lumen folicular. El simportador de sodio/yoduro, localizado en la membrana basolateral es una proteína clave para la captación del yoduro y la síntesis de las hormonas tiroideas. Hemos identificado una vía mediada por clatrina como responsable del tráfico basolateral de NIS, en la cual los complejos adaptadores de clatrina AP-1A y AP-1B segregan a NIS a nivel del *trans*-Golgi y de los endosomas de reciclaje. Hemos demostrado que la subunidad mediana de AP-1B controla el tráfico basolateral de NIS a través de los endosomas comunes de reciclaje. En su ausencia, NIS se transporta a la membrana apical donde sigue siendo funcional. AP-1A participa en el tráfico directo de NIS del *trans*-Golgi a la membrana basolateral a través de vesículas cubiertas de clatrina que cotransportan el receptor de transferrina. En ausencia de su subunidad mediana, AP-1B compensa su función. También estudiamos las vías de internalización de NIS y resultados preliminares muestran que el mecanismo es independiente de clatrina y que NIS es finalmente degradado en los lisosomas.

INDEX

ABBREVIATIONS

2D	two dimensional
3D	three dimensional
Act-Itgb1	activated Itgb1
Ac-tub	acetylated tubulin
AEE	apical early endosome
AJ	adherens junction
AMIS	apical membrane initiation site
AP	apical
AP-1	clathrin-associated adaptor protein 1
AP1M1	gene codifying the μ subunit of the AP-1A clathrin adaptor protein
AP1M2	gene codifying the μ subunit of the AP-1B clathrin adaptor protein
aPKC	atypical protein kinase C
ARE	apical recycling endosome
ASE	apical sorting endosome
BEE	basolateral early endosome
BL	basolateral
BM	basement membrane
CCV	clathrin-coated vesicles
CDE	clathrin-dependent endocytosis
Cdh16	cadherin-16
CFTR	cystic fibrosis transmembrane conductance regulator
CH	congenital hypothyroidism
Crb3	crumbs 3 protein
CRE	common recycling endosome
CRYAB	αB-crystallin
Ctr	control
DEHAL1	iodotyrosine dehalogenase 1
DIC	differential interference contrast
DIT	diiodotyrosine
DPPIV	dipeptidyl peptidase IV
DUOX1/2	dual oxidase 1 and 2
Dynrlb2	dynamin light chain roadblock-type 2
E	embryonic day
ECM	extracellular matrix
ER	endoplasmic reticulum
ERM	ezrin-radixin-moesin proteins
ESC	embryonic stem cell
F-actin	filamentous actin
FDR	false discovery rate
Fn1	fibronectin 1
FoxE1	transcription factor with forkhead box E1 domain
GEF	guanine nucleotide exchange factor
GPI	glycosylphosphatidylinositol
Hhex	transcription factor with homeobox domain
IGF1	insulin growth factor 1
ITD	iodide transport defect
Itgb1	β1-integrin
Kif	kinesin family

Ksp-cadherin	kidney-specific cadherin
LE	late endosome
LRP1	low-density lipoprotein receptor-related protein 1
Lys	lysosome
Map7	microtubule-associated protein 7
MIT	monoiodotyrosine
MT	microtubules
MUC1	mucin 1
MVB	multivesicular body
Myo5b	myosin Vb
Nid2	nidogen 2
NIS	sodium/iodide symporter
Nkx2-1	transcription factor with a homeobox domain also known as TTF1
NTF-1	NIS TSH-responsive factor
NUE	NIS upstream enhancer
Ocln	occludin
PAP	preapical patch
Pax8	transcription factor with a paired box 8 domain
PBF	PTTG1binding factor
PCX	podocalyxin glycoprotein
Pend	pendrin
PIP2/PtdIns(4,5)P2	phosphoinositol-4,5-diphosphate
PIP3/PtdIns(3,4,5)P3	phosphoinositol-3,4,5-triphosphate
PKA	protein kinase A
PM	plasma membrane
Polr2g	RNA polymerase II polypeptide G
PTB	phosphotyrosine-binding domain
PTTG1	pituitary tumor-transforming gene-1 product
RE	recycling endosome
SD	standard desviation
STAS	sulphate transporter and antisigma factor antagonist
Stx7	syntaxin 7
T_3	triiodo-thyronin
T_4	tetraiodo-thyronin
TD	thyroid dysgenensis
TfR	transferrin receptor
Tg	thyroglobulin
TGFβ	transforming growth factor beta
Tgm2	transglutaminase 2
TGN	*trans*-Golgi network
TH	thyroid hormone
TJ	tight junction
TMS	transmembrane segment
TPO	thyroperoxydase
TRH	thyrotropin-releasing hormone
TSH	thyroid stimulating hormone
TSHr	TSH receptor
TTF	thyroid transcription factor
VAC	vacuolar apical compartment
VSVG	vesicular stomatitis virus glycoprotein
vs.	versus

INTRODUCTION

1. The thyroid gland

The thyroid gland is the first endocrine structure recognizable during development. It consists of two lobes on either sides of the larynx connected by an isthmus that overlies the second and third ring of the trachea in man (Fig. 1, left panel). Two main cell types characterize the thyroid gland: the thyroid follicular cells or thyrocytes of endodermal origin (Grapin-Botton and Melton, 2000) that are responsible for thyroid hormones synthesis and secretion, and the parafollicular or calcitonin producing C-cells whose origin is still a matter of controversy as some authors report that they are derived from the neural crest (Le Douarin et al., 2007), while according to others they originate in the ultimobranchial body (Kameda et al., 2007). Thyrocytes are epithelial polarized cells that are organized into follicular structures in which a monolayer of thyrocytes encloses a luminal compartment filled with a colloidal mass where thyroid hormone precursors bound to thyroglobulin are formed and stored (Fig. 1A, right panel). Each thyroid follicle is supported by the stroma that contains interfollicular extracellular matrix (ECM), a capillary network and a few stromal cell types such as fibroblasts and inflammatory cells. C-cells are scattered in the interfollicular spaces. Thyrocytes in thyroid follicles present a specific structural polarity: their apical pole with numerous microvilli faces the follicle lumen, whereas their basal side with the basement membrane faces the stroma (Fig. 1B). This is a specialized structure and results in a functionally polarized process of thyroid hormone (TH) biosynthesis and release in a basal-apical (follicle lumen)-basal direction in thyrocytes (Fig. 1B), making follicles the functional unit of the gland (Fujita, 1975).

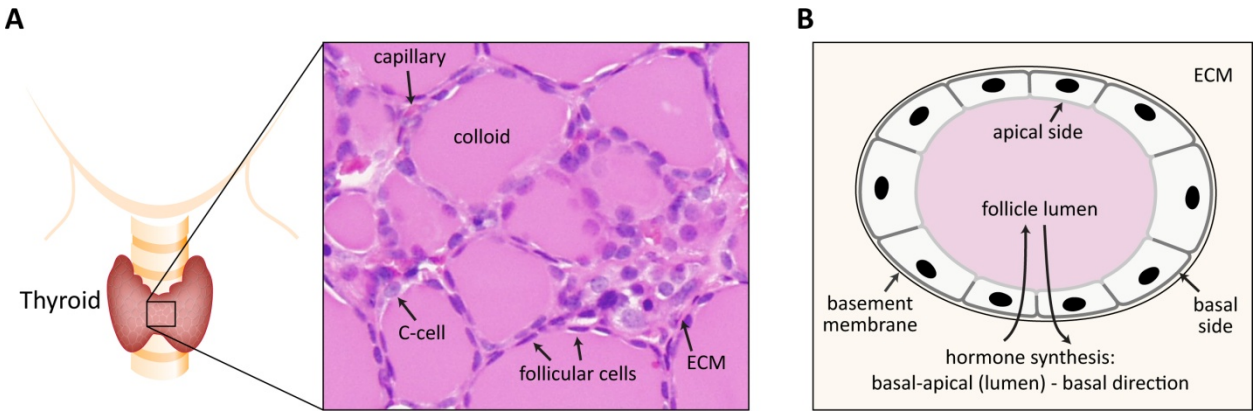

Figure 1. **Localization, morphology and structure of the thyroid gland.** A) Thyroid gland is composed of two lobes connected by the isthmus and localized at the anterior part of the trachea. Thyroid follicles are spherical structures composed of a single layer of epithelial follicular cells (black arrows) that surround the follicle lumen rich in colloid. Follicles are supported by extracellular matrix (ECM) and a capillary network, while C-cells are scattered between follicles (all indicated with black arrows) in a section of thyroid human tissue stained with hematoxylin and eosin, observed under an optical microscope with a 20x objective. B) Schematical representation of a thyroid follicle *in vivo* and in ECM gel culture (pink shading). Thyrocytes show specific cellular polarity: the apical side (bright grey) faces the lumen and the basal side (dark grey) surrounded by the basement membrane (black) faces the ECM. Thyrocytes undergo thyroid hormone synthesis and release in a basal-apical (lumen)-basal direction as the long black arrows indicate.

Since THs are iodinated, iodide (I^-) uptake is required for their synthesis. Active I^- transport from the bloodstream to the interior of the human thyrocytes is mediated by the Na^+/I^- symporter called NIS (*SLC5A5* gene), a transmembrane glycoprotein located in the basolateral membrane of the thyrocytes (Fig. 2) (Dai et al., 1996). Once inside, iodide is vectorially transported in a basal to apical direction and finally enters the follicular lumen through the apical I^-/Cl^- exchanger Pendrin (*PDS* gene) (Yoshida et al., 2004) and other iodide channels or transporters (Fong, 2011). Then, iodide oxidation takes place by the apically localized enzyme thyroperoxidase (TPO) that uses as a substrate H_2O_2 produced by the dual oxidases DUOX1/2 (Ohye and Sugawara, 2010). In the lumen, the previously synthesized and apically exocytosed glycoprotein thyroglobulin (TG) is iodinated in tyrosine residues in a peroxidase-mediated manner, giving the thyroid hormones triiodo (T_3) and tetraiodo-thyronine (T_4) within the thyroglobulin peptide chain (Degroot and Niepomniszcze, 1977). THs biosynthesis and secretion are stimulated by thyrotropin (thyroid stimulating hormone, TSH) secreted from the pituitary gland (Dumont et al., 1991) Depending on thyroid hormone requirement and in response to TSH stimulation, colloid droplets rich in thyroglobulin are endocytosed through micropinocytosis (Bernier-Valentin et al., 1991, Botta et al., 2011) and after lysosomal hydrolysis (Dunn et al., 1991) T_3 and T_4 are eventually secreted into the blood circulation through the thyroid hormone transporter MCT8 (Di Cosmo et al., 2010). TG proteolysis also releases mono- and diiodotyrosine (MIT and DIT), the precursors of T_3 and T_4 which are deiodinated by the iodotyrosine dehalogenase 1 (DEHAL1) (Moreno et al., 2008).

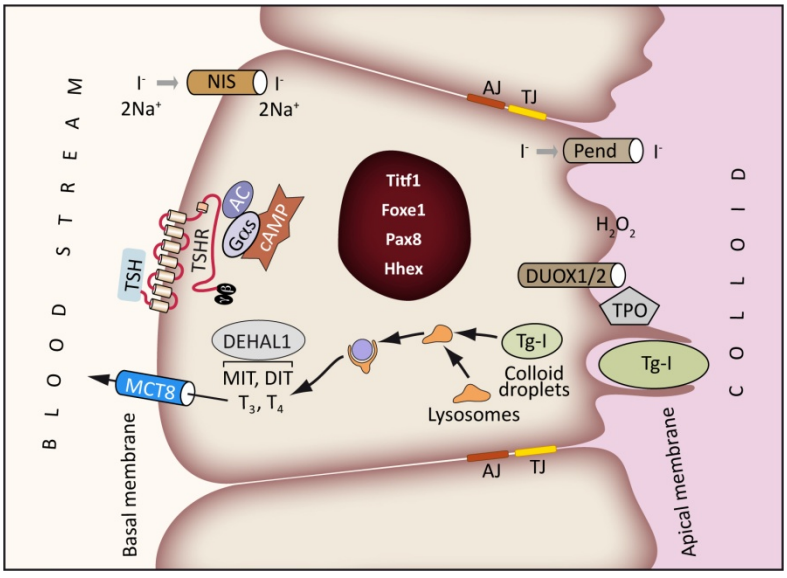

Figure 2. **Schematic representation of a human thyrocyte with the major proteins involved in biosynthesis and secretion of the thyroid hormones T_3 and T_4.** Thyrocytes concentrate iodide (I^-) from the circulation by the Na^+/I^- symporter (NIS) located in the basolateral membrane. Pendrin (PEND) at the apical membrane transports iodide into the follicular lumen. After I^- is oxidized, iodination of tyrosine residues within thyroglobulin (TG), which is released into the follicular lumen, takes place by the thyroid peroxidase (TPO) using H_2O_2 generated by the oxidases DUOX1/2. The iodinated TG is taken up by endocytosis of colloid and after fusion with lysosomes TG enzymatical cleavage results in MIT, DIT, T_3 and T_4 release. MIT and DIT are deiodinated by the dehalogenase DEHAL1, whereas T_4 and T_3 are released into the extracellular fluid through the MCT8 transporter. The cell nucleus contains the transcription factors TITF1, FOXE1, PAX8 and HHEX that regulate the transcription of the genes encoding for NIS, TPO, TG, TSH receptor (TSHR) and others. Thyroid cells connect to each other by tight junctions (TJ) and adherens junctions (AJ).

1.1. Thyroid embryonic morphogenesis

Thyroid gland organogenesis in mouse embryos begins at embryonic day (E) 8.5 in a process known as specification (Fig. 3). A group of cells in the floor of the primitive pharynx becomes committed to a thyroid fate by coexpressing the transcription factors Nkx2-1, Pax8, FoxE1 and Hhex. In this stage, the thyroid precursor cells compose the thyroid anlage. Later, on E9.5, these cells form a bud which on E10.5-E11.5 proliferates and then dissociates from the pharyngeal floor and begins a caudal descend as two lobes on either side of the larynx and the upper trachea. On E14.5 the thyroid precursors reach their definitive position and Tg expression begins (Postiglione et al., 2002). The first evidence of follicle formation is on day E15.5, when small follicles appear disseminated within the gland. At E16, the Tshr and Tpo proteins are detected and then thyroid functional differentiation takes place with the expression of Nis and the onset of thyroid hormone biosynthesis on E16.5 (Fagman and Nilsson, 2010).

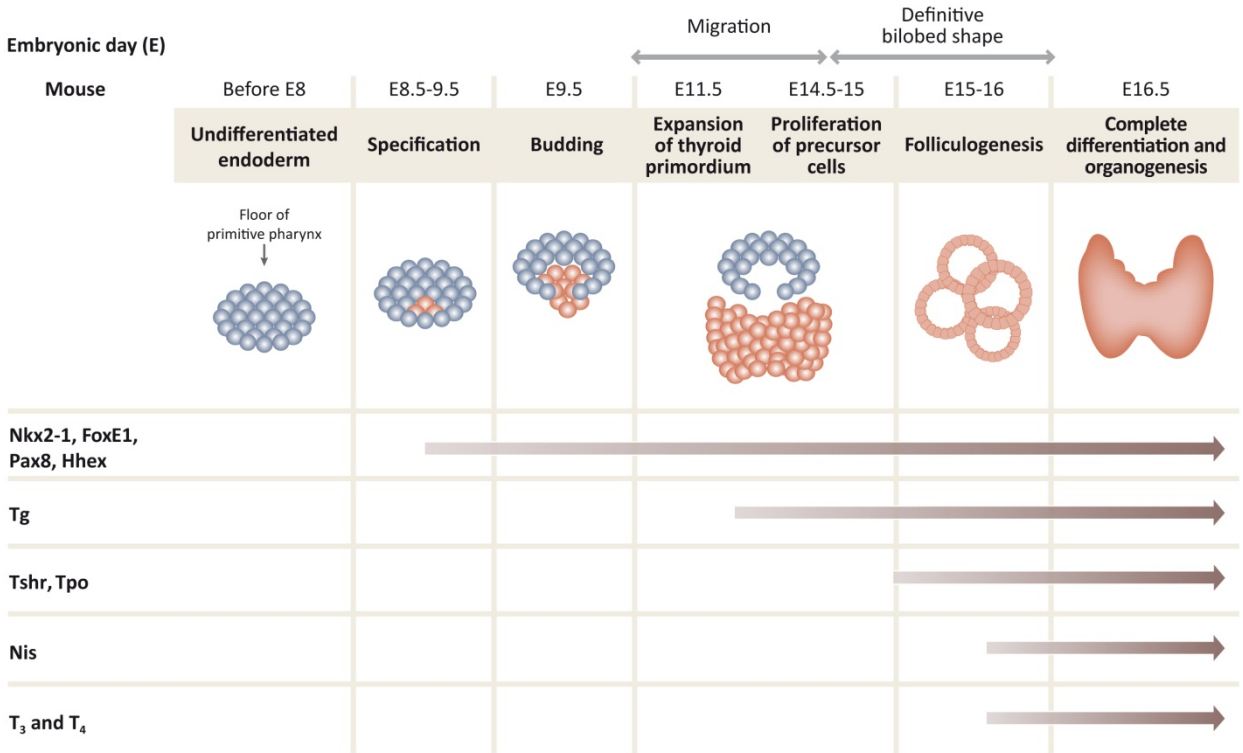

Figure 3. **Expression of thyroid specific proteins and the stages of thyroid development.** The expression of Nkx2-1, Foxe1, Pax8 and Hhex determine the specification of a group of cells from the ventral endoderm at E8.5–9.5 in mouse. Bud formation takes place at E9.5 and from E11.5 the cells of the thyroid primordium begin to migrate downward to their final position in the trachea. At the same time as migration, the thyroid precursor cells proliferate and expand laterally, in a process known as lobulation, which is completed when the thyroid gland reaches its definitive position at E14.5–15. At this time Tg is expressed in the primitive thyroid. However, expression of Tpo and Tshr is not activated until folliculogenesis begins at E16. At E16.5, the thyroid gland is completely formed and Nis is expressed. Synthesis of thyroid hormones T_3 and T_4 is initiated when the thyroid gland is completely functional. Abbreviation: E, embryonic day. (Adapted from Macchia, P. E. Recent advances in understanding the molecular basis of primary congenital hypothyroidism. *Mol. Med. Today* 6, 36–42, 2000).

1.2. Thyroid transcription factors in thyroid gland development and differentiation

Nkx2-1, Pax8, FoxE1 and Hhex transcription factors are expressed in several other embryonic and adult tissues. However, they are expressed together only in epithelial thyroid follicular cells and for this reason are collectively known as thyroid transcription factors (TTFs). Expression of the TTFs in thyroid precursor cells at E8.5 in combination with knockout mice experiments, have demonstrated their specific role in thyroid morphogenesis (De Felice and Di Lauro, 2004, De Felice and Di Lauro, 2011).

Nkx2-1 is a member of the homeodomain family and its main role during thyroid organogenesis is to preserve the survival of thyroid follicular cells. Primitive thyroid of Nkx2-1 null mice at E10 degenerates, possibly due to apoptotic mechanisms still not studied in depth (Kimura et al., 1999). Nkx2-1 is also important for the maintenance of the thyroid follicular structure in adult thyroids, as conditionally KO mice do not show cellular apoptosis, but instead microfollicular structures and degenerated follicles lacking colloid (Kusakabe et al., 2006).

Pax8 is a paired domain family member, essential for the survival of the thyroid precursor cells in later stages of thyroid development (De Felice and Di Lauro, 2004). The primitive thyroid in Pax8 null mice is smaller than normal on E11.5 and follicular structures are absent on E12.5. Consequently, mice have thyroid hypoplasia, low weight and growth retardation, and only twenty percent survive up to three weeks due to severe hypothyroidism (Mansouri et al., 1998). In humans, it is well established that heterozygous inactivating *PAX8* mutations in adults cause congenital hypothyroidism with or without thyroid hypoplasia (Macchia et al., 1998, Di Palma et al., 2010). The histology of a *PAX8* mutation carrying thyroid tissue has been poorly examined, however a case study has revealed dense aggregates of thyrocytes with absent or very small follicles (Narumi et al., 2011) suggesting a role of PAX8 in adult follicle formation and growth.

Foxe1 is a forkhead domain protein and controls migration of the thyroid gland during thyroid morphogenesis. Reintroduction of a normal *Foxe1* gene exclusively into thyroid precursor cells in mice deprived of the endogenous gene restores proper gland positioning (Fagman et al., 2006).

Hhex, which is also member of homeodomain family, regulates the expression of *Pax8* and *FoxE1* transcription factors controlling bud formation and survival of thyroid precursor cells in later stages of thyroid development (Parlato et al., 2004).

The fact that the thyroid anlage is formed normally in all TTFs mutants suggests that transcription factors do not participate individually in its formation, but that they are required for the emergence and survival of the thyroid bud by promoting thyroid cell specification and differentiation (Fernandez et al., 2015).

Differentiated thyroid follicular cells express proteins that are critical for biosynthesis, storage and secretion of the thyroid hormones T_3 and T_4. As described before, these proteins include Tg, TPO, NIS,

TSHR, DUOX1/2, Pendrin, DEHAL1 and MCT8. TTFs regulate the expression of genes that encode several of these proteins. In brief, all four TTFs regulate *Tg* transcription (Civitareale et al., 1989, Santisteban et al., 1992, Zannini et al., 1992, Pellizzari et al., 2000). Nkx2-1, FoxE1 and Pax8 also regulate *Slc5a5* and *Tpo* gene expression (Francis-Lang et al., 1992, Ohno et al., 1999, Endo et al., 1997, Aza-Blanc et al., 1993, Fernandez et al., 2013). Furthermore, Nkx2-1 regulates the expression of the other three TTFs, as well as of the *Tshr, Pds* and *Duox1* genes (Christophe-Hobertus et al., 2012). Moreover, TSH, the main regulator of thyroid function, controls the expression and the DNA binding activity of Pax8, FoxE1 and Nkx2-1 transcription factors and therefore modulates the expression of *Slc5a5*, *Tpo* and *Tg* genes (Postiglione et al., 2002, Marians et al., 2002). To exert its function TSH binds to its receptor, a seven-transmembrane domain protein that couples to G proteins in the basolateral membrane of thyroid follicular cells (Vassart and Dumont, 1992) (Fig. 2). Stimulation of the TSHR leads to the dissociation of trimeric G proteins into Gα and Gβγ subunits that in turn trigger complex signaling cascades. Most of the activities of the TSHR are mediated through Gs, one of the Gα proteins that activates the adenylyl cyclase/cAMP/protein kinase A (PKA) cascade. The simultaneous expression of these transcription factors is maintained in adult thyroid cells and guarantees the differentiated thyroid function (Damante et al., 2001, Parlato et al., 2004).

2. Thyroid folliculogenesis

Thyroid follicle formation or folliculogenesis is the most critical stage of thyroid organogenesis for the THs synthesis and the proper gland function. Thyroid folliculogenesis is a complex phenomenon that requires a combination of processes that induce the acquisition of cell polarity, lumen formation, follicular cell proliferation and differentiation. The precise cellular and molecular mechanisms associated to these processes are still poorly understood. However, recent advances in the molecular regulation of epithelial cell polarity (Rodriguez-Boulan and Macara, 2014), lumen morphogenesis (Datta et al., 2011) and epithelial tubulogenesis (Rodriguez-Fraticelli et al., 2011), provide valuable information to understand thyroid follicular cell biology.

2.1. Cell-matrix recognition

The initial cue for apical-basal polarization derives from proteins of the basal lamina or basement membrane (BM), a specialized part of the ECM made essentially of laminins, collagen IV, entactin and perlecan. Primary thyrocytes embedded in gels made of ECM components such as collagen I, fibronectin, laminin and reconstituted basement membrane, reconstruct follicle structures with physiological cellular polarity (Chambard et al., 1981, Mauchamp et al., 1998). The fact that isolated thyrocytes and established thyroid cell lines develop follicular structures with inverted polarity in

suspension culture conditions (Nitsch and Wollman, 1980), but regain correct apical-basal polarity when embedded in three dimensional (3D) gel-like environments (Chambard et al., 1981, Garbi et al., 1984, Garbi et al., 1987), made evident that interaction between the cell surface and the ECM orientates thyrocyte polarity. Thyroid follicular cells synthesize ECM components such as collagens, laminins, fibronectin, dystroglycan, elastins and others (Garbi et al., 1988, Frohlich et al., 1995), with collagen IV and laminin being the major components of the BM surrounding each follicle *in vivo* and shown to regulate *in vitro* thyroid cell proliferation and differentiation, respectively (Toda et al., 1995). To sense the extracellular environment follicular cells interact with the ECM proteins through heterodimeric integrin molecules consisting of α- and β-integrin pairs localized at the basal epithelial membrane. Specifically, β1-integrin-containing complexes have key roles in follicle formation (Cali et al., 1998), cell proliferation and shape through actin filaments organization (Vitale et al., 1997). However, the precise mechanism of thyrocyte-ECM interaction that leads to correct apical-basal cellular and follicular polarity remains unknown.

Conversely, the role of integrins and especially that of β1-integrin subunit in signal transduction from the ECM into cells to effect tissue polarization is clear enough in a variety of cell types. In Madin-Darby canine kidney (MDCK) 3D cultures, cyst polarity orientation relies on a pathway in which collagen-mediated activation of β1-integrins induces Rac1 signaling to laminin receptors in an actin-remodeling dependent manner. Laminin-receptor interaction facilitates the asembly of basement membrane at the cell surface through laminin organization (O'Brien et al., 2001, Yu et al., 2005) that in turn leads to cortical cytoskeleton organization (Colognato et al., 1999). Inhibition or loss of β1-integrin or the downstream GTPase Rac1 results in inversion of the normal cyst orientation so that the apical surface becomes orientated towards the matrix through inappropriate activation of a RhoA-ROCKI-myosin II pathway (Yu et al., 2008). Increased ROCK activity is shown to disrupt the integrity of Par polarity complex through phosphorylation of Par3 protein (Nakayama et al., 2008). Analysis of later blood vessel development in endothelial-specific β1-integrin knockout mice also reveals perturbed vessel polarity, filled lumens and mistargeting of cell-cell junction proteins (Zovein et al., 2010). In these knockouts the polarity protein Par3 was downregulated and Par3 re-expression partially rescued lumen occlusion, suggesting that polarity proteins are key β1-integrin targets. Thus, the ECM, β1-integrins, Rho GTPases, polarity proteins and actin cytoskeleton are key regulators of apical surface and lumen orientation.

2.2. Cell-cell recognition

While signals from the ECM provide one axis from which to orient apical domain and lumen positioning, adjoining cells through cell-cell contacts and intercellular junctions provide a second axis. Sensing neighbouring cells occurs via a multitude of adhesion receptors, including cadherins and nectins that form part of a cell-cell adhesion structure denominated adherens junction (AJ) (Tachibana et al., 2000).

The establishment of initial contacts between adjacent epithelial cells occur through exploratory lamellipodia in MDCK cells (Adams et al., 1998, Ehrlich et al., 2002) and IAR-2 cells (Krendel and Bonder, 1999); and/or filopodia in primary mouse keratinocytes (Vasioukhin et al., 2000) that penetrate and embed into neighbouring cells. Localized Rac1 activation at the newest sites of cell contact induces actin polymerization and the formation of actin-based protrusions that carry E-cadherin rapidly at the initial zone of E-cadherin-mediated cell-cell contacts (Ehrlich et al., 2002, Gavard et al., 2004). Conversely, E-cadherin localized in nascent sites of adhesion can exert an active influence to mark the site for actin assembly at the cell surface through Rac activation that in turn can stimulate the activation of Cdc42- and Arp2/3-mediated actin nucleation which may promote the establishment of the junctions (Kim et al., 2000, Kovacs et al., 2002). Interaction between these activated Rho family GTPases and Par6 leads to the activation of atypical PKC (aPKC), which has been shown to be required for the maturation of AJs from simple cell-cell adhesions to junctional complexes (Yamanaka et al., 2001). Therefore, AJ complex components together with polarity complexes, the balanced activities of Rho GTPases and the actin cytoskeleton are all required to establish and maintain junctions between adjacent cells in an epithelium.

At the beginning of thyroid morphogenesis, the initial hollow anlage becomes solid by the inward migration of its endodermal wall followed by connective tissue elements. In chick thyroid embryogenesis, the cells which eventually will form the follicles become arranged as cords or plates of two cells thick (Hilfer, 1964), whereas in rat embryos thyroid follicles develop from aggregates of unpolarized precursor cells (Shepard, 1967, Remy et al., 1980). *In vitro* studies have proposed two different models of thyroid follicle formation. According to the single cell origin model, single thyrocytes develop intracytoplasmic cavities, become cavity-embracing cells and then undergo cell division and reconstruct small follicles consisting of two cells. Alternatively, the plural cell origin model supports the formation of follicles after aggregation and link between many thyrocytes. It is believed that thyrocytes with higher proliferative ability follow the single cell origin mechanism, while those with lower proliferative ability follow the plural cell model (Toda et al., 1993). In all cases, the site of follicle formation is characterized by an area of contact between the adjoining cells where an immature junctional complex is formed (Remy et al., 1977, Nathaniel, 1986). The first indication of the junctional complex formation is the appearance of a ring-shape thickening in the cells plasma membrane observed with electron microscopy. During mouse thyroid morphogenesis E-cadherin is expressed in the lateral plasma membrane of progenitor cells where colocalizes with β-catenin from the E9.5 and during the entire development (Fagman et al., 2003). The importance of E-cadherin in initial cell-cell adhesion is demonstrated in follicle formation *in vitro* from isolated porcine primary cells that are unable to form aggregates after the blocking of E-cadherin function (Yap et al., 1995b). Conversely, E-cadherin

depletion at E15 resulted in smaller follicles with irregular shape, but had no effect on cell-cell junctions despite the significant reduction in α- and β-catenins probably due to the redundant expression and function of other cadherins such as R-cadherin and Ksp-cadherin localized at the lateral membrane of thyrocytes (Cali et al., 2007). Thus, E-cadherin seems crucial for gland development; however, it is not indispensable to junction formation. Recently, the previously considered kidney-specific cadherin (Ksp-cadherin) or cadherin-16 (Cdh16) was identified to be expressed during mice gland organogenesis from E10.5 (Cali et al., 2012). Interestingly, Cdh16 expression was demonstrated to depend on TSH and to be under the transcriptional regulation of Pax8 in thyroid follicular cells (Ruiz-Llorente et al., 2012, de Cristofaro et al., 2012).

2.3. Apical-basal polarization and membrane transport during follicle formation

In mammalian epithelial cells, it is well established that membrane trafficking and polarity-complex machineries work together to form the apical surface and lumen (Bryant et al., 2010). When epithelial cell aggregates start to polarize, junction proteins such as E-cadherin, occludin and exocyst components accumulate at the site of cell-cell contact (Fig. 4A). Apical membrane proteins, as the polarity protein Crumbs3 (Crb3) and the glycoproteins podocalyxin (PCX) and mucin 1 (MUC1) are initially distributed in the cell periphery. They become endocytosed and transported in vesicles towards recycling endosomes (RE) in a process regulated by Cdc42, INF2 (a Cdc42-activated formin) and MAL2 (a member of the MAL protein family) (de Marco et al., 2002, Madrid et al., 2010). Trafficking from RE is mediated by Rab11a that initiates a GTPase cascade recruiting the Rab guanine nucleotide exchange factor (GEF) Rabin8 that in turn activates Rab8a/b locally. This Rab cascade drives RE delivery to the cell-cell contact site by activating motor proteins such as the actin motor myosin Vb (Myo5b) (Roland et al., 2011) and interacting with microtubules through kinesins (Schonteich et al., 2008) as depicted in figure 4A. In that way, cell cytoskeleton provides a driving force for apical vesicle formation and transport. Studies with MDCK 3D cultures indicate that the vesicles are delivered to a discrete common landmark between neighbouring cells in order to initiate the lumen, a region termed the apical membrane initiation site (AMIS) (Bryant et al., 2010), demarcated by a polarity complex comprising Par3 and aPKC (Roland et al., 2011). This complex, although initially contributes to the immature junctional complex, it also focuses exocyst-dependent vesicle docking events allowing initiation of apical polarity through its interaction with exocyst proteins. Once vesicles reach the AMIS and fuse with the membrane through t-SNARE syntaxin 3, an early apical domain between cells called preapical patch (PAP) is defined (Ferrari et al., 2008)(Fig. 4B). Apical surfaces become separated and tight junctions are established at PAP borders. Crb3 delivery to the nascent lumen may exclude Par3 and other junction proteins from this region to tight junctions. Once PAP is formed, lumen initiation can take place while phosphoinositides also become asymmetrically distributed. In MDCK cysts, the apical accumulation of PTEN by the Par complex

leads to the exclusion of PtdIns(3,4,5)P3 and the apical enrichment of PtdIns(4,5)P2 (Martin-Belmonte et al., 2007). Once a lumen has been established, this polarized architecture is maintained during tissue growth by orienting cell division events in which Cdc42 has a key role. Apically localized Cdc42, in conjunction with Par3, recruits aPKC which in turn phosphorylates LGN excluding the spindle-orientating LGN-NuMa complex from the apical surface (Hao et al., 2010) (Fig. 4C). Moreover, Cdc42 localization at the centrosomes during mitosis and association between aPKC and midbody during cytokinesis also determine spindle orientation (Jaffe et al., 2008). As the cells divide and polarize in a coordinated way, the follicle structures grow bigger and lumen expands through polarized fluid transport.

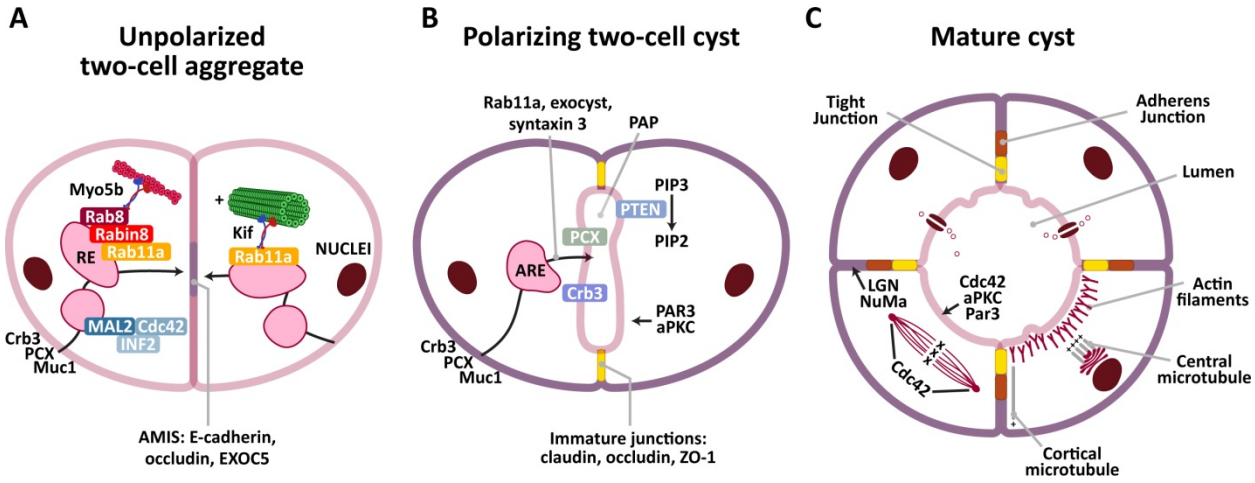

Figure 4. **Trafficking during polarization of MDCK cysts.** The steps that lead to the establishment of apica-basal polarity have been characterized in MDCK cell cysts generated from individual cells in Matrigel. A) At the two-cell stage polarization begins: E-cadherin, occludin and exocyst components such as EXOC5 are accumulated at the site of cell-cell contact, whereas Crumbs3 (Crb3) and podocalyxin (PCX) glycoproteins are enriched at the periphery. Formation of the apical membrane initiation site (AMIS) at the cell-cell contact requires a series of trafficking events: endocytosis of Crb3 and PCX from the periphery, their Rab11a-dependent endosomal transport (RE) and exocytosis at the AMIS. Rab11a activates Rab8 through the GEF Rabin8 and altogether recruit myosin Vb (Myo5b) and activate kinesins (Kif) to facilitate vesicular transport to the AMIS. B) Upon fusion of the Rab11a-positive apical recycling endosomes (AREs) with the membrane by exocyst components and the target-SNARE syntaxin 3, the AMIS progresses into a preapical patch (PAP), where the cell´s apical and basolateral surfaces are distinct. Exocytosis site is demarcated by the initial apical recruitment of Par3 and aPKC to the AMIS, however, upon Crumbs apical transport the Par3/aPKC complex moves at the PAP sides where immature tight junctions composed of claudin, occludin and ZO-1 are localized. Apical recruitment of PTEN excludes PIP3 from this region converting it in PIP2 which is necessary for apical membrane definition and lumen initiation. C) The mature cyst exhibits segregated tight junctions and adherens junctions, a fully developed single central lumen and polarized cytoskeleton and organelles. Actin filaments are beneath the apical membrane and Golgi is apically orientated. Polarized cyst architecture is maintained by orienting cell division events in which Cdc42, Par3 and aPKC play a key role by excluding the LGN-NuMa complex from the apical surface. This ensures mitosis occurs in the plane of the monolayer. Moreover, Cdc42 localizes to the centrosomes during mitosis and controls spindle orientation.

In thyroid gland, the molecular mechanisms and the signalling cascades involved in thyroid cell polarization and follicle formation are mainly unknown. In all cases, junctional complex formation provides cues and thus spatial coordinates for generation and positioning of apical membranes that are decisive for follicular lumen generation (Yap et al., 1995b). In normal tissue MAL2 protein is apically localized, whereas in polarized human primary thyrocytes 2D cultures is distributed in subapical

endosomal compartments positive for Rab11a, suggesting that basolateral-to-apical transcytotic pathway relies on MAL2 in thyroid epithelial cells (Marazuela et al., 2004). Moreover, MUC1 is restricted at the apical membrane in thyroid follicular cells (Bieche et al., 1997), although its transport in MAL2 positive vesicles or AREs has not been demonstrated yet. Nevertheless, it is clear that apical trafficking of vesicles containing apical membrane components at cell-cell contact site of developing thyroid follicles is the initial step in apical domain definition and follicular lumen formation. Coordinated TJ maturation and VACs fusion at the contacts between adjacent thyrocytes, provide attractive mechanisms to segregate newly inserted apical membrane proteins and thus facilitate cell polarization (Yap et al., 1995b). In mature follicles, the apical (luminal) surfaces have numerous microvilli that protrude into the follicular lumen increasing the surface area in contact with the colloid. Microvillus biogenesis and its apical restriction depend on ezrin, a critical plasma membrane-cortical actin cytoskeleton linker and the founding member of the ezrin-radixin-moesin (ERM) family of proteins (Bonilha et al., 2006, Fehon et al., 2010). Apical localization and activation of the ezrin kinases LOK and SLK, restrict the active-phosphorylated ezrin apically and determine microvillus formation at the apical membrane of epithelial cells (Viswanatha et al., 2012).

2.4. Thyroid lumenogenesis

Luminal space can be generated either by hollowing, cavitation or focalized contact and repulsion (Datta et al., 2011). In developing mouse aorta and in MDCK cysts *de novo* lumen formation occurs by hollowing (Strilic et al., 2009, Martin-Belmonte et al., 2008). Clusters of cells contacting the ECM initially adhere without a luminal space and then vesicles containing luminal components are exocytosed in a coordinated way to a central luminal region generating apical-basal polarization. When clusters of cells initially adhere without a luminal space and the inner cells that do not contact the ECM undergo apoptosis, luminal space is generated by cavitation. This process takes place in mammary terminal end buds (Mailleux et al., 2008). In the case of heart tube formation in Drosophila, neighbouring cells form adhesive contacts only at a discrete foci with non-contacting regions undergoing active repulsion (Bryant and Mostov, 2008). This leads to the formation of a luminal space between adhesions, called focalized contact. Although *de novo* lumen formation occurs through seemingly different morphogenetic events, all of them rely on the coordination of the common and consecutive principles of ECM and cell-cell recognition, apical-basal polarization and lumen expansion (Fig. 5, left). The process of lumen expansion requires filling through liquid pumping and depends on tight junction complexes that are the main regulators of paracellular transport in all polarized epithelia. Vectorial water transport requires the function of apical ion pumps, such as the cystic fibrosis transmembrane conductance regulator (CFTR) channel, which facilitates the osmotic filling of the lumen by increasing the luminal concentration of chloride ions (Li and Naren, 2010). Moreover, different sets of claudins are

transcriptionally regulated to modify the permeability of epithelial junctions during tubulogenesis, (Bagnat et al., 2007). In kidney, Claudin2 is responsible for increasing water leakiness, while brain ventricular lumen expansion requires Claudin5a (Zhang et al., 2010).

The exact mechanism of thyroid follicle lumen formation is not completely defined. It is postulated that follicular lumen originates either from intercellular spaces (Hilfer, 1979) or from intracellular cavities (Shepard, 1968, Nathaniel, 1986). In the case of the extracellular originated lumen, some authors suggest that adjacent cells form microvilli that interdigitate with each other. Then, cells secrete and store luminal material between the two surfaces resulting in the separation of the interdigitated microvilli and the formation of the follicular space (Hilfer, 1964, Remy et al., 1980) (Fig. 5A left).

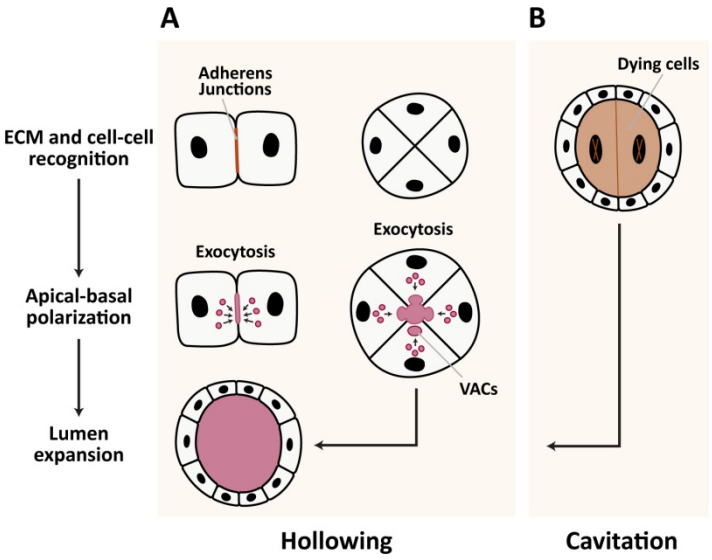

Figure 5. **Thyroid *de novo* lumen formation mechanisms.** Lumen formation relies on the coordination of three consecutive design principles: extracellular (ECM) and cell-cell recognition, apical-basal polarization and lumen expansion. Molecular instructions for whether, where and how lumens will be generated are provided from signals from the ECM (pink shading) and cell-cell contacts. In (A), lumen is formed by hollowing when two or more cells that are in contact with the ECM initially adhere without luminal space. Then vesicles containing luminal components are exocytosed directly into the intercellular space in the site of the adherens junctions and infolding of the membranes (left), or fuse and form vacuolar apical compartments (VACs) that are exocytosed to a central luminal region (right), generating apical-basal polarization. In (B), clusters of cells initially adhere without luminal space, while some of them do not contact with the ECM and undergo apoptosis. As a result, luminal space is generated due to inner cells death (cavitation process) and additional apical-basal polarization must occur. Black ovals, nuclei; pink shading, ECM; fucsia, apical membrane components and colloid; brown, dying cells.

According to the intracellular lumen origin, cytoplasmic vacuolar cavities are presumed to fuse with each other to form an apical intracellular follicular lumen that then either fuses with the junctional complex resulting in the coalescence of the cavities between the neighbour cells, or with the preformed intercellular follicular lumen (Yamashita et al., 1989) (Fig. 5A right). Both mechanisms involve exocytosis of Golgi derived vesicles rich in luminal components between the adjacent cells in a process similar to the hollowing. Additionally, a recent study of thyroid follicle formation and follicular lumen

differentiation in grass snake embryos revealed lumen formation by cavitation, as a population of centrally located cells was cleared through apoptosis to form the lumen (Rupik, 2012) (Fig. 5B).

Lumen growth and size depends on ion efflux through transport proteins, ion channels and pumps localized at the apical membrane such as iodide and chloride channels (Yap et al., 1994, van den Hove et al., 2006). The final size of the follicles is determined by the number of the composing follicular cells that proliferate in a TSH independent way (Fayet et al., 1982), and the amount of colloid that varies according to the functional activity of the follicular epithelium. Sealing of the paracellular space by TJ proteins located at the most upper interface between adjacent cells (Luciano et al., 1979), prevents the passive back-diffusion from degrading the ionic gradients established by active transport. Microtubules integrity is also necessary for the maintenance of paracellular permeability barrier in the thyroid epithelium possibly by regulating the contractile activity of the actin cytoskeleton (Yap et al., 1995a) and the correct targeting of TJ components (Yap and Manley, 2001). Therefore, coordinated lumen filling and tight junction maturation at the upper-lateral membranes is crucial for preventing colloid leakage and for permitting proper thyroid physiology.

3. Membrane-trafficking pathways in polarized thyroid cells

In thyroid cells, as in all epithelial cells, the different composition of the apical and basolateral plasma membrane domains is continuously supported by an intracellular mechanism that regulates the insertion of new proteins and lipids at specific plasma membrane domains. This occurs through the biosynthetic-secretory pathway and the constitutive or induced uptake of membrane components through the endocytic pathway (Fig. 6 and 7). All these processes require the presence of sorting signals inside the proteins and the recognition of the signals by a cellular machinery able to decipher them and therefore allow selective plasma membrane protein distribution.

3.1. Polarized biosynthetic-secretory pathways

Most membrane and secretory proteins, as well as many lipids, are synthesized in the endoplasmic reticulum (ER), the luminal environment of which is especially suited to facilitate the correct folding of the synthesized proteins and the initial steps of protein glycosylation. Proteins that are destined to be transported out of the ER move on to the Golgi complex, where further post-translational modifications can occur. The newly synthesized plasma membrane proteins specifically pass through the *trans*-Golgi network (TGN) where are sorted into distinct transport carriers for their delivery to the appropriate cell-surface domain (Mellman and Nelson, 2008). Conversely, indirect cargo transport from the TGN to the cell surface takes place through different endosomal compartments (Fig. 6). For some apical and basolateral proteins passage through the respective apical and basolateral sorting endosomes (ASEs and

BSEs, respectively) or apical and common recycling endosomes (AREs and CREs, respectively) has been described (Ang et al., 2004). However, there are proteins that can use both direct and indirect pathways as it is the case of the basolateral transferrin receptor (TfR), that chooses a direct or indirect pathway through CREs depending on the degree of cell polarity (Gravotta et al., 2007). Additionally, some proteins avoid the Golgi and are secreted by a non-canonical bypass pathway (Tveit et al., 2009).

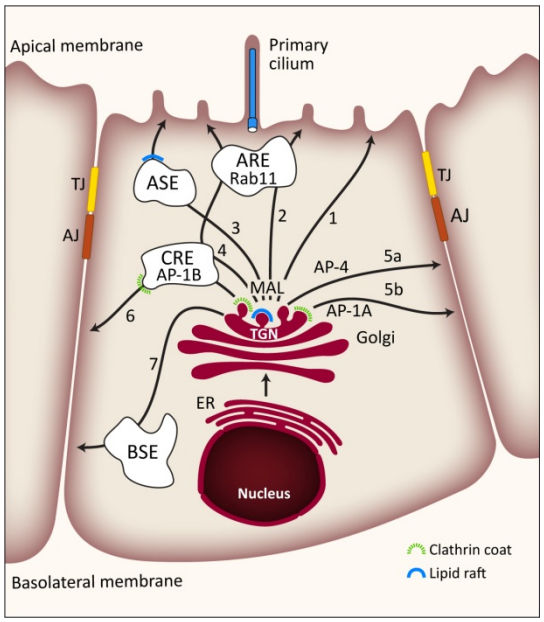

Figure 6. **Biosynthetic routes in epithelial cells.** Apical and basolateral plasma membrane proteins are synthesized at the endoplasmic reticulum (ER), transferred to the Golgi and sorted at the *trans*-Golgi network (TGN) into direct vesicular routes to the plasma membrane as shown in route 1 (apical) and in routes 5a and b (basolateral). In addition, apical plasma membrane proteins may use Rab11 positive AREs (route 2), ASEs (route 3) or CREs (route 4) as intermediate stations for apical transport. MAL proteolipid sorts at the TGN the overall apical cargos. Clustering of apical proteins in lipid-rafts (blue cap) takes place at the TGN and theses cargos reach the membrane through ASEs (route 3). Basolateral plasma membrane proteins may use CREs (route 6) or BSEs (route 7). Their sorting takes place at the TGN and at the CREs through the clathrin-associated adaptors AP-1A and AP-1B (routes 5b and 6, respectively, green cap) or clathrin-independent adaptors such as AP-4 and others (routes 5a, 7).

Cargos destined for the apical membrane (AP) present diverse sorting signals in their cytoplasmic, transmembrane or extracellular domains (Folsch, 2008, Weisz and Rodriguez-Boulan, 2009). The most common signals are N- or O-linked glycans attached to the luminal domains (Table 1). In addition, glycosylphosphatidylinositol (GPI) anchors serve as apical targeting determinants localized in the cytoplasmic protein domain. It is proposed that lectins of the galectin family bind glycan residues at the luminal side of vesicles, thereby facilitating apical targeting through clustering the cargos into different transport carriers. GPI-anchored proteins are usually clustered into lipid rafts at the TGN and this association is mediated by physical affinity to the raft's cholesterol or may be facilitated by galectin-4 that has an affinity to glycosphingolipids. On the other hand, apical targeting of raft-independent cargos such as endolyn or the neurotrophin receptor p75 depends on galectin-3. Interestingly, raft-associated cargos seem to be apically carried by ASE, while raft-independent may move through Rab11-positive ARE (Fig. 6).

Basolateral (BL) sorting signals are simple peptide motifs in the cytoplasmic domain of a protein recognized by cytosolic adaptor proteins. Tyrosine-based motifs such as YxxØ, NPxY (x indicates any amino acid and Ø a bulky hydrophobic amino acid), dileucine-based (LL/LI) and monoleucine (L/LV) motifs are critical for BL sorting (Folsch et al., 2009) (Table 1). Furthermore, stretches of acidic amino

acids, a glycine residue or aromatic motifs can increase the targeting efficiency of these signals. PDZ binding motifs formed by C-terminal sequences have also been shown to mediate BL localization of many growth factor receptors in polarized epithelial cells (Kim, 1997).

Adaptor proteins are components of protein coats associated with the TGN and/or the RE and may link or not cargo binding to clathrin (Bonifacino, 2014). The clathrin-associated adaptor protein 1 (AP-1) complex has a preeminent role in clathrin-mediated BL sorting of YxxØ, [DE]xxxL[LI] and non-canonical signals. AP-1 is a heterotretrameric complex which is present in two highly homologous isoforms in epithelial cells, the AP-1A and AP-1B that share three of four subunits (β1, γ and σ) and differ only in the medium subunit μ1A and μ1B, respectively (Folsch et al., 2001). Whereas AP-1A preferentially functions in biosynthetic route (Carvajal-Gonzalez et al., 2012, Gravotta et al., 2012), AP-1B sorts basolateral plasma membrane proteins in both biosynthetic and recycling routes (Gravotta et al., 2007, Gonzalez and Rodriguez-Boulan, 2009). However, it was recently suggested that both adaptors localize to the TGN and CRE, where they exert similar sorting functions, differing only in their affinity for BL cargo proteins (Guo et al., 2013). Conversely, clathrin-independent trafficking mechanisms through adaptors such AP-4 have been described in sorting of BL proteins. AP-4 is localized to TGN and mediates vesicle trafficking from the TGN to endosomes or BL plasma membrane through Yx[FYL][FL]E and non-canonical signals (Burgos et al., 2010). Among the proteins that follow clathrin-independent trafficking, is the transforming growth factor (TGF) whose traffic is mediated by Naked 2 through binding to motifs in its cytoplasmic domain (Li et al., 2007) and the key epithelial transporter Na,K-ATPase which is sorted basolateraly by a clathrin-independent machinery through a still unknown mechanism (Deborde et al., 2008).

Sorting signals	Sorting mechanisms, carriers-adaptors
Apical	
N-glycans	No rafts (galectin-3 mediated or not), ARE
O-glycans	No rafts (galectin-3 mediated), lipid rafts
GPI-anchor	Lipid rafts (galectin-4 mediated), ASE
Basolateral	
Tyrosine	
YxxØ	Clathrin dependent, AP-1B
Yx[FYL][FL]E	Clathrin independent, AP-4
Dileucine	
LL/LI	Clathrin dependent, AP-1
Monoleucine	
L/LV	Clathrin dependent, unknown adaptors/AP-1B

Table 1. Signals and mechanisms for sorting to the apical and basolateral membranes.

In thyrocytes and polarized Fisher rat thyroid (FRT) cells intracellular sorting of newly synthesized membrane proteins takes place at the TGN where they can be clustered into lipid rafts (Lipardi et al., 1999) or tissue specific vesicles (Zhang and Arvan, 2000). Then apical cargo can follow either a direct or an indirect route mediated by the MAL proteolipid, which is distributed in the Golgi region of human thyrocytes and FRT cells (Martin-Belmonte et al., 1998, Martin-Belmonte et al., 2000b), whereas proteins that follow a basolateral-to-apical transcytotic pathway are not transported in rafts (Sarnataro et al., 2000) but in MAL2 positive endosomes (Marazuela et al., 2004). An example of an apically localized protein by transcytosis depending on the degree of polarity of the thyroid cell line FRT is the dipeptidyl peptidase IV (DPPIV) (Zurzolo et al., 1992). Tg is likely sorted through its N-linked glycans-known to interact with lectin VIP36 (Fiedler and Simons, 1996), and is directly transported apically via a raft pathway in which MAL could be also involved (Martin-Belmonte et al., 2000a). The apical plasma membrane targeting of TPO is demonstrated to depend on the attachment of O-glycans and on N-oligosaccharides modifications at the TGN (Fayadat et al., 1998), although the carriers that mediate its transport in cell-type specific vesicles are still unknown. In the case of the apical iodide transporter Pendrin, TSH via PKA induced phosphorylation increases its translocation to the membrane (Pesce et al., 2012), whereas the presence of the sulphate transporter and antisigma factor antagonist (STAS) domain in the C-terminal determines its apical localization and function (Bizhanova et al., 2011). Interestingly, GPI-anchored proteins are apically sorted in the Golgi of FRT cells by an oligomerization mechanism driven by N-glycosylation and not cholesterol (Imjeti et al., 2011). However, thyrocytes can sort apically unglycosylated proteins through other signals and mechanisms such as ions and intracellular compartimentation, respectively (Prabakaran et al., 1999). On the other hand, the delivery of cargos at the basolateral plasma membrane (BL) of thyrocytes can be either direct from the TGN to the plasma membrane (PM) or through the BSE and CRE. Basolateral traffic of the thyroid protein marker TSHR is mediated by a signal independent of Y- and LL-based motifs, localized at the C-terminal of the protein, at a marked distance from the membrane (Beau et al., 2004). Nevertheless, Y-based, LL and LV sorting signals determine the basolateral targeting of membrane proteins such as the low-density lipoprotein receptor-related protein 1 (LRP1) and syntaxin 4 in polarized FRT cells (Donoso et al., 2009, Torres et al., 2011). AP-1 clathrin adaptor complex is also expressed in FRT cells and the medium subunit of AP-1B protein sorts both TfR and VSVG at the perinuclear region of the recycling endosomes during their biosynthetic delivery, as well as mediates recycling of TfR and LDLR in this cell line (Cancino et al., 2007).

3.2. Polarized endocytic pathways

Endocytosis encompasses a variety of processes that cells use to internalize plasma membrane proteins/lipids and extracellular molecules. The endocytic compartments, which include early endosomes, recycling endosomes, multivesicular bodies, late endosomes and lysosomes, are

dynamically interconnected both with each other and with the plasma membrane through mechanistically diverse regulated pathways (Fig. 7). Plasma membrane proteins can be internalized through clathrin-dependent or clathrin-independent endocytic pathways. Clathrin-dependent endocytosis (CDE) requires recognition of internalization signals in the cytoplasmic tails of the membrane proteins (Owen et al., 2004) (Table 2). There are three short linear motifs shown to be necessary and sufficient for the uptake of cargo into clathrin-coated vesicles (CCVs): YxxØ, [DE]xxxL[LI] and FxNPxY. The YxxØ and [DE]xxxL[LI] motifs are both recognized by the most abundant adaptor in plasma membrane-derived CCVs, the AP-2 adaptor complex, which is composed of α, β2, μ2 and σ2 subunits. FxNPxY motifs interact with the phosphotyrosine-binding (PTB) domains of some alternative clathrin adaptors, including Dab1, Dab2, ARH and Numb (Bonifacino and Traub, 2003). Additional, clathrin-independent endocytic pathways include caveolae carriers coated with caveolin-1, a cholesterol-binding protein that resides on the cytoplasmic side of lipid rafts and mediate the transport of some GPI-linked proteins. However, some membrane GPI-linked proteins undergo endocytosis via a clathrin- and caveolin-independent endocytic pathway that can be dynamin dependent or independent (Sabharanjak et al., 2002).

Endocytic mechanisms	Sorting signals	Carriers, adaptors
Clathrin-dependent	YxxØ	Clathrin, AP-2
	[DE]xxL[LI]	Clathrin, AP-2
	FxNPxY	Clathrin, DAB1/2, Numb, ARH
Caveolin-dependent	GPI-anchor	Caveolae, caveolin-1
Clathrin- and caveolin-independent	GPI-anchor	
Dynamin-dependent		Dynamin, RhoA, Rac1
Dynamin-independent		Cdc42

Table 2. Endocytic mechanisms, signals and adaptors.

Upon internalization, apical and basolateral cargo enter spatially distinct, peripherally localized apical or basolateral early endosomes (AEEs and BEEs respectively, Fig. 7) (Parton et al., 1989). Cargo can then undergo rapid recycling to the cell surface, like TfR which provides the cell with blood nutrients, or may be partitioned into multivesicular bodies (MVBs) which fuse to generate late endosomes (LEs) containing lysosome-directed cargo internalized from both apical and basolateral surfaces. An alternative cargo fate involves routing of considerable fraction of cargo to CREs that can contain intermixing of apical and basolateral cargos both endocytic and from indirect biosynthetic pathways.

Within the CREs, apical and basolateral cargos are again sorted and directed towards their appropriate surface. Apically destined proteins may be further routed through AREs as shown in figure 7, route A5.

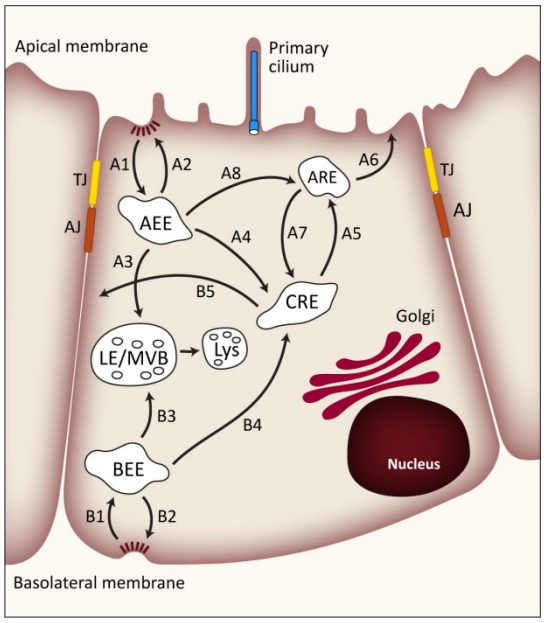

Figure 7. **Membrane-trafficking endocytic routes in polarized epithelial cells.** Membrane proteins and lipids are internalized from the apical (A1) or basolateral (B1) surfaces and delivered to apical early endosomes (AEEs) or basolateral early endosomes (BEEs) respectively. Cargos can recycle back to the cell surface (A2,B2), be delivered to late endosomes (LEs)/multivesicular bodies (MVBs; A3, B3) from which they will end up to lysosomes (Lys), or they can be delivered to the common recycling endosome (CRE; A4,B4). CRE cargos are shuttled to the basolateral cell surface (B5), or delivered to AREs (A5), from where they gain access to the apical cell surface (A6). Apical-to-basolateral transcytosis may involve cargo transit from the ARE to CRE (A7). There may also be a direct pathway from the AEEs to the apical recycling endosomes (AREs; A8).

In thyroid cells, Tg is internalized by micropinocytosis which can result from both non-specific endocytosis (fluid-phase) or receptor-mediated endocytosis (Marino and McCluskey, 2000). Both forms of internalization involve AP membrane invagination to form intracellular vesicles that subsequently fuse with endosomes, followed by endosome-lysosome fusion and its consequent proteolytic cleavage. In cultured polarized thyrocytes, the endocytic uptake and the intracellular trafficking of Tg, that leads to the BL secretion of thyroid hormones, are triggered in tandem by increased expression of the endocytic catalysts Rab5a and Rab7 in response to cAMP (Croizet-Berger et al., 2002). Moreover, TSHR internalization and recycling back to the BL membrane is triggered upon stimulation with TSH (Singh et al., 2004). In CHO cells, TSHR localizes at the perinuclear region, positive to endosomal marker RhoB, and then recycles back to the PM within 10 minutes of TSH stimulation. The role of AP-2 in protein internalization has not been demonstrated yet in thyroid cells, although it is abundantly expressed in FRT cells (Lipardi et al., 2002).

4. Sodium/iodide Symporter, a membrane protein necessary for thyroid function

Thyroid function depends on the adequate supply of iodide (I^-) which is an essential constituent of the THs. I^- reaches the thyroid via the Na^+/I^- symporter NIS, the key plasma membrane transport protein localized in the basolateral surface of thyrocytes. The experimentally tested secondary structure model of rat NIS depicts a hydrophobic protein of 618 amino acids with 13 transmembrane segments (TMSs),

an extracellularly facing amino terminus, and an intracellular carboxy terminus (Levy et al., 1998, Dohan et al., 2003). NIS has three N-linked glycosylation sites, one in the loop between TMS VI and VII, and two in the loop between TMS XII and XIII (Fig. 8). However, NIS glycosylation is not essential for its function as demonstrated by the high activity and the same K_m for I^- displayed by a NIS mutant protein in which all three glycosylated Asn were replaced with Gln (Levy et al., 1998).

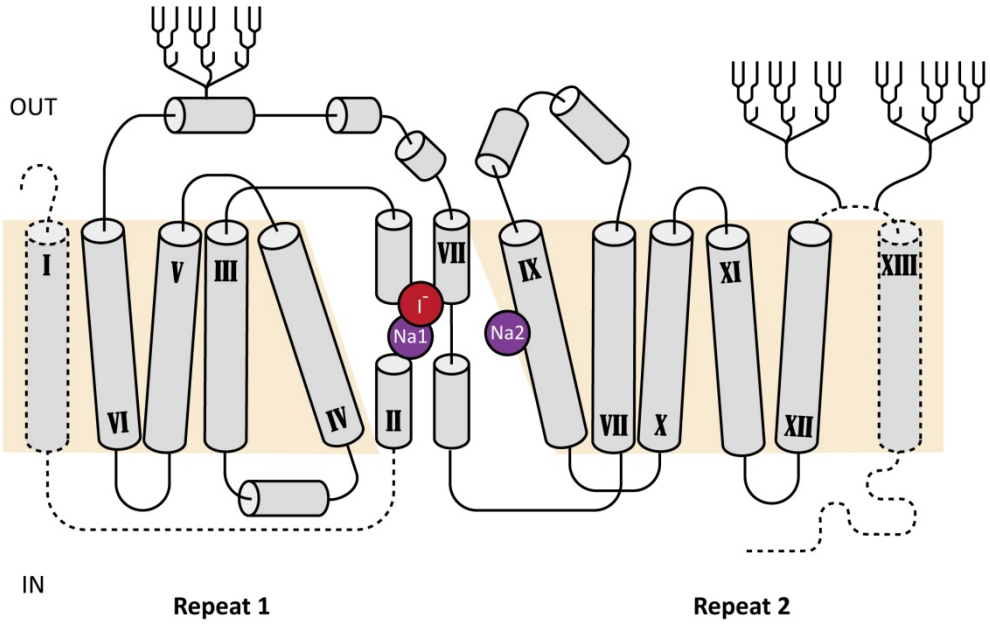

Figure 8. **NIS secondary structure.** The secondary structure model for NIS based on biochemical data and the protein's structural homology with transporters whose three dimensional structures are known. NIS is a 13-TMS protein, with the N-terminus facing the extracellular milieu and an intracellular C-terminus. TMSs I and XIII, and the loops between TMSs I and II and XII and XIII, are represented by dotted lines as their position relative to the other TMSs in the secondary structure has not been defined yet. Ten helical TMSs form an internal inverted topology repeat consisting of 5 transmembrane helical bundles (repeat 1, comprising TMSs II–VI, and repeat 2, comprising TMSs VII–XI), related to each other by a 2-fold pseudosymmetry axis running parallel to the membrane plane through the centre. There are 3 glycomoieties (black trees), 1 between TMSs VI and VII and 2 between TMSs XII and XIII. TMSs II and VII are proposed to define the substrate cavity accommodating both the I^- and Na1, and TMS IX contributes to coordination of Na2. TMS= transmembrane segment. (Modified from Portulano *et al.* The Na+/I- Symporter (NIS): Mechanism and Medical Impact, Endocrine Reviews, February 2014, 35:106)

Important information about NIS structure and function has been elucidated by the study of amino acids that are mutated in patients with congenital hypothyroidism (CH) due to an I^- transport defect (ITD). To date, 13 such mutations have been reported in NIS coding region and 1 in the 5-untranslated region (Portulano et al., 2014). Interestingly, some of these mutations resulted in intracellular NIS retention, indicating the amino acidic sequences that could be involved in NIS maturation and plasma membrane traffic.

4.1. NIS transcriptional and post-transcriptional regulation

Nkx2-1, Pax8 and FoxE1 transcription factors regulate *Slc5a5* transcription upon binding to its promoter. Proximal rat promoter has one site for Nkx2-1 that has a modest effect on *Slc5a5* transcription and a site

for NIS TSH-responsive factor (NTF-1), whereas human proximal promoter only has two NTF-1 sites. Conversely, rat *Slc5a5* upstream enhancer (NUE) consists of two Pax8, two Nkx2-1 and one cAMP response element (CRE)-like binding site, while human consists of one Pax8 binding site and one CRE-like site (Ohno et al., 1999). Binding of Pax8 to the NUE, in response to TSH stimulation (Costamagna et al., 2004), is the primary requirement for significant activation of NUE. Pax8 also collaborates with Ctcf, Sp1 and β-catenin in the transcription of *Slc5a5* (Ruiz-Llorente et al., 2012, Sastre-Perona and Santisteban, 2014). FoxE1 binding to rat *Slc5a5* promoter was recently demonstrated in our lab, in a complex interaction and in cooperation with NF1/CTF transcription factors (Fernandez et al., 2013).

4.1.1 Regulation of NIS by TSH

TSH is the primary regulator of NIS expression in thyroid gland. Stimulation of TSHR activates adenylyl cyclase resulting in elevation of endogenous cAMP that in turn induces *Slc5a5* transcription by stimulating several signal pathways of cis-regulatory elements in a Slc5a5 locus, including the NUE, the most potent TSH responsive enhancer contained in the *Slc5a5* promoter (Kogai et al., 2006). A TSH-mediated increase in NIS expression and I^- accumulation is demonstrated in human thyroid primary cultures and FRTL5 cells and the time lag between iodide uptake and NIS protein induction suggested the post-translational regulation of NIS by TSH (Saito et al., 1997, Kogai et al., 1997). Conversely, withdrawal of TSH from FRTL5 cell media results in reduction of both cAMP levels and I^- transport activity (Weiss et al., 1984, Riedel et al., 2001). However, intracellular active NIS molecules in conditions of prolonged TSH deprivation explain the persistence of I^- transport in membrane vesicles and indicates that mechanisms other than transcription may be involved in regulating NIS activity in response to TSH (Kaminsky et al., 1994). NIS can be detected intracellularly in FRTL5 cells up to 10 days after TSH withdrawal and this observation is consistent with its extremely long half-life of 5 days in the presence of TSH and 3 days without TSH in FRTL5 cells, as established by metabolic labeling and immunoprecipitation experiments (Riedel et al., 2001). Thus, it is believed that TSH not only stimulates its transcription and biosynthesis, but it is also required for targeting NIS to and/or retaining it at the plasma membrane. Moreover, TSH is shown to modulate NIS phosphorylation mostly on its C-terminus. Considering that phosphorylation has been implicated in activation and subcellular distribution of several transporters, it was initially proposed as a TSH-dependent mechanism regulating NIS transport to the membrane (Riedel et al., 2001). Eventually, site-directed mutagenesis of 5 *in vivo* phosphorylation sites demonstrated that NIS localization is independent of phosphorylation (Vadysirisack et al., 2007).

4.1.2. Regulation of NIS by other factors

Both NIS transcription and its expression at the plasma membrane are impaired in the presence of two of the main factors that regulate thyroid cell function: insulin growth factor 1 (IGF1) and transforming

growth factor beta (TGFβ) (Garcia and Santisteban, 2002, Costamagna et al., 2004). IGF1 inhibits the cAMP-induced NIS expression in FRTL5 cells through PI3K activation, whereas TGFβ through Smad3 interferes with Pax8 transcriptional activation of *Slc5a5* gene. Furthermore, several studies have shown that overexpression of the RET-RAS-BRAF oncogenes in thyroid carcinomas decreases NIS mRNA and protein levels through the MAPK pathway, and that BRAF impairs the localization of NIS in the basal membrane of follicular thyroid cells both *in vitro* and *in vivo* (Riesco-Eizaguirre et al., 2006, Knauf and Fagin, 2009). Interestingly, our lab demonstrated that the repression of NIS function induced by BRAF is mediated through TGFβ secretion via an autocrine loop (Riesco-Eizaguirre et al., 2009). Additionally, the NUE is negatively regulated by the pituitary tumor-transforming gene-1 product (PTTG1) and the PTTG1-binding factor (PBF) (Boelaert et al., 2007). PBF is shown to reduce iodide uptake and cell surface NIS expression in NIS-introduced Cos7 cells after exogenous PBF expression (Smith et al., 2009). PBF is also significantly increased in thyroid cancers suggesting that its abundant expression is likely associated with the reduced cell surface NIS expression in those cancers (Stratford et al., 2005). Interestingly, in Cos7 cells, PBF is predominantly expressed in CD63-positive late endosomes where colocalizes with internalized NIS. CD63 is a tetraspanin involved in protein trafficking associated to clathrin, indicating a possible interaction between NIS and the clathrin-coated machinery. In fact, the cytoplasmic, C-terminus of NIS contains a dileucine motif that could be recognized by clathrin adaptors (Dohan et al., 2003). In addition, NIS is reported to have a PDZ target motif important for protein-protein interaction and three acidic dipeptide motifs that could function as retrieval signals in its C-terminus. All those motifs are likely to be involved in the post-translational regulation of NIS; nevertheless they have not been studied yet.

4.2. NIS and thyroid functional polarity

NIS expression in the basolateral plasma membrane of thyrocytes and the subsequent iodide accumulation in human developing thyroid are observed only when small follicles are formed (Szinnai et al., 2007). *Slc5a5* is the last gene to appear during thyroid mice morphogenesis (see figure 3), and its expression is strongly correlated with the sudden onset of thyroid hormone synthesis in human, mouse and rat (Postiglione et al., 2002). Furthermore, functional NIS and iodide uptake are much more stimulated in 3D than in 2D TSH-induced human thyrocytes cultures (Kogai et al., 2000) and porcine primary reconstructed follicles (Bernier-Valentin et al., 2006), indicating that polarized efflux into the follicular lumen contributes to iodide concentration after follicle formation and support the hypothesis that NIS function may involve intracellular sorting and membrane localization of NIS or NIS regulatory factors. Thus, all this data makes evident that proper thyroid function requires thyrocytes polarization followed by their organization into a polarized follicular structure in order to guarantee the polarized NIS expression and subsequent iodide accumulation into the thyroid lumen available for THs synthesis.

OBJECTIVES

1. **To reveal the cellular and molecular mechanisms that control thyroid epithelial cell polarity acquisition and follicle formation.**

- To establish an appropriate three dimensional culture system in which thyroid follicular cells acquire apical-basal cell polarity and form follicle structures.

- To identify thyroid specific regulators of three dimensional follicular organization.

- To define novel thyroid-specific pathways involved in follicle formation.

2. **To define the biosynthetic and internalization trafficking pathways of the basolateral transmembrane sodium/iodide symporter NIS in polarized epithelial cells.**

- To identify the exocytic machinery and the sorting mechanisms involved in NIS biosynthetic and recycling routes.

- To identify the endocytic machinery and the trafficking mechanisms involved in NIS internalization routes.

MATERIALS AND METHODS

1. Materials

1.1. Cell lines

FRT and PCCl3: Epithelial thyroid rat cell lines obtained from Fisher rats of 6 weeks or 18 months age, respectively (Ambesi-Impiombato et al., 1980, Fusco et al., 1987). PCCl3 cells retain the functional properties but not the morphogenetic characteristics of thyrocytes as they express all thyroid transcription factors (Nkx2-1, Pax8, FoxE1, Hhex) and the more important thyroid differentiation markers (Tg, TPO, NIS and TSHR), but have lost the ability to get polarized. In contrast, FRT cells are dedifferentiated as they only express Pax8 transcription factor and none of the thyroid differentiation markers, but become fully polarized (Nitsch et al., 1984) and therefore consist in the only suitable cell line to study thyroid cell polarization and follicle formation.

FRTshPax8, FRTshCdh16: FRT cells stably silenced for Pax8 and Cdh16 expression described in Methods 2.6.1.

MDCK, MDCKhNIS: Madin-Darby Canine Kidney epithelial cells (strain II) are generated from dog kidney (Valentich, 1981). These cells become fully polarized and form three-dimensional cysts in appropriate conditions (Montesano et al., 1991). Thus, are widely used as a polarized model system to study epithelial development and function. MDCKhNIS cells are MDCKII cells stably expressing human NIS cDNA (Zuckier et al., 2004), kindly provided by Dr. Nancy Carrasco (Yale School of Medicine, Connecticut, USA).

µ1B-KD: MDCK cells stably knockdown for µ subunit of AP-1B protein (AP1M2 gene) (Gravotta et al., 2007) were kindly provided by Dr. Enrique Rodriguez-Boulan (Weill Cornell Medical College, New York, USA).

µ1B-KDhNIS: µ1B-KD cells stably expressing human NIS described in Methods 2.7.2.

µ1A-KDhNIS, µ1AB-KDhNIS: MDCKhNIS and µ1B-KDhNIS cells stably knockdown for µ subunit of AP-1A protein (AP1M1 gene) respectively, as described in Methods 2.6.1.

1.2. Animals

Experimental FVB/C57 mice were housed in temperature (22±2˚C) and light (12:12 light-dark cycle; lights on at 7 a.m.) controlled conditions and had free access to food and water. Adult, 16-weeks old animals were sacrificed by CO_2 inhalation and the thyroid glands were rapidly dissected out and further preceded for primary thyrocytes culture. Animals were handled according to Spanish laws (R.D. 1201/2005).

1.3. Antibodies/Dyes

Table 3.

Primary Ab	Reference	Immunogen	WB dilution	IF dilution
β-actin	1616R Santa Cruz	rabbit	1:1000	-
γ-adaptin	610385 BD Biosciences	mouse	-	1:500
AP-2	610501 BD Biosciences	mouse	-	1:200 (Triton)
E-cadherin	610182 BD	mouse	1:1000	1:200
Cadherin 16	15107 ProteinTech	rabbit	1:1000	1:100
β-catenin (C-18)	1496 Santa Cruz	rabbit	-	1:500
Clathrin	610500 BD Biosciences	mouse	-	1:500
CRYAB	13497 Abcam	rabbit	1:4000	1:400
EEA1	610457 BD Biosciences	mouse	-	1:500
phospho-ERM	3141 Cell Signaling	rabbit	-	1:100
Ezrin	661-P0 Thermo	mouse	-	1:300
GFP	6455 Invitrogen	rabbit	-	1:200
GM130	610822 BD	mouse	-	1:100
gp135	Gift from Dr. G. Ojakian	mouse	1:50	1:200
HA (16B12)	MM3-101P Covance	mouse	-	1:100
HA-FITC (3F10)	11988506001 Roche	rat	-	1:200
Itgb1 (N20)	6622 Santa Cruz	goat	1:500	-
Itgb1(HUTS21)	Gift from Dr. F. Sánchez	mouse	undiluted	1:2
LC3	2775 Cell signaling	rabbit	1:1000	-
α-Na,K ATPase	MA3-928 Thermo	mouse	1:500	-
hNIS	Gift from Dr. N. Carrasco	rabbit	1:1000	1:500
hNIS	FP5A LabVision	mouse	-	1:200
rNIS	Gift from Dr. N. Carrasco	rabbit	1:1000	1:1000
Pax8	PA0300 Biopat	rabbit	1:2000	1:500/1000
Rac1	610651 BD Biosciences	mouse	1:1000	1:200
Stx7	72016 Abcam	sheep	-	1:300
TfR	13-6890 Invitrogen	mouse	1:500	1:400
Tg	A0251 Dako	rabbit	1:5000	1:1000
TGN38	AHP499G AbD Serotec	sheep	-	1:800
TGN46	ABT95 Merck	rabbit	-	1:200/500
α-tubulin (B7)	5286 Santa Cruz	mouse	1:1000	-
α-tubulin acetylated	T 6793 Sigma	mouse	-	1:500
ZO-1 (R40.76)	33725 Santa Cruz	rat	-	1:200

Table 4.

Secondary Ab	Reference	Dilution
Goat anti-mouse AF488, 546, 647	Molecular probes	1:500
Goat anti-rabbit AF488, 546, 647	Molecular probes	1:500
Goat anti-rat AF488, 546, 647	Molecular probes	1:500
Donkey anti mouse AF488, 546	Molecular probes	1:500
Donkey anti-rabbit AF555, 647	Molecular probes	1:500
Donkey anti-rat AF488	Molecular probes	1:500
Donkey anti-sheep AF633	Molecular probes	1:500

Table 5.

Dyes	Reference	Dilution/Concentration
Dapi	D1306 Molecular Probes	1:10,000
Falloidin546	A22283 Molecular Probes	2.5:100
Falloidin647	A22287 Molecular Probes	2.5:100
Lysotracker-RedDND-99	L7528 Molecular Probes	100nM

Tables 3, 4 and 5. List of antibodies and dyes used in Wester-blot and immunofluorescence.

1.4. Plasmids

Expresion vectors:

- pcDNA3.1-human**NIS**, provided by Dr. Antonio de la Vieja Escolar (Instituto de Salud Carlos III, Madrid-Spain)
- pEGFP-N1-dog**Cdh16**, generated by Dr. Ilenia Bernascone, Dr. Fernando Martín-Belmonte laboratory (Centro de Biología Molecular "Severo Ochoa", Madrid-Spain)
- pcEFL-human**Rac1QL-HA**, provided by Dr. Piero Crespo (Instituto de Biomedicina y Biotecnología de Cantabria, Spain)
- pcDNA3-human**TfR-HA**, (Belouzard et al., 2004). Provided by Dr. María del Mar Malagón (Department of Cell Biology, Physiology and Immunology, University of Córdoba, Spain)
- pBC6-mouse**µ1A-HA** and pBC6-humanµ1B-HA (Folsch et al., 2001). Provided by Dr. Heike Folsch (Department of Biochemistry, Molecular Biology, and Cell Biology, Northwestern University, Evanston-IL)

Lentiviral vectors:

- Lentiviral plackaging plasmids pMD2-VSVG and pCD-NL-BH: These vectors contain cDNAs for VSVG envelope protein and gag, env and pol structural proteins, respectively. Expression of these four proteins is necessary for the correct packaging of the viral particles.
- Short hairpin (sh) RNA expression pGIPZ vectors against Pax8 (pGIPZ, RHS4430-101170241), Cdh16 (pGIPZ, RMM4431-99940298), AP1M1 (pGIPZ, RHS4430-200279346) mRNAs and a GIPZ non-silencing lentiviral shRNA control (pGIPZ-shRNAmir-NS, RHS4346) all from Open Biosystems.

1.5. Oligonucleotides

Gene	Sequence	Product size	Species
AP1M1	F: 5′ CCCTCAGCCACATCAGTGTT 3′ R: 5′ AAACATAGACAGGGTGGCGG 3′	128bp	Dog
AP1M2	F: 5′ AGGTGTTTCTGTCGGGAATG 3′ R: 5′ AATTTCACGTCCTCCAGCTC 3′	112bp	Dog
Cdh16	F: 5′ TTCCTGGAGGTTTCTGATGG 3′ R: 5′ AAAGGCTGAACTGGGAACTG 3′	89bp	Rat
Dynlrb2	F: 5′ CCACAAAGGGGTCATCGGAA 3′ R: 5′ TCAGGTCATTCTGGGGGTCA 3′	161bp	Rat
Fn1	F: 5′ AACTTCTGGTCCTCTCCCGT 3′ R: 5′ CCTAGGTAGGTCCGTTCCCA 3′	358bp	Rat
GAPDH	F: 5′ CATCAACGGGAAGTCCATCT 3′ R: 5′ ACTCAGCACCAGCATCACC 3′	78bp	Dog
LamC2	F: 5′ ATCACCCTGAGTTCCCTCCA 3′ R: 5′ GCTGCGGTCTAGAGATCCTTC 3′	111bp	Rat
Map7	F: 5′ GCTCTCGTCCTCATCTGCAA 3′ R: 5′ CAGTTTTGAAGGGCGTGGTG 3′	194bp	Rat
Myo5b	F: 5′ AGTGGGGATGAGGGTTTCAT 3′ R: 5′ TTCCAGCATGGCAGAAACTA 3′	180bp	Rat
Nid2	F: 5′ CGCCCCAAAGAGTCCTACAA 3′ R: 5′ ATGGTCACCTCCAACTGTGG 3′	237bp	Rat
Ocln	F: 5′ ACGGCAAAGTGAATGGCAAG 3′ R: 5′ TTATCGTTGCTGCTGTACCG 3′	139bp	Rat
Pax8	F: 5′ GGACAGTTGTCGACTGAGCA 3′ R: 5′ GAATGAGGATCTGCCACCAC 3′	300bp	Rat

Polr2	F: 5′ GCAGGACGATGAGATACGCT 3′ R: 5′ ATCAAAGCAAGCTGGAGGCT 3′	133bp	Rat
Rab17	F: 5′ AACACCATTGCCCAGGAG 3′ R: 5′ AGGCTGAGCTATCCTCCAC 3′	169bp	Rat
Tgm2	F: 5′ CCGGGAATACGTCCTCACAC 3′ R: 5′ ACATAGATGGGACTGCTGCG 3′	192bp	Rat
Wnt4	F: 5′ GCTGTACCTGGCCAAGCTGT 3′ R: 5′ GAACTGGTACTGGCACTCCTC 3′	172bp	Rat
Wnt7A	F: 5′ GCCTGGACGAGTGTCAGTTT 3′ R: 5′ GTGGTACTGGCCTTGCTTCT 3′	221bp	Rat

Table 6. List of oligonucleotides used for q-PCR.

All the oligonucleotides were designed with Primer3 online program and ordered at Sigma.

2. Methods

2.1. Cell culture methods

2.1.1. Unpolarized monolayer cell culture

PCCl3 and FRT cells were grown in Coon's modified Ham's F-12 medium containing 5% donor calf serum and a six-hormone mixture consisting of 1nM TSH, 10µg/ml insulin, 10ng/ml somatostatin, 5µg/ml transferrin, 10nM hydrocortisone, and 10ng/ml glycyl-L-histidyl-L-lysine acetate (Sigma). In the present Thesis we will refer to this medium as **6H**.

The effect of TSH hormone on NIS expression and localization was studied by starving almost-confluent PCCl3 cells for TSH and insulin in the presence of 0.2% serum. We will refer to this culture medium as **starvation medium** and it will be indicated as **-TSH** in the figures. TSH was added to the starvation medium at the final concentration of 0.5mU/ml.

To label lysosomes in PCCl3 cells we used the Lysotracker-red probe (see Materials 1.3.) at different concentrations (45, 70 and 100nM) and time points (30 minutes and 1 hour) and then cells were fixed and prepared for confocal immunofluorescence analysis as described in Methods 2.3.4.1. Once the best concentration and incubation time for immunofluorescence colocalization analysis were defined, we incubated 24 hours-starved-PCCl3 cells with 100nM Lysotracker for 30 minutes and then performed immunofluorescence and confocal analysis.

To inhibit lysosomal degradation in PCCl3 cells and follow NIS degradation pathway we cultured cells in starvation medium for 40 hours and then we treated them with 100mM of protease inhibitor Leupeptin and 20mM NH_4Cl (that alkalizes lysosome pH) for different time points. Consequent to lysosomal

inhibition, lysosomal fusion with autophagosomes is also inhibited and to monitor this process we used the autophagosomal marker LC3 that localizes in autophagosomes and autolysosomes in its lipidated form LC3-II (Tanida et al., 2005). NIS and LC3 expression levels after lysosomal inhibition were evaluated by Western blotting.

MDCK cells were grown in Dulbecco's MEM (DMEM) culture medium containing 5% fetal bovine serum (FBS). MDCKhNIS cells were grown in DMEM with 5% FBS supplemented with geneticin G418 (0.6mg/ml). All MDCKhNIS knockdown cell lines: µ1B-KDhNIS, µ1A-KDhNIS and µ1AB-KDhNIS were grown in DMEM with 5% FBS and supplemented with puromycin (2.5µg/ml) and G418 (0.6mg/ml).

2.1.2. Primary thyrocytes isolation and culture in a monolayer

Mouse thyrocytes were isolated from thyroid lobules of aseptically dissected 3-months old mice (Jeker et al., 1999). Lobules were chopped and then digested in a solution composed of type I collagenase (Sigma: 112U/ml) and dispase (Sigma: 1.2U/ml) during 45 minutes in a rotatory mixer at 37˚C. After digestion the tube was centrifuged for 3 min at 1,200rpm and the pellet was resuspended in 1ml of 6H medium. The resuspended follicles were plated in 35mm Petri dish and cultured in a 37˚C water saturated incubator, under air/CO_2 (95%:5%). The initially isolated thyroid follicles (Fig. 9, day 0) attached to the Petri dish within the first 24 hours and consequently lost their three-dimensional structure (Fig. 9, day 1). Three days post isolation a single layer of thyrocytes was formed (Fig. 9, day 3) and cells continued growing (Fig. 9, day 5) until they reached confluence. Their thyroid identity was then confirmed through the protein expression of the thyroid transcription factors (not shown).

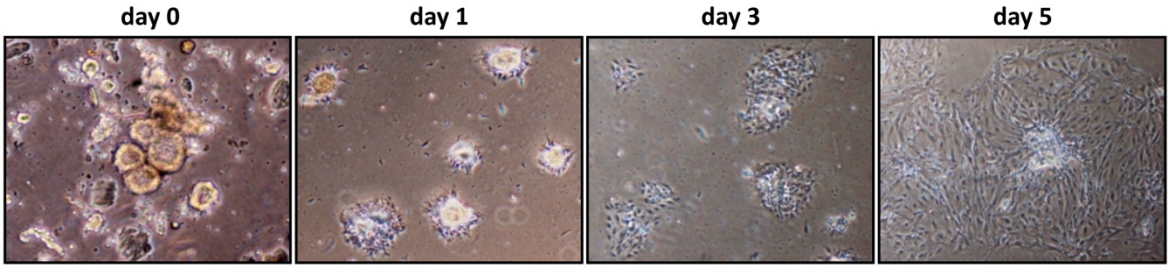

Figure 9. **Establishment of mouse primary culture.** Primary thyrocytes the day of isolation (day 0) and at different days of culture (day 1, 3, 5) visualized with a bright-field microscope under a 40x objective.

2.1.3. Polarized monolayer culture on Transwell

Suspended FRT- and MDCKhNIS-derived cells were seeded on 0.4mm pore size Transwell polycarbonate membrane inserts (Corning) at a density of $0.4x10^5$ or 10^6 cells for 12mm or 24mm inserts, respectively. Cell line-respective culture medium was added at both sides of the insert and was replaced every 2 days without washing. Confluent monolayers were let 5 days to become fully polarized before they were

assessed for cell surface immunofluorescence detection or domain-selective membrane protein biotinylation.

2.1.4. Three-dimensional culture in Matrigel

FRT cells and primary thyrocytes were trypsinized to a single cell suspension of 10,000cells/ml and mixed with 10% of reconstituted basement membrane matrix gel-Matrigel (BD Biosciences 356234). Cells-Matrigel mix was plated on chambers coated with previously gelled Matrigel at 37˚C for 15 minutes. 6H culture medium was changed without washing every 2 days and cells were let to grow and form three dimensional follicle-like structures. Small follicles were observed at 4 days of culture and continued growing up to 8 days (see Results 1.1., Fig. 12). In this Thesis we will refer to 3D thyroid follicle formation in Matrigel as morphogenesis assay.

2.2. RNA

2.2.1. RNA extraction

Each cell line was grown in its respective culture medium as unpolarized monolayer or follicles in Matrigel. Medium was removed and cells were washed with PBS pH 7 at 4˚C and RNA was extracted using Trizol (Sigma) according to provider's instructions. In the case of follicular culture an additional centrifugation at 12,000xg for 10 minutes at 4˚C was performed after initial Trizol addition and homogenization in order to remove Matrigel. RNA cuantification and purity were determined by absorbance measurements at 260 and 280nm using the spectrophotometer Nanodrop ND1000 (Thermo Scientific). Removal of genomic DNA from RNA preparations was performed using the DNAase I recombinant, RNase free (Roche) according to provider´s instructions. DNase inactivation and RNA precipitation was then carried out by adding 0.1 volumes of 3M sodium acetate (pH 5.2) followed by vortex and addition of 2.2 volumes of ice cold 100% ethanol. The samples were mixed thoroughly and placed in the freezer for at least 2 hours. RNA was withdrawn after mix of the ethanol precipitate and centrifugation at 14,000xg for 10 minutes at 4˚C. Pellet was washed with ice cold 70% ethanol, centrifuged at 7,500xg for 10 minutes at 4˚C and let to dry. RNA was finally dissolved in 5-10µl of RNase free water.

2.2.2. Reverse Transcription-Polymerase Chain Reaction (RT-PCR)

To obtain complementary DNA (cDNA) from RNA samples, 1µg of total RNA were reverse transcribed according to the following protocol. First RNA was mixed with 200ng of dNTPs and 200ng of random primers in a total reach the final volume of 14µl. To denature RNA secondary structure RNA was incubated at 65˚C for 10 minutes and then quickly chilled on ice 2 minutes to let the primers anneal to the RNA. Then a mix made with 200U of reverse trasctiptase M-MLV (Promega), 40U of RNase inhibitor

(RNaseOUT, Invitrogen) and M-MLV RT buffer was added to a final volume of 20µl. RT reaction was performed at 25˚C for 10 minutes, then shifted to 37˚C for 15 minutes, 40˚C for 15 minutes, 42˚C for 30 minutes and finally at 95˚C for 5 minutes to inactivate the enzyme. cDNA was diluted 5 times with destiled water to reach the final volume of 100µl.

2.2.3. Real-time quantitave PCR (q-PCR)

To detect relative gene expression levels q-PCRs were performed with the Mx3000P q-PCR system (Agilent) using a reaction mix of SYBR green composed of KAPA SYBR FAST 2x and ROX low 50x (Kapa Biosystems). Each reaction was performed with 10 or 20 ng of cDNA, 10µM of each primer in a final volume of 10µl and in triplicate. Amplification conditions used were the following: polymerase activation at 95˚C for 5 minutes followed by amplification during 40 cycles consisting in denaturalization at 95˚C for 20 seconds, annealing at 60˚C for 20 seconds and extension at 72˚C for 30 seconds. Then, primers specificity was determined by the dissociation curve. Basal fluorescence was subtracted by MxPro q-PCR software and relative gene expression was calculated by the $2^{-\Delta\Delta Ct}$ algorithm (Giulietti et al., 2001). Presented data are normalised to Polr2g expression for FRT samples, and to GAPDH expression for MDCK-derived samples. All the primers used are resumed in Materials 1.5.

2.3. Protein detection methods

2.3.1. Total lysate extraction

Whole cell extracts were prepared by washing the monolayers twice with ice cold PBS and cell lysis was performed by incubation with RIPA buffer (1% Nonidet p-40, 0.1% SDS, 1% sodium deoxycholate in PBS) plus a protease-inhibitor mixture (Roche) for 30 minutes on ice followed by centrifugation at 12,000rpm for 10 minutes at 4˚C. Protein concentration was measured according to the Bradford method (Bradford, 1976) using the Bio-Rad Protein Assay Dye Reagent Concentrate (Bio-Rad) and through a bovine serum albumin (BSA) standard curve.

2.3.2. Cell surface proteins extraction by biotinylation assay

Cell surface proteins were isolated using a biotinylation assay consisting in conjugation of sulfo-NHS-SS-Biotin (Pierce) to the primary amines present on the N-termini of membrane proteins. PCCl3 cells grown as a monolayer in 60mm Petri dishes to 80% confluence were subjected to biotinylation according to the method described previously (Riedel et al., 2001). Membrane, cytosolic and total extracts were recollected during the process.

Domain-selective biotinylation from the apical (AP) and basolateral (BL) domains was performed with polarized MDCKhNIS cells grown on 24mm-Transwells as described in cell culture methods. Cells were placed on ice and rinsed twice with ice-cold PBS supplemented with 100mM $CaCl_2$ and 1mM $MgCl_2$

(PBSCM) at both upper and lower compartments, and once with biotinylation buffer (BB, pH 8.4) composed of 25mM triethanolamine-HCl (pH 7.8), 0.25M sucrose, 0.5mM $CaCl_2$ and 1mM $MgCl_2$. Next, cells were incubated twice with 1.5mg/ml sulfo-NHS-SS-Biotin in BB added either to the apical (0.9ml) or to the basolateral (0.6ml) sides (while the opposite compartment was incubated with PBSCM) at 4˚C for 20 minutes. Cells were gently rinsed twice with BB and unreacted biotin was quenched using 100mM glycine in PBSCM three times during 5 minutes each. Filters were removed from the inserts and cells were lysed with 1ml of Transwell Lysis Buffer composed of 50mM Tris-HCl (pH 7.4), 150mM NaCl, 25mM KCl, 2mM EDTA, 1% Na-deoxycholate, 0.1% SDS, 1% Triton X-100 and supplemented with the protease inhibitors for 30 minutes at 4˚C. Lysates were cleared by centrifugation (16,000xg for 10 min at 4˚C) and 0.2ml were separated as total protein fraction. Biotinylated proteins were retrieved from cleared lysates in the same way as the cell surface proteins and were finally eluded with 50µl of LB+DTT 2x in lysis buffer for 5 minutes at 75˚C with agitation. Samples were chilled on ice during 10 minutes and proteins were taken off with a spin and kept on ice until SDS-PAGE analysis followed by Western-blot.

2.3.3. Western-blot

Whole cell protein extracts (30µg) or cell surface proteins (≥100µg) were separated by electrophoresis in SDS-PAGE gels according to the protocol of Laemli (Laemmli, 1970) and then transferred to a nitrocellulose membrane (Protran) using the wet transfer technique (Towbin et al., 1979). Next, membranes were incubated with blocking solution (5% milk powder in PBS 1x with 0.1% Tween-20) for 2 hours at room temperature and, subsequently, with the appropriate primary antibodies (Materials 1.3. Table I) prepared in blocking solution at 4˚C overnight or at room temperature for 2 hours. Finally, the membranes were incubated with the appropriate Horse Radish Peroxidase (HRP)-conjugated secondary antibodies diluted in blocking solution for 1 hour at room temperature. All membrane incubations were made with gentle rocking. The antibody binding targets were visualized via chemiluminescence using the Western-blot Luminol detection system (Thermo Fisher). Films (AGFA) were exposed at different times to ensure the bands were not saturated and films were scanned for densitometric analysis using NIH Image J software (http://rsbweb.nih.gov/ij/) to obtain a relative comparison between protein bands. We demonstrate representative blots from at least 2 independent experiments.

2.3.4. Immunofluorescence assay

In order to monitor the expression and/or subcellular localisation of proteins cells were grown in monolayer, on Transwell or embedded in Matrigel and prepared for immunofluorescence analysis.

2.3.4.1. Monolayers

Unpolarized cell were grown on glass coverslips to a 70% confluence and then medium was removed, cells were washed twice with PBS 1x and fixed with 4% (v/v) para-formaldehyde (PFA) in PBS for 10

minutes. To remove the excess of PFA cells were washed twice for 5 minutes with PBS and cells were next blocked and permeabilized for 20 minutes with a solution composed of 0.5% BSA, 0.1% saponin, 50mM NH_4Cl and 0.02% sodium azide in PBS. Overnight incubation with primary antibodies diluted in the same solution at 4˚C was followed by 3 washes of 5 minutes with PBS and subsequent 45 minutes incubation with appropriate secondary antibodies at room temperature. Nuclei were stained with 4-, 6-diamidino-2-fenilindol (DAPI) for 10 minutes and then coverslips were washed, dried and mounted with Mowiol or Prolong Gold antifade reagent (Invitrogen). Single confocal sections form FRT and MDCK, MDCKhNIS cells were collected with laser-scanning TCS SP5 Leica confocal microscope (SIdI-UAM, Madrid), using a HCX PL APO lambda blue 63x/1.40 oil-immersion objective, 1024x1024 pixels resolution and processed with LAS AF Lite software (Leica). PCCl3 samples were analyzed with LSM 700, Zeiss confocal microscope and images were captured with a Plan-Apochromat 63x/1.40 oil immersion objective (CNR-IBP, Naples). Further image processing was carried out with Image J software. Quantitative colocalization analysis was performed with the ICA plugin (Li et al., 2004) and the JACoP plugin (Bolte and Cordelieres, 2006) and expressed as Pearson´s correlation coefficient (Rr) and the Manders´coefficient (R). As both plugins gave same Rr results, we present data derived only from the ICA plugin. For each condition more than 10 cells were analyzed and values are the mean±SD.

2.3.4.2. Transwell

Polarized cells grown on 12mm-Transwells as described in cell culture methods, were prepared for immunofluorescence analysis of membrane proteins according to the following protocol. Cells were fixed with 4% PFA in PBSCM for 30 minutes and then excess of PFA was rinsed off with PBS 1x. To gain access to intracellular epitopes, cells were permeabilized with 0.1% saponin in PBS 1x at 4˚C for 15 minutes with gently shaking, followed by two quick washes with PBS 1x at room temperature. Blocking was performed with 3% BSA in PBS 1x at room temperature for 30 minutes. Then, the polycarbonate membranes were excised from inserts and incubated with specific primary antibodies against the luminal domains of the respective antigens, overnight at 4˚C at pre-optimized dilutions in blocking solution. After washing the excess antibody, bound antibodies were detected with appropriate combinations of secondary antibodies at room temperature for 1 hour. Samples were mounted on microscopy slides with Prolong Gold antifade reagent after nuclei and filamentous actin staining for 5 minutes. All incubations and washes were performed at both sides of the insert. For orthogonal views z-stack series (step 0.14µm) were collected with TCS SP5 Leica confocal microscope (SidI-UAM, Madrid), HCX PL APO lambda blue 63x/1.40 oil immersion objective, a 2x zoom, 1024x1024 pixels resolution and processed with LAS AF Lite software (Leica). Further image processing was carried out with Image J software.

2.3.4.3. Matrigel

Immunofluorescence of Matrigel embedded thyrocyte- or FRT-derived follicles was performed in 8-well coverglass chambers with removable media chamber (Lab-Tech II chamber system, NUNC) according a protocol for MDCK cysts preparation (Yu et al., 2005) modified to our system needs. Briefly, follicles were washed gently with PBS 1x (pH 7.4) containing 1mM $CaCl_2$ and 0.5mM $MgCl_2$ and fixed with 4% PFA in PBS-washing solution for 40 minutes. Permeabilization was performed with 0.025% saponin in PBS-washing solution for 40 minutes followed by 10 minutes neutralization with 75mM NH_4Cl and 20mM glycine in PBS-washing solution. Blocking was carried out with 0.0025% saponin, 1% gelatin and 1% BSA in PBS-washing solution for 30 minutes, and subsequent incubation with primary antibodies in blocking solution was done overnight at 4˚C. After secondary incubation for 1 hour at room temperature, cells were fixed again with 4% PFA in cacodylate buffer (pH 7.4) for 30 minutes. Nuclei were stained with DAPI in PBS-washing solution at 37˚C for 10 minutes. Finally, the media chamber was removed and the slide was mounted with Prolong Gold antifade reagent. Single images and z-stack serial sections were taken with the TCS SP5 Leica confocal microscope, HCX PL APO lambda blue 63x/1.40 oil immersion objective, a 2.5x zoom, 1024x1024 pixels resolution and processed with LAS AF Lite software (Leica). Further image processing was carried out with Image J software. Lumen formation and polarized protein distribution were determined by z-stack analysis of follicles that have 4 to 6 cells at the equatorial section. At least 150 follicles from three independent experiments were analyzed, statistical significance was determined by t-test analysis (two-tailed) and differences were considered significant for $p<0.05$.

2.4. Time-lapse microscopy

To visualize the follicle formation process we performed live imaging time-lapse microscopy using the Cell Observer.Z1 microscope (Zeiss). Single FRT cells or primary thyrocytes were seeded in 8-well µ-Slide (IBIDI) as described in Methods 2.1.4. and 5 hours later were transported to the microscope´s chamber at 37˚C and 5% CO_2 for live-cell imaging during 7 days. z-stack images were acquired in DIC with a Plan-APOCHROMAT 20x/NA 0.40 dry objective every 40 minutes, exposure time 2.8 milliseconds, using a high resolution camera (Cascade 1K). Image and video analysis was performed with Axiovision Rel.4.8 software. Medium was added the fourth day of growth.

2.5. Expression microarray

In order to detect differential gene expression between polarizing FRT cells in 3D Matrigel culture and 2D confluent monolayer, a microarray-based differential expression analysis was conducted using the Agilent Rat Gene Expression G3 60K. We prepared four biological replicates of each condition and we

compared every 3D condition to a pool of 2D conditions and a dye swap between 3D and 2D pools. RNA was isolated the fifth day of culture according to Methods 2.2.1. and 1µg of total RNA for each condition was sent to the Genomics Core Unit of the Spanish National Cancer Research Centre (CNIO, Madrid) for RNA quality evaluation, amplification, labelling and hybridization to Agilent Rat Gene Expression G3 60K according to manufacturer´s protocols. Microarray background subtraction was carried out using normexp method. To normalize the dataset, we performed loess within arrays normalization and quantiles between arrays normalization. Differentially expressed genes (DEGs) were obtained by applying linear models with R limma package (Smyth GK) (Bioconductor project, http://www.bioconductor.org). To account for multiple hypotheses testing, the estimated significance level (p value) was adjusted using Benjamini & Hochberg False Discovery Rate (FDR) correction. Those genes with FDR<0.01 were selected as differentially expressed between the two conditions (Annex I). From the resulting list of 4,520 differentially expressed genes we validated by q-PCR the expression pattern of 12 genes, 10 upregulated and 2 downregulated in 3D *versus* 2D condition. For the experimental validation of the microarray data we used three new 2D and 3D RNA samples.

The 4,520 differentially expressed genes (DEGs) identified were subjected to bioinformatic analysis to reconstruct potential molecular pathways, performed by Dr. Gonzalo Gómez from the Bioinformatic Unit of CNIO. Gene set enrichment analysis (GSEA) (Subramanian et al., 2005) was applied using annotations from a curated version of Biocarta, KEGG, Reactome and NCI. Genes were ranked based on limma moderated t statistic. After Kolmogorov-Smirnoff testing, those gene sets showing FDR<0.05, were considered enriched between the classes under comparison. Comparative enrichment analysis with customized data sets upon bibliographic research related to epithelial polarity program, lumenogenesis, tubulogenesis and MDCK cyst formation processes was also performed. We also overlapped our microarray DEGs with the Pax8-dependent DEGs found in rat PCCl3 cells silenced for Pax8 transcription factor (Ruiz-Llorente et al., 2012) and we identified 71 common genes (FDR<0.01) that were upregulated in 3D follicles and downegulated in siPax8 condition (Annex V).

2.6. RNAi

2.6.1. shRNA, virus production and transduction

Stable RNAi was achieved by viral short hairpin RNA (shRNA) for Pax8, Cdh16, AP1M1 mRNAs and non-targeting (control) using respective lentiviral vectors described in Materials 1.4. Second generation lentiviruses were produced after transfection (Methods 2.7.2.) of 10^6 Hek293T cells in 100mm Petri dishes with 10µg of the corresponding lentiviral expression vector plus 5µg of each packaging vector (pMD2-VSVG and pCD-NL-BH). Sixteen hours after transfection cells were washed with DMEM complete medium and dishes were filled with 5ml of virus production medium (Ultraculture 12-725F,

supplemented with 1% glutamine, 100mM sodium piruvate, 1% sodium bicarbonate (7,5%) and 5mM sodium butyrate). Supernatant full of viral particles was recollected 48 hours post transfection and passed through a 45µm filter. Cells to be infected were seeded in 6-well plates ($2x10^5$/well) and 24 hours later were infected with 3ml of the corresponding lentiviral supernatant supplemented with 80µg/ml polybrene. Cells were incubated for 30 minutes and then were centrifuged at 1,100xg at 37˚C for 30 minutes. Finally, cells were twice washed with PBS and fresh medium was added. After 48 hours of shRNA expression FRT cells and primary thyrocytes infected with lentiviruses expressing shPax8, shCdh16 and shControl were selected with puromycin 1µg/m, whereas MDCKhNIS cells infected with lentiviruses expressing shAP1M1 and shControl were selected with 2.5µg/ml for 48 hours.

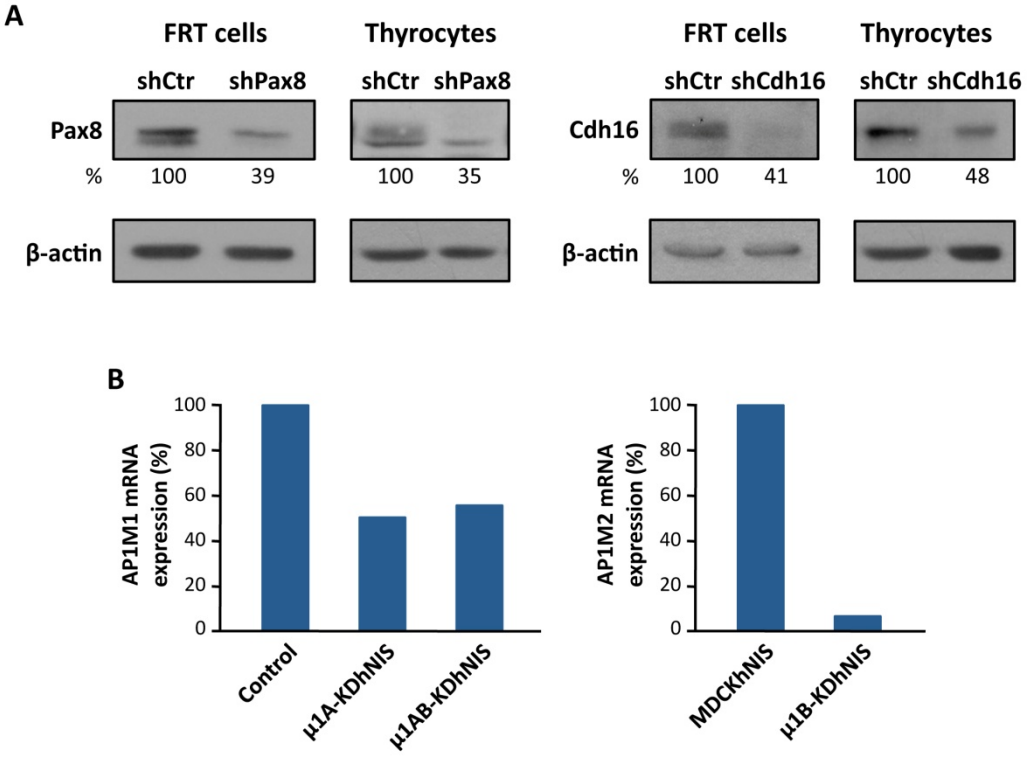

Figure 10. **Silencing by short hairpin RNAs.** (A) Protein expression levels of Pax8 and Cdh16 in FRT cells and mouse thyrocytes after infection with lentiviruses: shPax8, shCdh16 and shControl (shCtr). Cells were grown in 6H medium and total lysates were subjected to Western-blot analysis in order to evaluate Pax8 and Cdh16 silencing. Lysates were also immunoblotted for β-actin to ensure equal loading. (B) mRNA expression levels of AP1M1 in MDCKhNIS and µ1B-KDhNIS cells after infection with shAP1M1 and shControl lentiviruses. AP1M2 silencing in µ1B-KDhNIS cells compared to its expression in MDCKhNIS cells was also confirmed by q-PCR. mRNA expression is normalized to GAPDH expression and referred to control expression levels.

Resistant cells were assessed for Pax8 and Cdh16 knockdown efficiency by Western-blot compared to control cells (Fig. 10A), while AP1M1 knockdown was confirmed by q-PCR and normalizing to GAPDH expression (Fig. 10B). MDCKhNIS cells already interfered for AP1M2 that were infected with shAP1M1 and shControl lentiviruses, were selected by flow cytometry and AP1M1 expression was detected by q-

PCR normalized to GAPDH expression (Fig. 10B left graph). AP1M2 mRNA levels were evaluated in MDCKhNIS and µ1B-KDhNIS cells by q-PCR as shown in the right graph of figure 10B.

2.6.2. siRNA

FRT cells seeded in 60mm Petri dishes (600,000cells/dish) were transfected with 25nM of Pax8 siRNA (Rat Pax8 ON-TARGETplus SMARTpool) or with scrambled siRNA (ON-TARGETplus Non-targeting Pool) using DharmaFECT1 Transfection Reagent and following the manufacturer's protocol (Thermo Scientific). Cells were trypsinized 24 hours later and were seeded in 12mm-Transwells and in a 60mm Petri dish as described in Methods 2.1.3. At 96 hours after transfection polarized cells were prepared for immunofluorescence analysis of membrane proteins as described in Methods 2.3.4.2. Total protein was also extracted from the Petri dishes at both time points in order to evaluate the Pax8 silencing by Western blotting (Fig. 11).

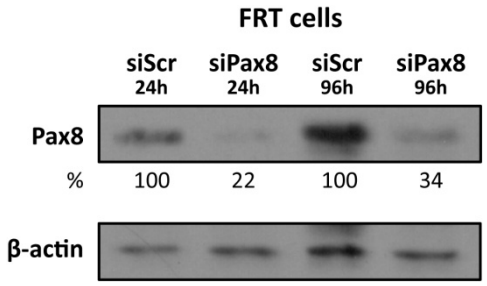

Figure 11. **Pax8 silencing by small interference RNA.** Pax8 protein levels from FRT cell lysates 24 and 96 hours after transfection with scramble and Pax8 siRNAs. Immunoblotting for β-actin was performed to ensure equal loading.

2.7. Transfections

2.7.1. Transient transfections

Hek293T cells were transfected with the lentiviral expression and packaging vectors for lentiviral production using calcium phosphate (Chen and Okayama, 1988). FRTshPax8 cells were transfected with pEGFP-N1-Cdh16 and pcEFL-Rac1QL-HA expression vectors using Lipofectamine 2000 (Invitrogen) according to the manufacturer's instructions. At 24 hours after transfections cells were trypsinized and seeded for 3D morphogenesis assays in Matrigel. MDCKhNIS and MDCKhNIS knockdown cells were transfected with pcDNA3-TfR-HA expression vector using Lipofectamine 2000 and 15 hours later cells were trypsinized and seeded on 24mm-Transwells for domain-selective membrane protein detection by biotinylation as described in Methods 2.3.2.

2.7.2. Stable transfections

µ1B-KD cell line (Gravotta et al., 2007) was stably transfected with pcDNA3.1humanNIS expression vector in order to generate the µ1B-KDhNIS cell line. Clones resistant to G418 were isolated and NIS expression levels were detected by Western-blot. Three positive clones with different NIS expression levels were further analysed in Transwell cultures through membrane immunofluorescence assay. The results presented in this Thesis are all from the same clone.

2.8. Radio-iodide transport assay

Polarized MDCKhNIS and µ1B-KDhNIS cells were assayed for iodide transport as described before with several modifications (De la Vieja et al., 2005). After cell polarization on 12mm-Transwells (Methods 2.1.3.) cells were incubated with 400µl PBS 1x containing 20µM KI and 10µCi/µl $^{125}I^-$ at the upper, lower or both sides of the insert at 37˚C and for different time points up to 360 minutes. Radio-iodide free side of the insert was incubated with 400 µl PBS 1x. Every condition was performed in duplicate and for each time point two aliquots of 10µl each were measured. Radioactivity was quantified in a ɣ-counter as counts per minute (cpm). The graphs shown in Results depict iodide uptake and accumulation at each insert side as the average of radio-iodide activity in two Transwells during incubation time (minutes).

RESULTS

1. Follicular cell polarity acquisition and follicle formation

1.1. FRT cells form three dimensional follicle-like structures in Matrigel.

In order to study epithelial folliculogenesis we made use of a three dimensional (3D) culture system consisting in FRT cells embedded in Matrigel. Several cell lines such as MDCK, Caco-2 and MCF-10A generate polarized cysts and acini respectively when embedded in Matrigel (O'Brien et al., 2001, Ivanov et al., 2008, Debnath et al., 2003). FRT cells, although have been extensively employed as polarized epithelial monolayers grown on two dimensional surfaces (Zurzolo et al., 1992, Lipardi et al., 2002, Imjeti et al., 2011), have not been previously used in a 3D Matrigel culture system. After numerous combinations of different amounts of bottom applied Matrigel and 6H medium-Matrigel supplemented overlay, we achieved the optimal conditions for the formation of spheroid follicle-like structures (called follicles from now on) after eight days of culture, consisting of a single layer of FRT cells surrounding a central hollow lumen (Fig. 12).

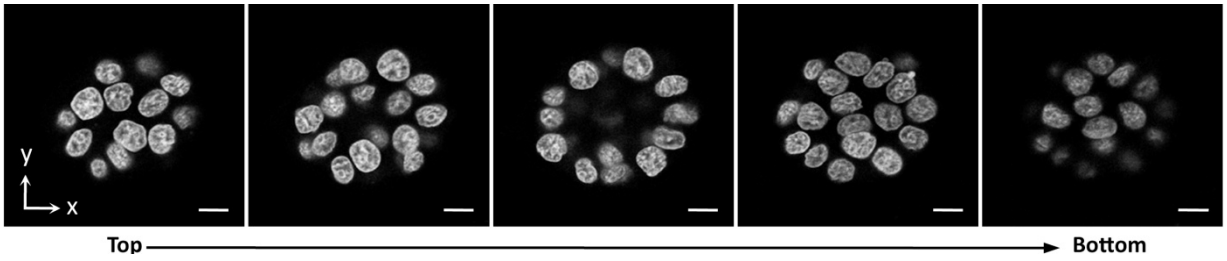

Figure 12. **Three dimensional FRT follicles.** From the top to the bottom confocal z-sections of a representative FRT follicle after eight days of growth in Matrigel. Nuclei are stained with DAPI (in grey) and images were taken with a 63x objective. Bars, 10µm.

Next, we observed step by step the process of folliculogenesis during seven days by time-lapse microscopy. As demonstrated in figure 13, individual FRT cells embedded in Matrigel present many small intracellular vacuoles revealed by differential interference contrast (DIC) microscopy at the first image taken (t0). Some of the vacuoles seem to fuse and generate bigger ones centrally localized. The first cell division takes place after approximately twenty hours. One large intracellular vacuole is visualized under the plasma membrane that separates the two adjacent cells and many smaller in the other cell the first day after seeding (Fig. 13, d1). As the spherical structure is being formed (d2, d3), cells proliferate, small vacuoles keep coalesce and the bigger generated move towards the apical side of the cells probably consisting in vacuolar apical compartments (VACs) that store and transport only apical membrane components (Vega-Salas et al., 1987). Fusion of the VACs with the plasma membrane gives rise to an initial open lumen between the apposing cells which is visible at the fourth day of culture (d4, black arrow), that develops to a bigger central lumen by the seventh day (d7, black arrow). Spheroid structures gradually grow larger through further proliferation of component cells (d5 and d6).

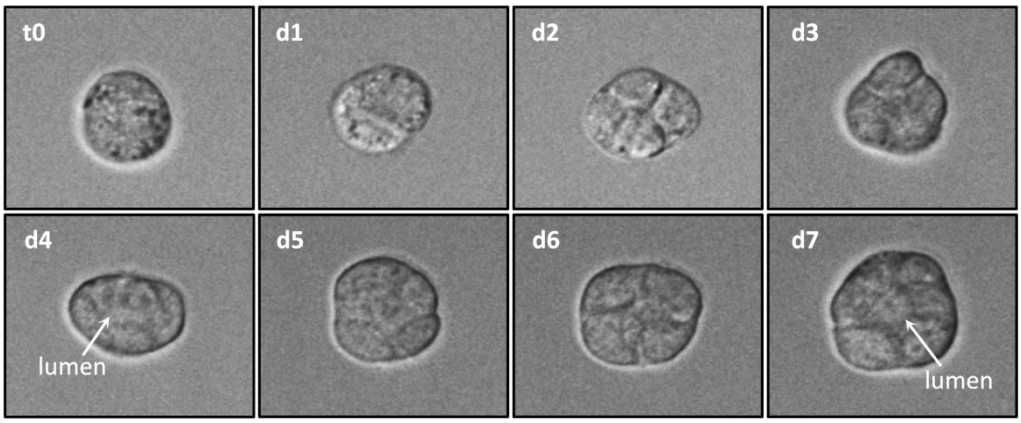

Figure 13. **Three-dimensional morphogenesis of FRT follicles.** Representative live-cell microscopy DIC images of follicle formation from a single FRT cell embedded in Matrigel from the beginning of the assay (t0) and for seven days of culture (d1-7). White arrows indicate the lumen in the growing follicles (d4 and d7). Images were taken with a 20x objective.

1.2. Mouse primary thyrocytes are able to reorganize into follicles in Matrigel.

Primary thyrocytes have been widely used in 2D and 3D culture systems regarding studies of thyroid biology, regeneration and disease (Toda et al., 2011). Among them, the 3D collagen gels have been the most employed for thyroid folliculogenesis studies as thyrocytes reconstruct follicle structures with physiological polarity when embedded in type I collagen gels (Toda and Sugihara, 1990, Toda et al., 1992). We performed a 3D morphogenetic assay using individual mouse thyrocytes embedded in Matrigel that has been rarely used for follicle reorganization from isolated thyrocytes (Frohlich et al., 1995, Bravo et al., 2013). We followed thyrocytes growth by live-cell imaging during seven days and as it is shown in figure 14, a small round follicle with a central lumen was formed (d7) from one single thyrocyte (t0). During this process, first, the individual thyrocyte develops many intracellular vacuoles that accumulate and some of them coalesce through time. Characteristic foot processes (d1, marked with black stars) appear to come out of the cell into the Matrigel and afterwards the first cell division takes place. Intracytoplasmic vacuoles localize under both sides of the plasma membrane that links the two cells, probably consisting in VACs that seem bigger that in the FRT cells. The same process is repeated with the reappearance of foot processes and many small vacuoles (d2), followed by cell division and vacuoles coalescence (d3). The fusion of the VACs with the plasma membrane results in the coalescence of the cavities between the adjacent cells and eventually the formation a primitive extracellular follicular lumen that can be appreciated in the center of the follicle at the fourth day (d4). As the follicle grows the lumen gradually expands (d5, d6) giving rise to a bigger spherical structure with a larger central lumen at the seventh day (d7).

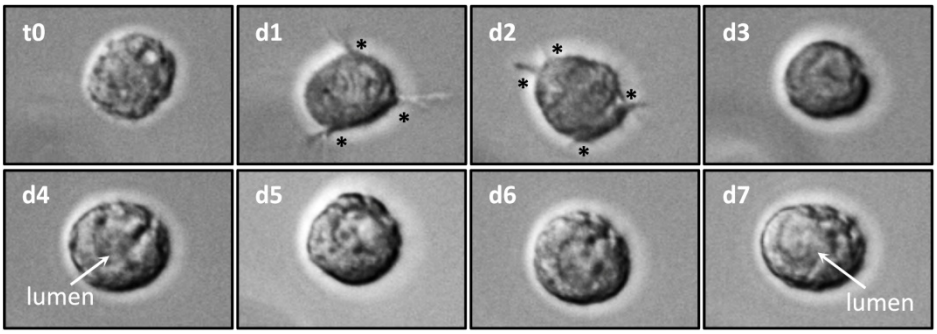

Figure 14. **Three-dimensional follicle reorganization of primary thyrocytes.** Representative live-cell microscopy DIC images of a single cell origin follicle embedded in Matrigel from the day of seed (t0) until the last day of folliculogenesis (d7). Black stars indicate the foot processes in the under-division thyrocytes and white arrows the lumens in the growing follicles. Images were taken with a 20x objective.

Up to now, two modes of thyroid folliculogenesis have been described in primary thyrocytes grown in 3D collagen gel cultures: the single and the plural cell origin (Toda et al., 1993). Matrigel is a softer kind of gel compared to the widely used collagen gels, thus it allows looser cell mobility and enhances cell-cell communication mediated by autocrine or paracrine growth factors and cytokines. As a result, it was common to see in FRT and thyrocyte 3D cultures, two or more cells (Fig. 15A and 15a respectively) to migrate immediately after being embedded in Matrigel, then contact (A, a), aggregate (B, b) and link after hours (C, c).

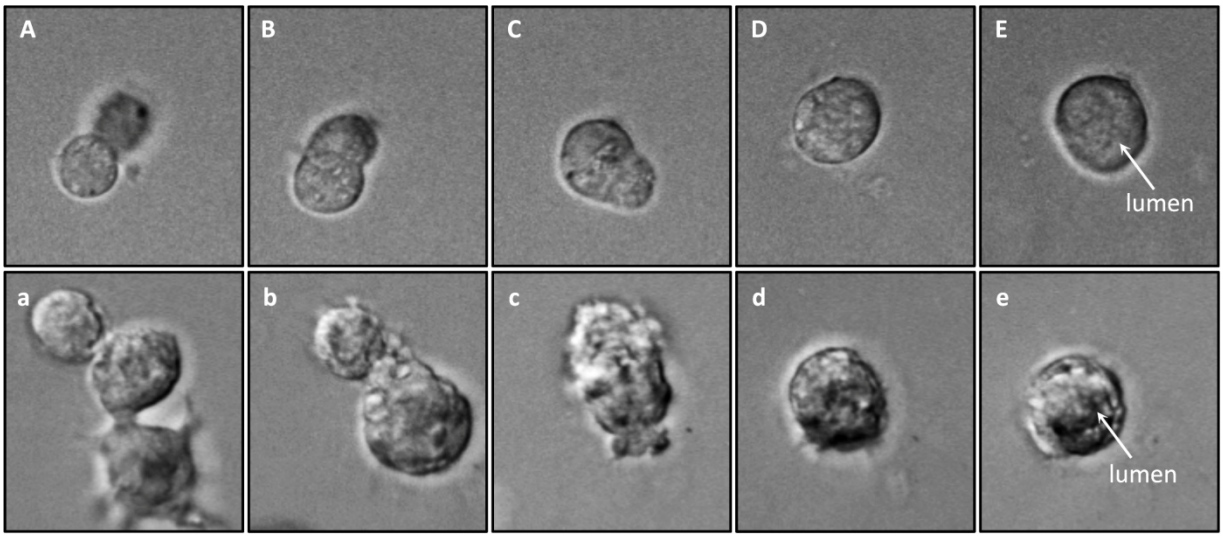

Figure 15. **Plural cell origin folliculogenesis.** Representative DIC images from live-cell microscopy of FRT (upper panel) and primary thyrocytes (lower panel) origin follicles grown in Matrigel for six days. Thyrocytes migrate, contact (A, a), aggregate (B, b) and link (C, c). At day 4, the spherical structures undergo morphogenetic changes (D, d) in order to acquire the follicle structure characterized by a central open lumen (white arrow) visible at day 6 (E,e). Images were taken with a 20x objective.

Finally some of them reorganized into follicle structures like those originated from one single cell (E, e). Images D and d correspond to structures at the fourth day of 3D growth and we observe that the initial

lumen is formed correctly and without delay. Six-days growing follicles (E, e) showed a centrally localized open lumen (Fig. 15).

1.3. FRT cells and primary thyrocytes acquire cell polarity from the first cell division and form fully polarized follicles with a central lumen in Matrigel cultures.

Once the 3D culture system was established we aimed to study the cellular and structural polarity acquisition process in thyroid follicles. For this purpose, we performed 3D morphogenesis assays followed by immunofluorescence confocal microscopy analysis of the expression and localization of polarity markers in growing follicles from FRT cells and primary thyrocytes (Fig. 16). We observed that both FRT and thyrocyte derived follicles present apical and basolateral domains specified at the second day of growth in Matrigel after the first cell division has taken place (Fig. 16, day 2). The membrane interface between the cells is demarcated into a lateral surface where adherens junctions are localized and here visualized by β-catenin (day 2A, B, D and E in red) that is interrupted by an apical domain defined by ezrin (day 2A and D in green), a plasma membrane-actin cytoskeleton linker that is apically targeted in polarized epithelial cells (Fievet et al., 2004). Tight junctions (TJ) separate the two membrane domains and are localized upper-laterally just above the adherens junctions as the TJ protein ZO-1 reveals in FRT and thyrocyte derived two-cell follicles (day 2B and E in green). We also examined intracellular polarity at this early stage using the Golgi apparatus as a reference and we observed that it was apically positioned and close to the tight junctions probably in order to facilitate the delivery of apical proteins to the nascent apical surface (day 2B, GM130 in magenta). After five days of growth in Matrigel, the spherical follicles had distinct adherens junctions visualized by β-catenin staining at the basolateral domains (Fig. 16, day 5A, B, D and E) and tight junctions visualized by ZO-1 staining localized at the upper-lateral domains (day 5B and E). Ezrin was found delineating the open and centrally localized follicular lumen (day 5A and D). Polarized actin cytoskeleton was also observed through filamentous actin (F-actin) localization using fluorescent phalloidin (Fig. 16C and E in magenta). Interestingly, F-actin colocalized with ezrin at the apical domains before and after lumen formation (Fig. 16C) demonstrating ezrin´s ability to link the F-actin cytoskeleton to the apical surface of the thyroid follicles. In addition, thyroid differentiated state was confirmed through the expression of the thyroid differentiation markers NIS and Tg that localized at the basolateral membrane and inside the follicular lumen correspondingly, as demonstrated in the right and left panel of the figure 5F, respectively. The above observations suggest that during thyroid folliculogenesis, epithelial cells acquire membrane and intracellular polarity at the first cell division and mature follicles are developed through coordinated cell division and further polarization of the membranes, junctional complexes, cytoskeleton and organelles in parallel with lumen formation (Fig. 16, day 5).

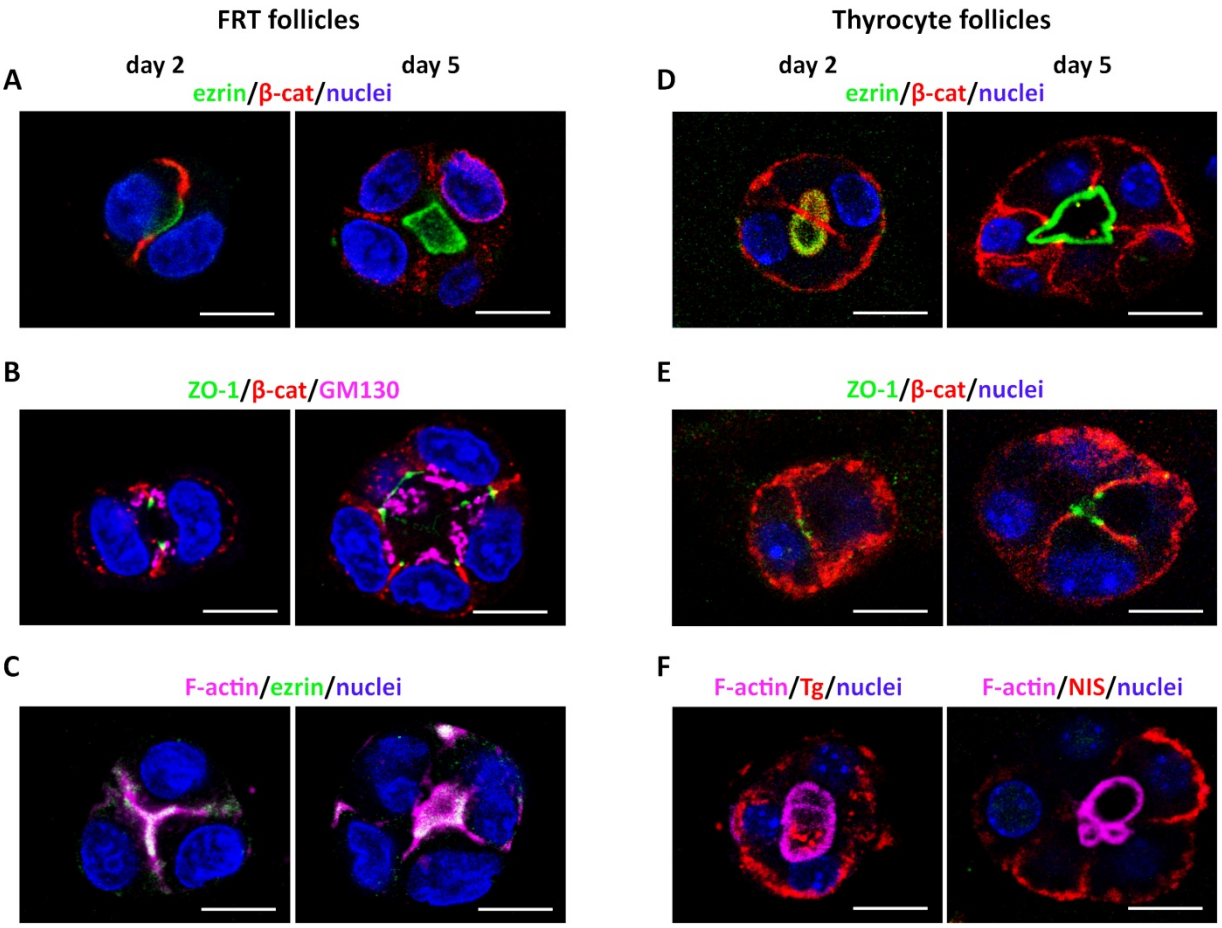

Figure 16. **FRT and thyrocyte derived follicles are fully polarized from the first cell division.** FRT and thyrocyte single cells were grown for 2 and 5 days in 3D Matrigel culture and follicles were then fixed and stained. Representative single confocal sections through the middle of FRT follicles stained for (A) ezrin (green), β-catenin (red) (B) ZO-1 (green), β-catenin (red) and GM130 (magenta) and (C) F-actin (magenta), ezrin (green). Thyrocyte follicles were stained for (D) ezrin (green), β-catenin (red) (E) ZO-1 (green), β-catenin (red) and (F, day 2) F-actin (magenta), thyroglobulin (red), (F, day 5) F-actin (magenta) and NIS (red). Nuclei are all stained with DAPI (blue). The tight junction associated protein ZO-1 localized at the upper-lateral domains, the adherens junction β-catenin was found mostly lateral and the plasma membrane-cytoskeleton linker ezrin was apical. Filamentous actin was stained with phalloidin (magenta) and colocalized with ezrin at the apical domains of the FRT follicles. Basolateral NIS (red) (F, right panel) and lumen concentrated Tg (red) (F, left panel) confirmed the differentiated phenotype of the thyrocyte follicles. All images are taken with a 63x objective, scale bar 10µm.

1.4. *De novo* lumen morphogenesis requires apical vesicular transport and fusion with the plasma membrane in FRT and thyrocyte follicles.

Soon after newly polarizing thyroid cells embedded in Matrigel recognize the extracellular matrix (ECM) and their neighbours, luminal space can be generated. Due to the importance of lumen morphogenesis for the proper thyroid structure and function we studied this process in FRT and thyrocyte 3D cultures using fluorescence confocal microscopy. Once the first cell division takes place, intracellular vesicles positively stained for ezrin are subapically localized (Fig. 17A, day 1, left panel). Vesicles are transported at the contact site and are targeted to a common point in the plasma membrane between apposing cells. Vesicle fusion with the membrane converts this part of the cell-cell contact, previously positive for

the adherens junction protein β-catenin, to an apical plasma membrane surface positive for ezrin (Fig. 17A, day 1, right panel). These observations make us consider this specific site as the equivalent to the apical membrane initiation site termed AMIS in MDCK cysts (Bryant et al., 2010). Through further delivery and docking of vesicles containing apical membrane components with the plasma membrane, the initial site is extended and apical domains between cells are created (day 2), although the nascent lumen in the centre of the structure is not expanded yet (day 3). Finally, opening of the luminal space makes visible a central lumen delineated by ezrin as shown by day 5 (Fig. 17A). F-actin is recruited in the apical domains from the beginning of cell polarization and lumen initiation (see Fig. 16C, day 2), and could generate force for lumen expansion and maintenance. These observations suggest that apical exocytosis and polarity machinery operate in cooperation to establish and expand an apical domain during lumen initiation in FRT cultures.

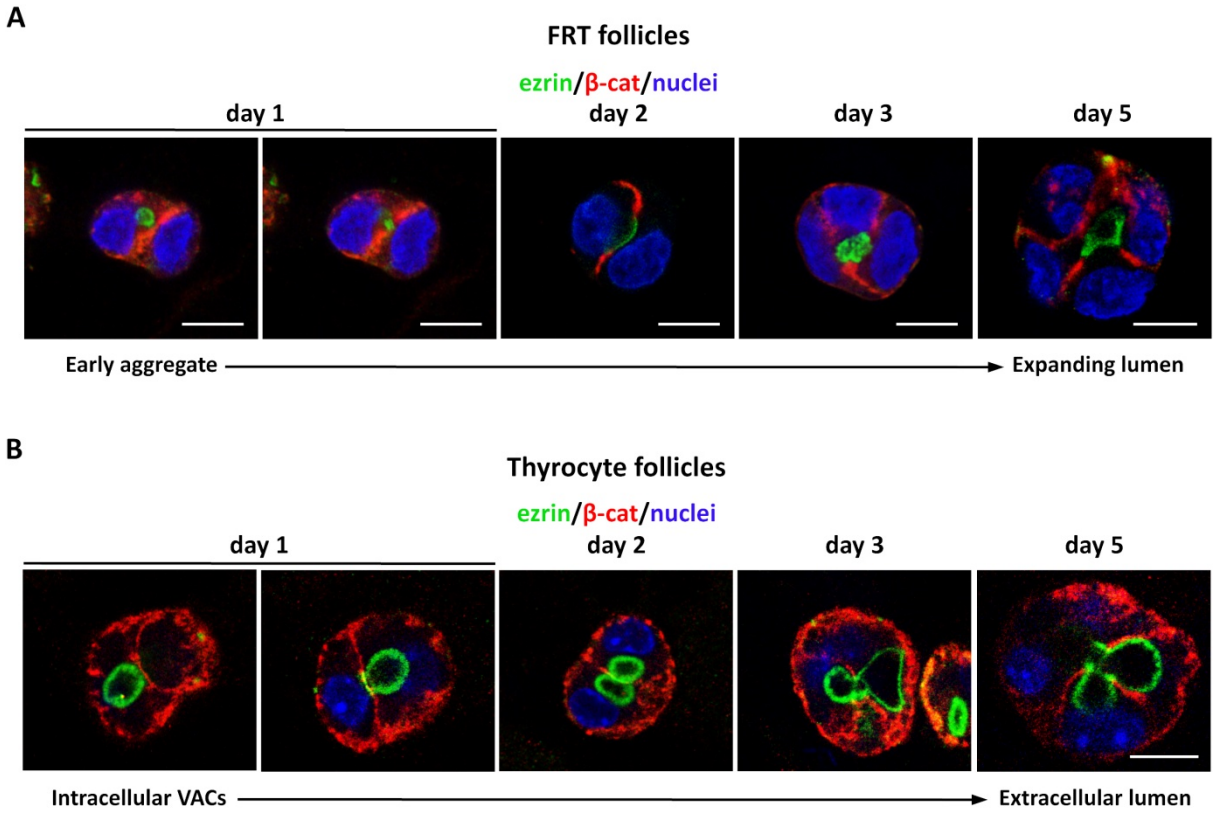

Figure 17. ***De novo* lumen morphogenesis requires vesicle and vacuolar apical trafficking in FRT and thyrocyte follicles.** (A, B) Lumen initiation site (day 1, 2), nascent lumen (day 3) and expanding lumens (day 5) were observed in FRT cells and primary thyrocytes in 3D Matrigel cultures. Growing structures were fixed and stained for nuclei (blue), β-catenin (red) and ezrin (green). Representative single confocal sections through the middle of the structures are shown using an objective of 63x. Scale bar is 10µm.

In a similar way, follicular lumen initiation in thyrocytes requires apical delivery and fusion of big intracellular vacuoles with the plasma membrane between cells, as shown in figure 17B. Subsequent to

the first cell division, intracellular vacuoles or VACs positive for ezrin accumulate apically (Fig. 16B, day 1 left panel). VACs fusion with the plasma membrane, where the junctional complex between the adjacent cells is initially localized (here visualized by β-catenin), is followed by its local loss and the formation of the apical domain as shown by the ezrin staining in the plasma membrane (day 1 right panel). As a result, the cavities between neighboring adherent cells can then coalesce (day 2) facilitating the formation of extracellular space in the center of the structure (day 3). As follicle grows, intracellular vacuoles from new polarizing cells move apically and coalesce with the extracellular central lumen (day 5). F-actin localization first at the subapical VACs, then at the cell-cell contact and finally at the apical domains that face the hollow lumen (see Fig. 16F), indicate that the polarized actin cytoskeleton could mediate VACs transport and fusion with the plasma membrane in order to form the apical domains (Malacombe et al., 2006). Additionally, thyroglobulin was found to be transported by the VACs and later released and accumulated inside the central lumen as shown in the left panel of figure 16F.

Altogether, these observations demonstrate that the vectorial transport of apical membrane and lumen components at a coordinated point between two closely apposed cells is common between FRT and thyrocyte follicles and it consists in the first step in order to create a luminal space *de novo*. This mechanism of lumen morphogenesis where cells contacting the ECM initially adhere without luminal space and then vesicles containing luminal components are exocytosed in a coordinated way to a central luminal region generating apical-basal polarization is named hollowing in MDCK cysts (Martin-Belmonte et al., 2008).

1.5. Differential gene expression in three dimensional *versus* two dimensional culture system reveals common regulators of 3D epithelial polarization.

In order to identify regulators of 3D epithelial thyroid polarization and follicle formation we conducted a microarray-based differential expression analysis comparing the transcriptome of FRT cells undergoing apical-basolateral polarization either in the traditional monolayer culture (2D) or as 3D follicles grown in Matrigel. Notable transcriptional differences were observed during 3D morphogenesis as a total of 4,520 differentially expressed genes were identified in 3D *versus* (*vs.*) 2D condition with false discovery rate (FDR) lower than 0.01 (Annex I). We technically validated the expression data by q-PCR analysis of 10 upregulated and 2 downregulated genes in 3D follicles (see Results 1.5.1., Fig. 19).

With the aim to characterize cellular processes significantly enriched (FDR<0.05) in both experimental conditions, we performed gene set enrichment analysis applying four different data bases and using our 2,265 upregulated (positive) and 2,255 downregulated (negative) genes in 3D *vs.* 2D condition. To prioritize functional analysis we focused on the upregulated genes in 3D condition and we found no gene sets to fulfil the FDR restriction. Gene sets implicated in epithelial polarization but with FDR slightly

higher than 0.05, such as the Notch signaling pathway (Human_NCI, FDR=0.056) and the polarity lipids pathways: glycerolipid metabolism (KEGG, FDR=0.0967) and phosphatidylinositol signaling system (KEGG, FDR=0.099) were identified. Positively regulated genes in 3D were also found to participate in other pathways such as membrane trafficking (Reactome), regulation of actin cytoskeleton (KEGG) and integrin-cell surface interaction (Human_NCI), although they were not significantly enriched.

In order to identify differentially expressed genes involved in 3D polarization and follicle formation process and taking into account that cellular functions are not fully defined in the available data bases, we created a gene set of three dimensional epithelial polarity and lumen morphogenesis components based on bibliographic research (Datta et al., 2011, Rodriguez-Fraticelli et al., 2011, Rodriguez-Boulan and Macara, 2014). Gene set enrichment analysis using an initial set of 81 genes resulted in 51 common genes (Annex II) whose enrichment plot is shown in figure 18A (FDR=0.059), demonstrating that genes positive in 3D follicles are involved in 3D epithelial morphogenesis. Among them there was a subset of 11 genes (Annex III) that was significantly enriched (FDR=0.008) in epithelial tubulogenesis (Rodriguez-Fraticelli et al., 2011)(Fig. 18B).

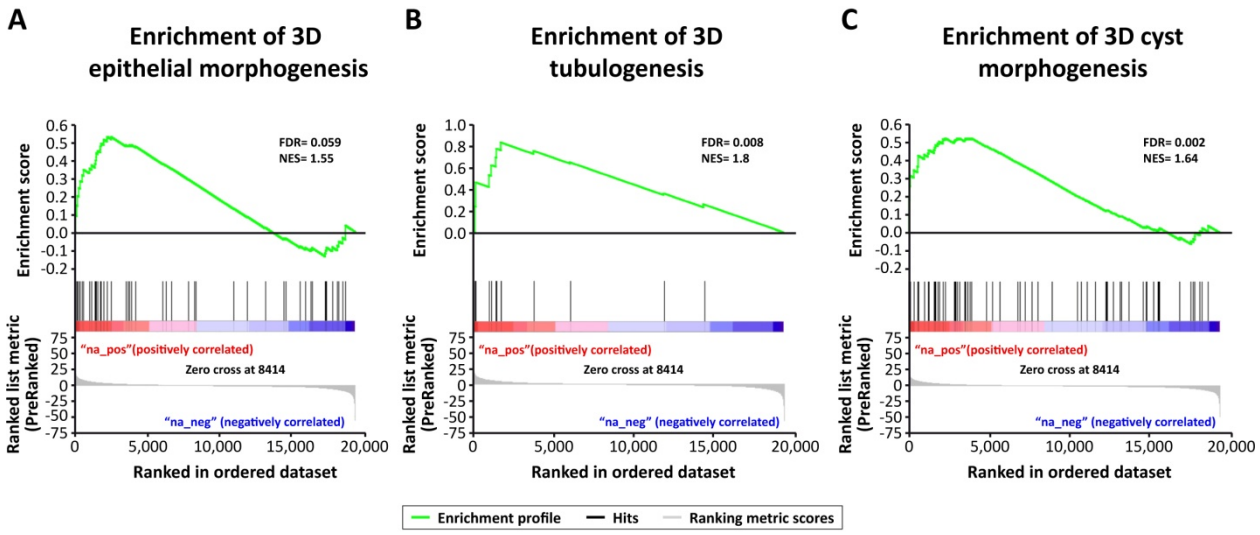

Figure 18. **Common regulators of epithelial 3D polarization.** Gene Set Enrichment Analysis (GSEA) statistics plots of our 3D *vs.* 2D gene expression profile compared to different gene sets. (A) Gene set enrichment plot of 3D epithelial morphogenesis components upon bibliographic research. (B) Gene set enrichment plot of molecular regulators of tubulogenesis reported by Rodríguez-Fraticelli *et al.* (C) Gene set enrichment plot of the 3D MDCK cyst morphogenesis set defined by M. Galvez-Santisteban *et al.* FDR, false discovery rate q-value; NES, normalized enrichment score.

Finally, we compared our array data with a set of upregulated genes from MDCK cells grown in 3D *vs.* 2D conditions (Galvez-Santisteban et al., 2012). Interestingly, we found 66 genes significantly enriched in 3D cyst morphogenesis (FDR=0.002, Fig. 18C, Annex IV).

Altogether, these results demonstrate that the regulators of three dimensional epithelial polarization are common and well conserved among epithelial cells of different organ origin.

1.5.1. Pax8 transcription factor and its target genes are upregulated in 3D *versus* 2D conditions.

Concerning thyroid specific genes, we observed that *Pax8* transcription factor, oxidase *Duox2* and the Duox maturation factor *Duoxa1* were positively regulated in 3D FRT follicles. Pax8 is the only thyroid specific transcription factor expressed in this cell line and its expression is critical for thyroid gland development during embryogenesis and for thyroid differentiation in adults. In our laboratory were recently identified new Pax8 target genes through ChIP-Seq and microarray analysis in rat PCCl3 follicular cells (Ruiz-Llorente et al., 2012). In order to discover Pax8-regulated genes important in FRT follicle formation, we crossed our 3D upregulated genes (Annex I) with Pax8 negatively regulated genes in PCCl3 cells silenced for Pax8 (siPax8) and we found 71 common genes with FDR<0.01 (Annex V). Amongst them, there were genes codifying for proteins consisting in cellular components or members of biological processes such as cell-extracellular matrix interactions, tight and adherens junctions, cell cytoskeleton, vesicular traffic and endocytosis, glycerolipid biosynthesis, ion channels regulation, gene transcription and thyroid development shown in Table 7.

Cellular components/ Biol. Processes	Genes
Cell-ECM	**Tgm2**, **Nid2**, RT1-Db1, Gne, Cask, Rasd1
Tight junctions	**Ocln**
Adherens junctions	**Cdh16**
Cell cytoskeleton	Rhpn2, **Dynlrb2**, **Map7**, Sh3kbp1, Sptbn2
Vesicular traffic	**Rab17**, Mlph, **Myo5b**, Syt5, Spg20, Grtp1
Endocytosis	Sh3kbp1, Folr1, Synj2
Glycerolipid biosynthesis	Pemt
Ion channels	Atp11b, Hspa14, Kcnk1, Atp10d, Nedd4l
Gene transcription	Rbm4b, Calr, Parp1, Klf5, Per2, Brwd3, Hmgn3
Thyroid development	Fgfr2, **Wnt4**

Table 7. Common 3D upregulated genes and Pax8 positively regulated genes from 3D *vs.* 2D and control *vs.* siPax8 expression arrays classified according to their participation in biological processes. FDR cutoff is 0.01. In bold are the upregulated genes in 3D FRT follicles validated by q-PCR as shown in the following figure 19.

We next validated the mRNA enrichment of some common genes (Table 7 in bold) in 3D follicles through q-PCR shown in figure 19. We chose four genes essential for the epithelial polarized phenotype: the adherens junction protein cadherin-16 (Cdh16), the apical recycling and transcytosis protein Rab17, myosin Vb (Myo5b) which participates in apical exocytosis and Wnt4 that is necessary for epithelial integrity. Interestingly, all these genes are direct Pax8 transcriptional targets and significantly

upregulated in 3D follicles. We also validated two genes codifying for proteins participating in ECM-cell interactions, the highly upregulated transglutaminase 2 (Tgm2) that mediates integrin activation at the cell surface and the basement membrane protein nidogen 2 (Nid2). Moreover, genes for the tight junction protein ocludin (Ocln), the tubulin associated protein dynein light chain roadblock-type 2 (Dynlrb2) that binds dynein to cargo and adaptor proteins, and the microtubule-associated protein 7 (Map7) were also confirmed to be enriched. We finally validated two negatively regulated in 3D condition genes: fibronectin 1 (Fn1) that was negatively regulated by Pax8, and Wnt7a whose expression is not described to be affected by Pax8. In total, Pax8 upregulation in 3D follicles together with the enrichment of its direct and indirect targets involved in epithelial polarized phenotype suggest the presence of diverse Pax8-dependent paths that could regulate 3D morphogenesis. Taking in account the importance of Pax8 in proper thyroid gland development and function, we considered that the role of Pax8 in thyroid follicle formation needed to be studied.

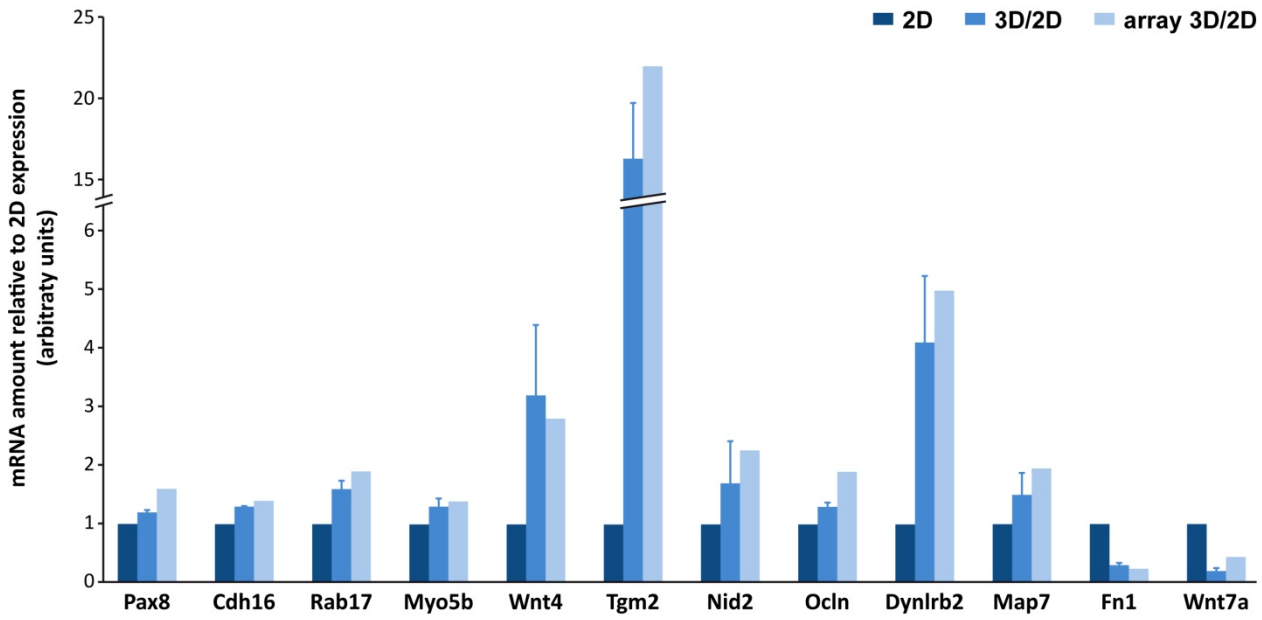

Figure 19. **q-PCR validation of selected genes.** Relative mRNA expression of ten upregulated and two downregulated genes in 3D follicles. FRT cells were grown in 2D and 3D conditions and lysates were collected after 5 days of culture. After mRNA extraction and cDNA polymerization, samples were analyzed by q-PCR and quantitative data was referred to 2D genes expression levels after normalization with Polr2g expression. Values are mean±SD from two or three replicates.

1.6. Pax8 silencing specifically disrupts apical membrane polarity orientation, lumen formation and polarized cytoskeleton distribution in a 3D environment.

In order to study the involvement of Pax8 in 3D follicular cell polarity acquisition and follicle formation, we stably silenced Pax8 expression using lentiviruses expressing shPax8. Next, we performed 3D

morphogenesis assays followed by immunofluorescence confocal analysis of apical-basolateral polarization during follicle formation. Lumen formation was evaluated at the end of folliculogenesis after 5 days of growth in Matrigel. Polarization and follicle formation process was observed in 2-day and 5-day follicles by the apical localization of ezrin, the upper-lateral staining of the tight-junction protein ZO-1 and the basolateral labelling of the adherens junction marker β-catenin (Fig. 20A, upper panels).

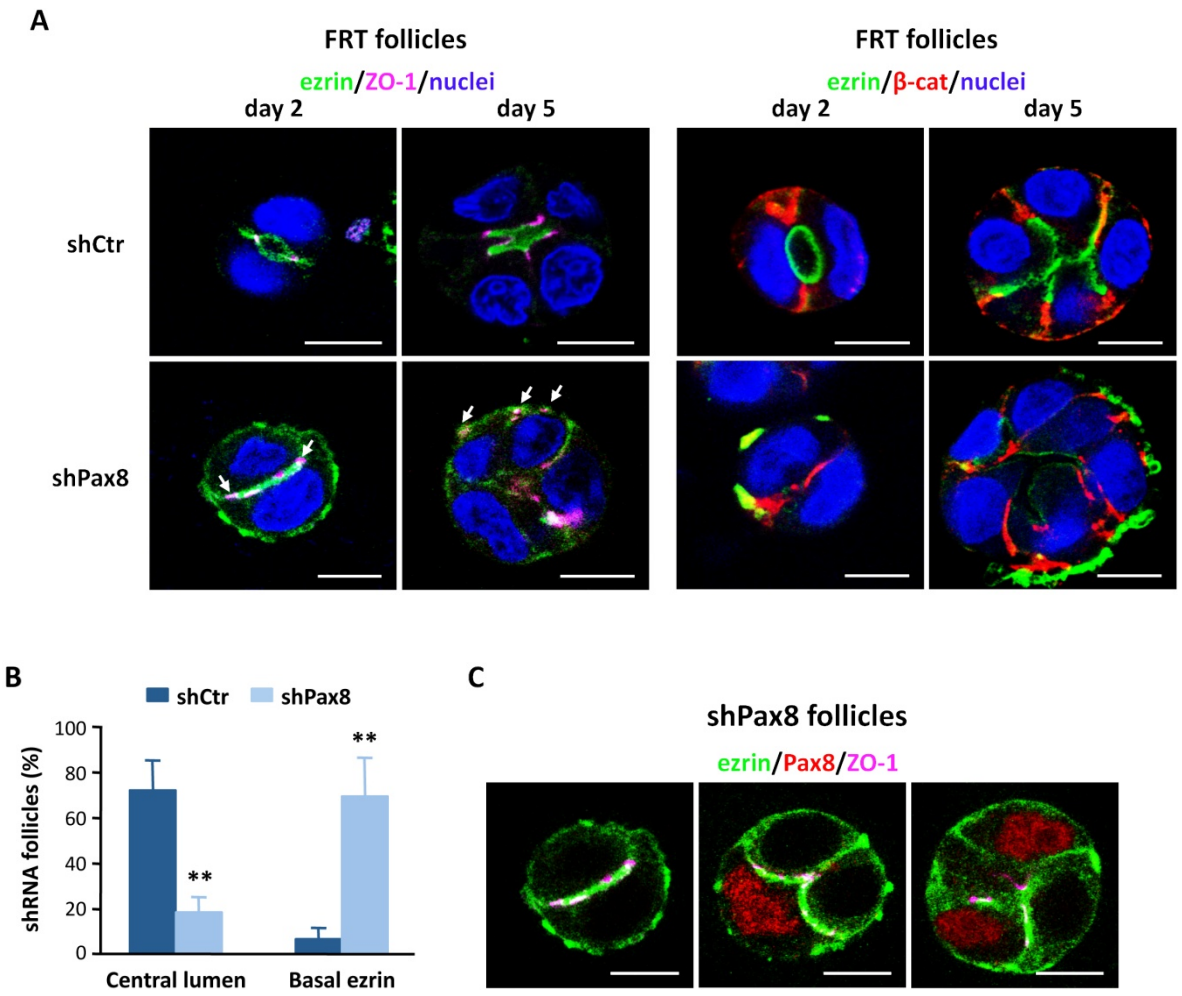

Figure 20. **Pax8 silencing disrupts apical membrane polarity in FRT follicles.** (A) Infected shControl (shCtr) and shPax8 FRT cells were grown for 2 and 5 days in 3D Matrigel culture. Representative single confocal sections through the middle of FRT follicles stained for apical and basolateral polarity markers: ezrin (green), ZO-1 (magenta, white triangles indicate basal ZO-1 localization) and β-catenin (red). (B) Quantitation of lumen formation and ezrin localization. Graph denotes the percentage of shCtl or shPax8 FRT follicles forming a central lumen and presenting ezrin delocalization at the basal membrane at 5 days of growth. Values are mean±SD from three replicates, n≥30 follicles per replicate. **P<0.001. (C) Representative single confocal sections of growing shPax8 FRT follicles stained for ezrin (green), Pax8 (red) and ZO-1 (magenta). All nuclei were stained with DAPI (blue). Scale bar, 10µm.

After 5 days of 3D growth, 92.6% of control follicles (shCtr) established the apical pole in the follicle interior and 72.4% developed central lumens (Fig. 20B). On the contrary, shPax8 follicles showed an extremely significant decrease in lumen formation as only 19.2% of shPax8 follicles presented a single

lumen in the centre of the structures (Fig. 20B). Instead, we observed a significant delocalization of the apical pole at the follicle periphery in a 69.4% of shPax8 follicles (Fig. 20B) as verified by the basal localization of ezrin (Fig. 20A lower panels) and the lower-lateral ZO-1 (Fig. 20A, left set of panels, white arrows). The majority of the shPax8 follicles exhibited a partial apical inversion as either not all the cells exhibited apical markers at the periphery or the whole structure presented apical marker distribution at both domains, although weaker in the center of the follicle. We attribute these phenotypic differences to the progressive loss of shRNA expression in the growing follicles as demonstrated in figure 20C. Concerning basolateral polarity in Pax8 depleted follicles, β-catenin always localized at the cell-cell contact in 2-cell follicles and the lateral surfaces in both control and shPax8 5-day follicles follicles, indicating that follicles maintain the ability to restrict basolateral domains in the absence of Pax8 (Fig. 20A, right set of panels). These results demonstrate that depletion of Pax8 impairs membrane polarity orientation and lumen formation leading to disrupted follicular organization.

Next we examined the distribution of the actin cytoskeleton in shPax8 follices and we observed that actin filaments were completely or partially delocalized at the periphery of the follicles and that fully colocalized with ezrin (Fig. 21A). Ezrin activation through phosphorylation is necessary for its association with the cortical actin cytoskeleton (Fievet et al., 2004). Therefore, we examined the localization of active ezrin in shCtr and shPax8 follicles using an anti-phospho-ERM antibody that recognizes phosphorylated ezrin at threonin 567. As shown in figure 21B, ERM proteins were phosphorylated at the apical membrane of control cells and had the same localization as ezrin (see Fig. 20A), whereas in shPax8 follicles immunoreactive signals of phospho-ERM were observed at the basal membrane or at both the apical and the basolateral membrane. These observations suggested that the basally localized ezrin is active and could interact with the actin cytoskeleton in shPax8 follicles. Concerning microtubules polarized distribution we studied the localization of the acetylated tubulin in control and Pax8 depleted follicles and we observed that it was restricted to the subapical domains in shCtr follicles (Fig. 21C, upper panels), while showed a basal cytoplasmic distribution in shPax8 follicles (Fig. 21C, lower panels). Altogether these results demonstrate that in the absence of Pax8, the polarized distribution of both actin filaments and acetylated microtubules is inverted and thus, the follicles that are formed show defects in the polarized organization of cell cytoskeleton.

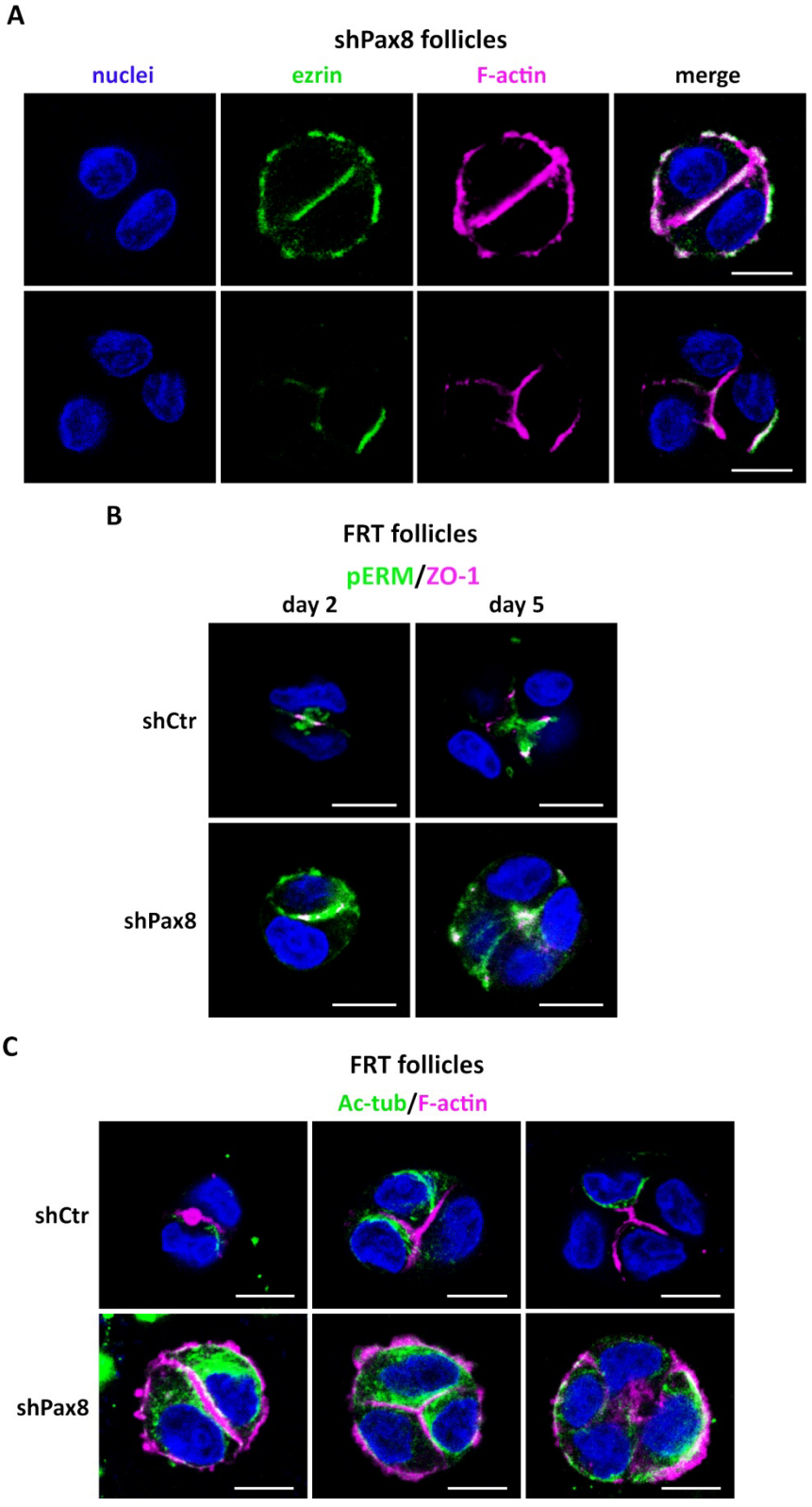

Figure 21. **Polarized organization of actin and microtubule cytoskeleton is disturbed by the lack of Pax8 in FRT follicles.** (A) Filamentous actin is delocalized at the basal membrane of Pax8 depleted FRT follicles where colocalizes with ezrin. Representative single confocal sections of shPax8 FRT follicles of different size stained for ezrin (green), F-actin (magenta) and β-catenin (red). (B) Activated ERM proteins localize basally in the absence of Pax8. Representative single confocal sections of shCtr and shPax8 follicles at 2 and 5 days of growth stained with phospho-ERM antibody (green) and ZO-1 (magenta) in order to detect the phosphorylated ezrin at threonin 567. (C) Subapical distribution of acetylated tubulin in control follicles becomes basal in Pax8 silenced follicles. Representative single confocal sections of shCtr and shPax8 FRT follicles of different sizes stained for acetylated tubulin (Ac-tub; green) and F-actin (magenta). All nuclei were stained with DAPI (blue). Scale bar 10µm.

Pax8 silencing in primary thyrocytes also led to inversion of apical membrane polarity (Fig. 22). Confocal sections of two-cell follicles demonstrated that in the absence of Pax8 the apical domain is not established between the adjacent cells as all the shPax8 thyrocyte follicles presented both ezrin and actin filaments delocalized at the periphery of the follicles (Fig. 22A). In some cases, actin filaments were also present in the plasma membrane between the two cells (Fig. 22B). Vacuoles carrying apical membrane components were basally orientated instead of apically and this may explain the apical protein accumulation in the basal membrane which is in contact with the ECM as shown in the upper panel in figure 22A. Staining with pERM antibody revealed that basal ezrin is phosphorylated and localized in characteristic surface blebs that protrude towards the ECM. Active ezrin could interact with F-actin at the base of these structures, as actin filaments were restricted in the basal membrane (Fig. 22B lower panel). As a consequence, lumen initiation site was not defined and no open lumen was formed in shPax8 thyrocyte follicles after 5 days of growth (Fig. 22B, day 5). On the other hand, both adherens and tight junctions were established in Pax8 depleted thyrocyte follicles (Fig. 22A). β-catenin appeared all over the plasma membrane as in control conditions; while ZO-1 showed basal localization supporting apical inversion. Finally, neither NIS (Fig. 22A, lower panel) nor Tg expression (Fig. 22B, upper panel) was observed in shPax8 thyrocyte follicles further confirming the lack of Pax8 expression.

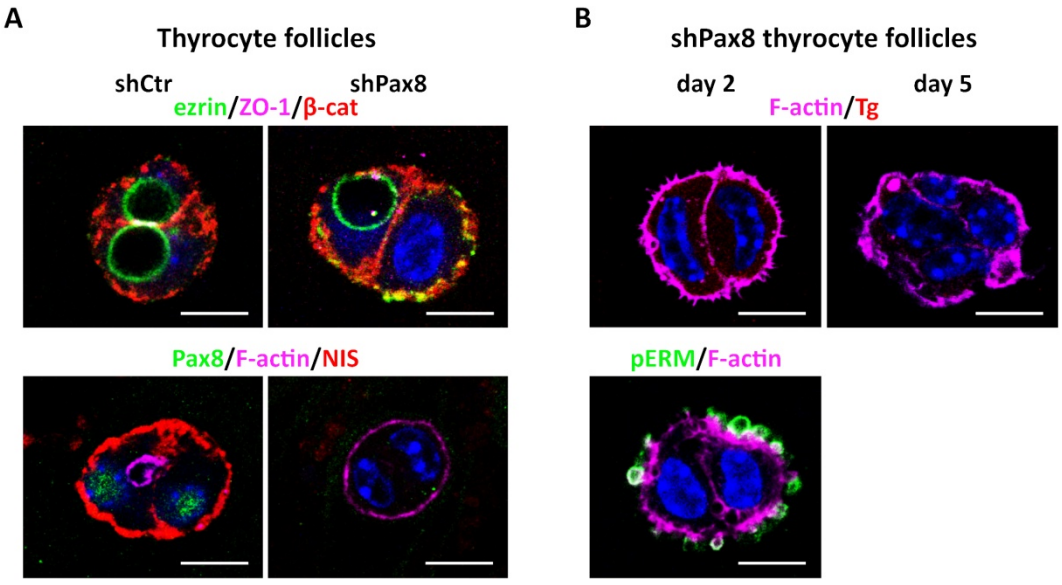

Figure 22. **Pax8 silencing disrupts apical polarity and inhibits lumen formation in thyrocyte follicles.** (A) Infected shCtr and shPax8 thyrocytes were grown for 2 days in 3D Matrigel culture and follicles were then fixed and stained. Representative single confocal sections through the middle of thyrocyte follicles stained for ezrin (green), ZO-1 (magenta) and β-catenin (red) (upper panels), Pax8 (green), F-actin (magenta) and NIS (red) (lower panels) in order to observe polarity acquisition. (B) Representative single confocal sections of shPax8 thyrocyte follicles after 2 and 5 days of growth in 3D Matrigel culture stained for (upper panels) F-actin (magenta), Tg (red) and (lower panel) pERM (green), F-actin (magenta). Nuclei are all stained with DAPI (blue). Images are taken with a 63x objective. Scale bar is 10µm.

All the above observations from both cell systems indicate that Pax8 is necessary for apical membrane definition, lumen formation and cytoskeleton organization during follicle formation.

Then, to investigate how the extracellular environment could modulate the effects of Pax8 depletion, we examined the polarization of FRT cells transfected with a control (scramble) and a Pax8 siRNA and then grown as a polarized monolayer on a Transwell during four days. Through confocal microscopy we observed that the localization of ezrin and ZO-1 was the same in both siScramble and siPax8 cells (Fig. 23). Both markers defined the apical pole at the free cellular surface in contact with the medium. Thus, the absence of Pax8 did not alter apical polarization in cell monolayers despite the similar Pax8 silencing levels between Transwell-grown and Matrigel-grown RNAi follicles (shown in Methods 2.6.).

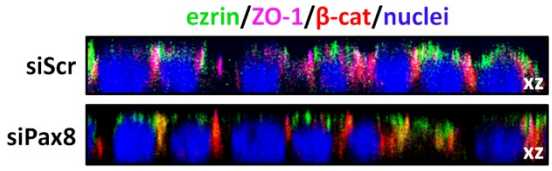

Figure 23**. Pax8 depletion does not alter the polarity of monolayers.** Immunocytochemical analysis of apical polarization in control (siScr) and Pax8 depleted (siPax8) FRT cells grown as polarized monolayers on Transwell for four days. Antibodies against ezrin (green), ZO-1 (magenta) and β-catenin (red) were used to reveal cell polarity orientation. Nuclei are stained with DAPI in blue. Representative x-z orthogonal views are shown; images are taken with a 63x objective.

Altogether, these findings indicate that Pax8 is specifically required for proper apical-basal polarization of follicles in Matrigel and that extracellular environment modulates the polarity effects of Pax8.

1.7. Cadherin-16 is downregulated in the absence of Pax8 and its silencing affects lumen formation and polarized cytoskeleton organization during follicle formation.

In order to unravel the molecular mechanisms that link Pax8 to thyroid follicle polarity we focused on the Pax8 downstream targets identified previously in our laboratory (see Results 1.5.1.). Among them, there was a member of the cadherin family, the cadherin-16 (Cdh16) gene expressed in the developing mouse thyroid gland (Cali et al., 2012) under the transcriptional control of Pax8 *in vivo* (de Cristofaro et al., 2012) and *in vitro* (Ruiz-Llorente et al., 2012). Taking into account that Cdh16 is upregulated in 3D FRT follicles, positively regulated by Pax8 and that links to actin cytoskeleton through αB-crystallin (CRYAB) in kidney cells (Thedieck et al., 2008), we questioned its role in the maintenance of the architecture and integrity of the thyroid follicles. In order to test our hypothesis we first confirmed the effect of Pax8 depletion on Cdh16 expression and localization in FRT follicles. As shown in figure 24, the protein levels of Cdh16 were greatly decreased in the absence of Pax8 (Fig. 24A) and its clear lateral localization, just below the tight junctions in control follicles; was lost in shPax8 conditions (Fig. 24B).

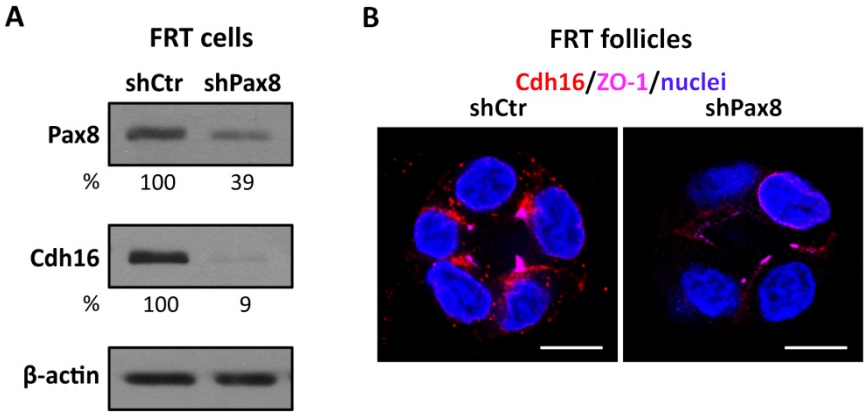

Figure 24. **Cdh16 protein levels are dramatically decreased due to Pax8 depletion.** (A) Protein expression of Pax8 and Cdh16 in FRT cells after infection with shCtr and shPax8 lentiviruses. Cells were grown in 6H and total lysates were subjected to Western-blot analysis in order to evaluate Pax8 silencing and Cdh16 expression levels. Lysates were also immunoblotted for β-actin to ensure equal loading. (B) Lateral localization of Cdh16 in control follicles is lost after Pax8 silencing. Representative single confocal sections of FRT shCtr and shPax8 follicles stained for Cdh16 (red) and ZO-1 (magenta). Nuclei are stained with DAPI (blue). Images are taken with a 63x objective. Scale bar is 10μm.

Then, we abolished Cdh16 expression through shRNA and we performed 3D morphogenesis assays with the aim to study polarity acquisition during follicle formation. Confocal immunlofluorescence analysis of growing shCdh16 follicles demonstrated inverted apical domains as evidenced by the aberrant phosphorylated ezrin localization at basal or both basal and apical membranes (Fig. 25A). Concomitantly, tight junctions visualized by ZO-1 had a lower-lateral or basal localization in the Cdh16 depleted cells where ezrin was also mislocalized as shown in figure 25A. After 5 days of growth, 45.5 % of the shCdh16 follicles formed a central lumen and 24.5 % of them showed basal ezrin localization (Fig. 25B). The distribution of cell cytoskeleton was also affected in Cdh16 silenced follicles. Polarized acetylated microtubules were localizing basally beneath the active ezrin (Fig. 25A) instead of subapically as it happens in the correctly polarized follicles. Actin filaments were localized at the periphery of the shCdh16 follicles (Fig. 25C) suggesting that F-actin loses its apical polarized organization due to the lack of Cdh16 and follows ezrin localization. Basolateral polarity revealed by β-catenin staining was not affected (data not shown).

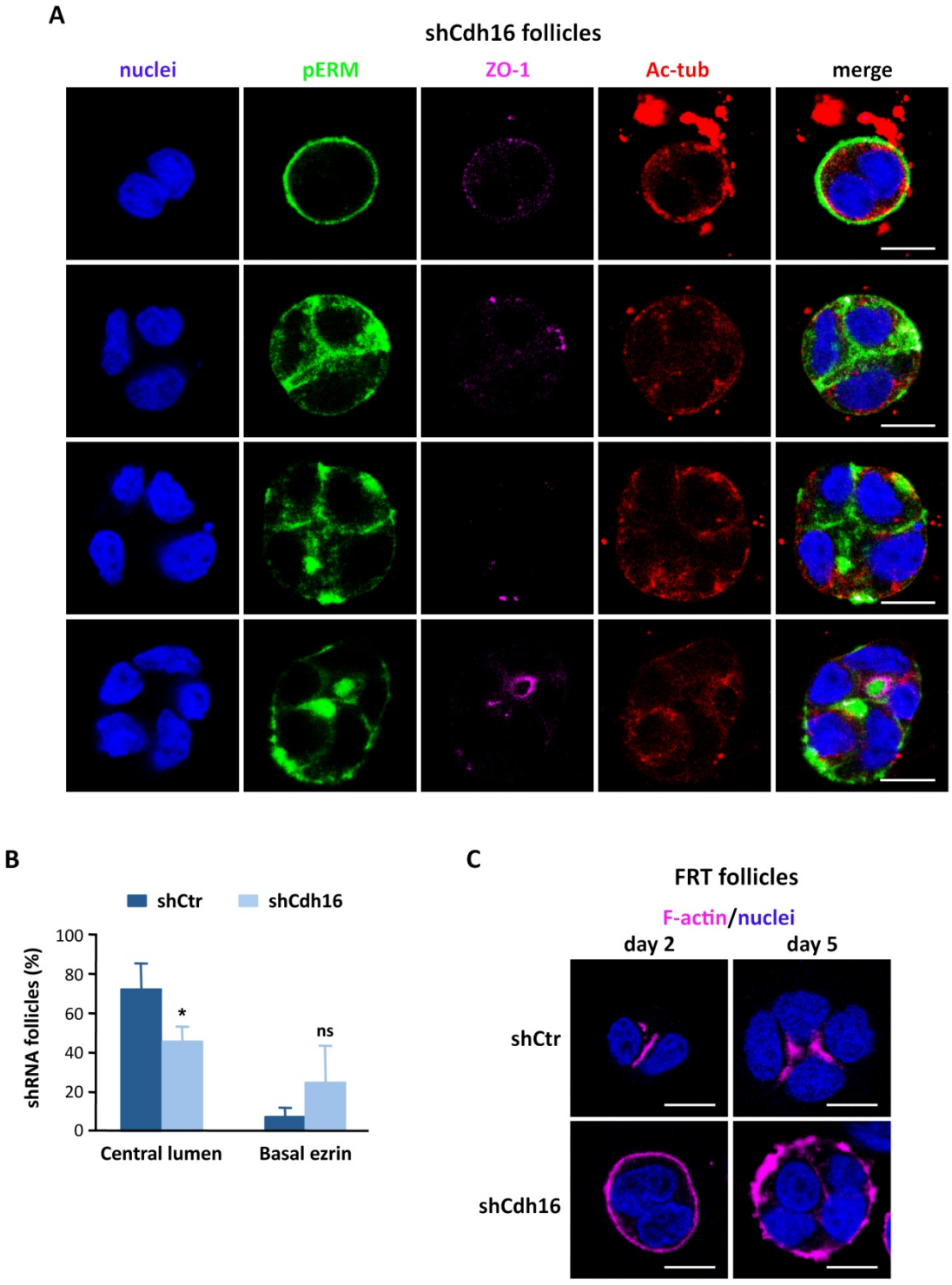

Figure 25. **Cdh16 silencing disrupts apical membrane polarity and affects polarized cytoskeleton organization in FRT follicles.** (A) Infected shCdh16 FRT cells were grown in 3D Matrigel culture and immunolabeled for apical and tight junctions markers as wells as for polarized microtubules distribution. Representative single confocal sections through the middle of FRT follicles stained for phosphorylated ERM (pERM, green), ZO-1 (magenta) and acetylated tubulin (Ac-tub, red). (B) Quantitation of lumen formation and basal ezrin localization. Graph denotes the percentage of shCtr or shCdh16 FRT follicles forming a central lumen and presenting ezrin delocalization at the basal membrane at 5 days of growth. Values are mean±SD from three replicates, n≥30 follicles per replicate. *P<0.05; ns: not significant. (C) Representative single confocal sections of shCtr and shCdh16 FRT follicles at 2 and 5 days of growth stained for F-actin (magenta) in order to visualize actin filaments polarized distribution. All nuclei were stained with DAPI (blue). Scale bar, 10µm.

We also confirmed the down-regulation of Cdh16 protein expression in the absence of Pax8 in primary thyrocytes (Fig. 26A), and then we silenced Cdh16 and performed 3D morphogenesis assays in order to confirm the above described results concerning cell polarity acquisition and follicle formation obtained in FRT follicles. Preliminary results in thyrocytes suggested that suppression of Cdh16 affected apical domain definition and subsequently lumen formation as our apical marker ezrin was localized basally and was never found delineating the follicular lumen (Fig. 26B, upper panels). Actin filaments were also mislocalized basally demonstrating the inversion of the apical polarity in the thyrocytes (Fig. 26B, lower panels). These findings were consistent with the previous immunofluorescence observations in shCdh16 FRT follicles.

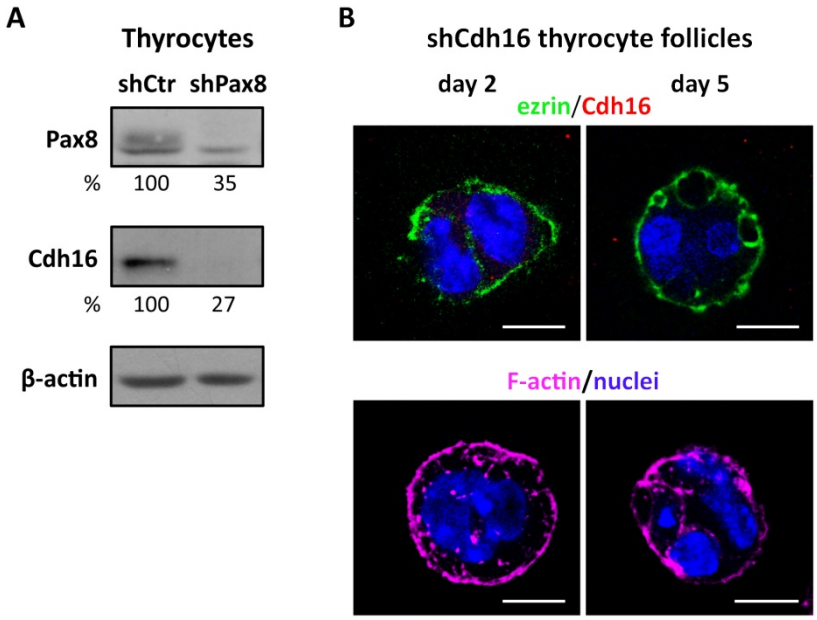

Figure 26. **Cdh16 is downregulated in the absence of Pax8 and its silencing disrupts apical polarity and inhibits lumen formation in thyrocyte follicles.** (A) Protein expression of Pax8 and Cdh16 in primary thyrocytes after infection with the lentiviruses shCtr and shPax8. Cells were grown in 6H and total lysates were subjected to Western-blot analysis in order to evaluate Pax8 silencing and Cdh16 expression levels. Lysates were also immunoblotted for β-actin to ensure equal loading. (B) Infected shCdh16 thyrocytes were grown for 2 and 5 days in 3D Matrigel culture and follicles were then fixed and stained. Representative single confocal sections through the middle of thyrocyte follicles stained for ezrin (green) and Cdh16 (red) (upper panels) in order to visualize the apical domains in absence of Cdh16. Follicles were stained with F-actin (magenta) (lower panels) in order to observe polarized actin cytoskeleton localization. Nuclei are all stained with DAPI (blue). Images are taken with a 63x objective. Scale bar is 10μm.

Taken together, these findings demonstrate that lack of Cdh16 leads to apical polarity disruption in a similar way as Pax8 depletion suggesting a Pax8-Cdh16 pathway that participates in apical domain orientation and regulates actin and microtubule cytoskeleton dynamics. The participation of Cdh16 in apical polarized distribution of F-actin was also reinforced by preliminary results of gain of function experiments in which shPax8 FRT cells that were transiently transfected with a Cdh16-GFP expression vector, formed follicles with correct F-actin apical localization (Fig. 27). Reversion of actin basal

distribution caused by the lack of Pax8 in 3D follicles (shown previously in figure 21A) due to exogenous Cdh16 expression imply a direct relation between adherens junctions and actin cytoskeleton in polarized 3D follicles.

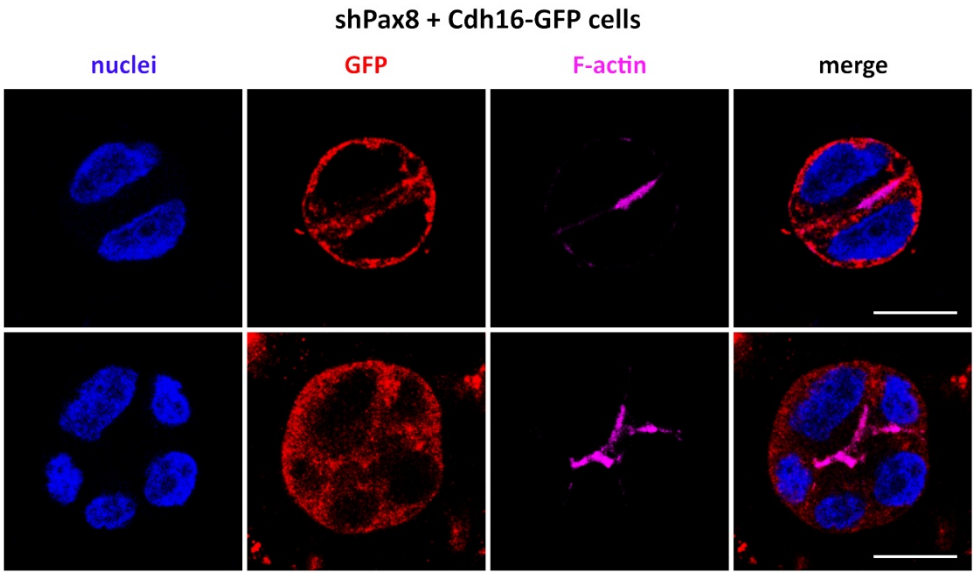

Figure 27. **Exogenous Cdh16 expression reestablishes apical distribution of actin filaments.** Infected shPax8 FRT cells were transiently transfected with Cdh16-GFP expression vector and grown in three-dimensional Matrigel culture. Representative single confocal sections through the middle of the follicles stained for GFP (red) and F-actin (magenta) in order to observe polarized actin cytoskeleton localization when exogenous Cdh16 is expressed in the shPax8 follicles. Nuclei are all stained with DAPI (blue). Images are taken with a 63x objective. Scale bar is 10µm.

1.8. CRYAB is downregulated in the absence of Pax8 independently of Cdh16 expression and localizes close to actin filaments in submembrane regions in FRT cells.

αB-crystallin (CRYAB) is a small heat shock protein involved in the stabilization and regulation of cytoskeletal proteins such as actin, vimentin and tubulin, among others (Wang and Spector, 1996, Nicholl and Quinlan, 1994, Arai and Atomi, 1997). So far, CRYAB is the only identified cytoplasmic partner of Cdh16 and the linker between Cdh16 and actin filaments in the basal side of renal collecting ducts (Thedieck et al., 2008). Willing to further characterize the Pax8-Cdh16-polarized cytoskeleton and ezrin pathway, we questioned the role of CRYAB as a potential linker between Cdh16 and actin cytoskeleton in our cell system. To answer this question, we first evaluated CRYAB expression after Pax8 and Cdh16 silencing and we found that CRYAB protein levels were diminished only in the absence of Pax8 in both FRT cells and mouse thyrocytes (Fig. 28A and B). Unexpectedly, in some cases that Cdh16 was depleted, Pax8 expression was increased and a consequent up-regulation in CRYAB expression levels was observed as shown in figure 28 in both cells. These results demonstrate that Pax8 upregulates CRYAB expression in thyroid in a Cdh16 independent manner, and these observations are in accordance

to the evidence that CRYAB is a direct Pax8 target as it was identified in the ChIP-seq analysis for Pax8 binding sites using rat PCCl3 follicular cells (Ruiz-Llorente et al., 2012, additional file 5).

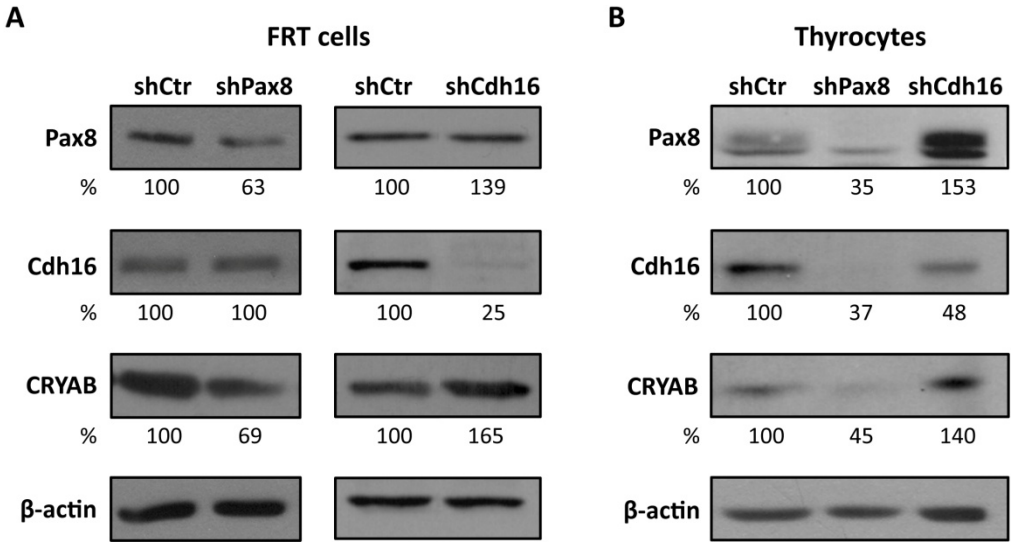

Figure 28. **CRYAB expression is upregulated by Pax8 transcription factor in a Cdh16 independent way.** Protein expression of Pax8, Cdh16 and CRYAB in (A) FRT cells and (B) primary thyrocytes after infection with the lentiviruses shCtr, shPax8 and shCdh16. Cells were grown in 6H and total lysates were subjected to Western-blot analysis in order to evaluate CRYAB expression levels after Pax8 and Cdh16 silencing. Lysates were also immunoblotted for β-actin to ensure equal loading. Protein levels are quantified as percentages (%) referred to shCtr levels.

The subcellular localization of CRYAB and its association with ezrin and filamentous actin were studied in FRT cells. Immunofluorescence analysis of FRT cells grown in 2D conditions revealed a diffuse CRYAB signal in the cytoplasm and a stronger labelling in submembrane regions, close to the colocalizing F-actin and ezrin at the cell membrane (Fig. 29).

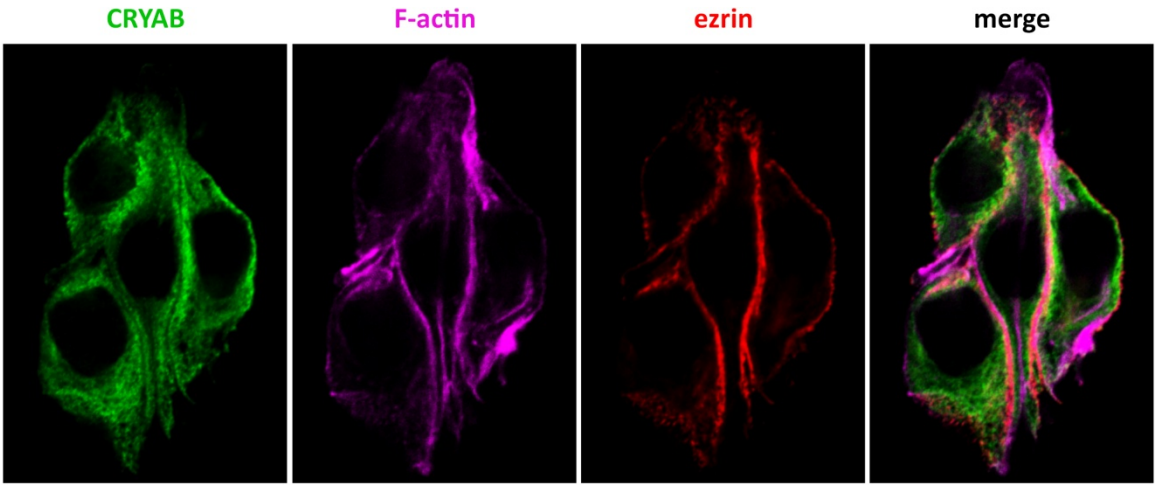

Figure 29. **CRYAB has a cytosolic submembrane localization in FRT cells.** FRT cells were grown as monolayers and then were fixed and stained for CRYAB (green), F-actin (magenta) and ezrin (red) in order to determine the subcellular localization of CRYAB. Representative single confocal immunofluorescence images were taken with 63x objective. Scale bar is 10μm.

1.9. Rac1 is delocalized at the basal membrane leading to the loss of apical polarity in Pax8 and Cdh16 depleted thyroid follicles.

Studies in MDCK cells have demonstrated that the interaction of epithelial cells with the ECM creates an intracellular signalling pathway in which activation of β1-integrins orients the apical pole of polarizing cysts via Rac1 activation and laminin organization in the basement membrane (BM) through actin reorganization and other signalling events (Yu et al., 2005, Colognato et al., 1999). As cell-ECM interaction relies on the availability and activation of integrins at the cell surface, we initially analyzed the expression of β1-integrins (Itgb1) in control, Pax8 and Cdh16 depleted FRT monolayers by Western-blot as shown at the left panels of figure 30. Then we evaluated the expression of the activated Itgb1 in 3D FRT follicles using an active-state-specific β1-integrin antibody (act-Itgb1 or HUTS21). Western-blot analysis showed that β1-integrins are activated in FRT follicles and that loss of Cdh16 downregulates their expression in both 2D and 3D conditions (Fig.30, right panel). These results suggest a possible link between Pax8-dependent polarity orientation and β1-integrins regulation through Cdh16.

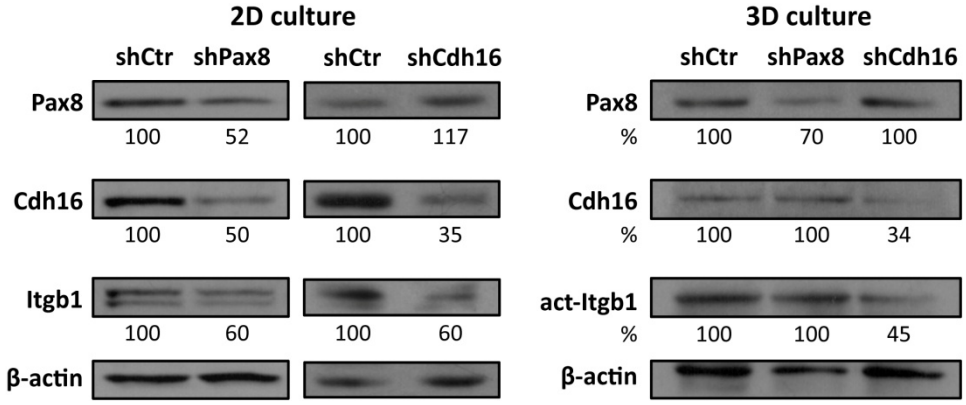

Figure 30. **Cdh16 depletion downregulates β1-integrins expression in 2D and 3D FRT cultures.** Protein expression of Pax8, Cdh16, β1-integrins (Itgb1) and activated Itgb1 (act-Itgb1) in FRT cells grown in 2D and 3D Matrigel culture system after infection with the lentiviruses shCtr, shPax8 and shCdh16. Cells were grown in 6H and total lysates were subjected to Western-blot analysis in order to evaluate Itgb1 expression levels after Pax8 and Cdh16 silencing. Lysates were also immunoblotted for β-actin to ensure equal loading. Protein levels are quantified as percentages (%) referred to shCtr levels.

On the other hand, integrin-mediated adhesion of cells to the ECM is required for Rac1 membrane localization (del Pozo et al., 2004), which in turn determines apical domain polarity acquisition. We checked Rac1 localization in control, shPax8, and shCdh16 FRT follicles and we observed that Rac1 was apically transported and then accumulated in the nascent apical domain of the control two-cell follicles, whereas it had a basal or a mixed apical and basal localization in shPax8 and shCdh16 follicles (Fig. 31A, upper strip of images at each condition). When Pax8 and Cdh16 silenced follicles became bigger (lower strip of images), apical domain was either completely or partially inverted giving place to follicles with

no central lumen. These results indicated that correct membrane localization of Rac1 determines apical polarity in thyroid follicles as evidenced by actin filaments and Rac1 colocalization (Fig. 31A).

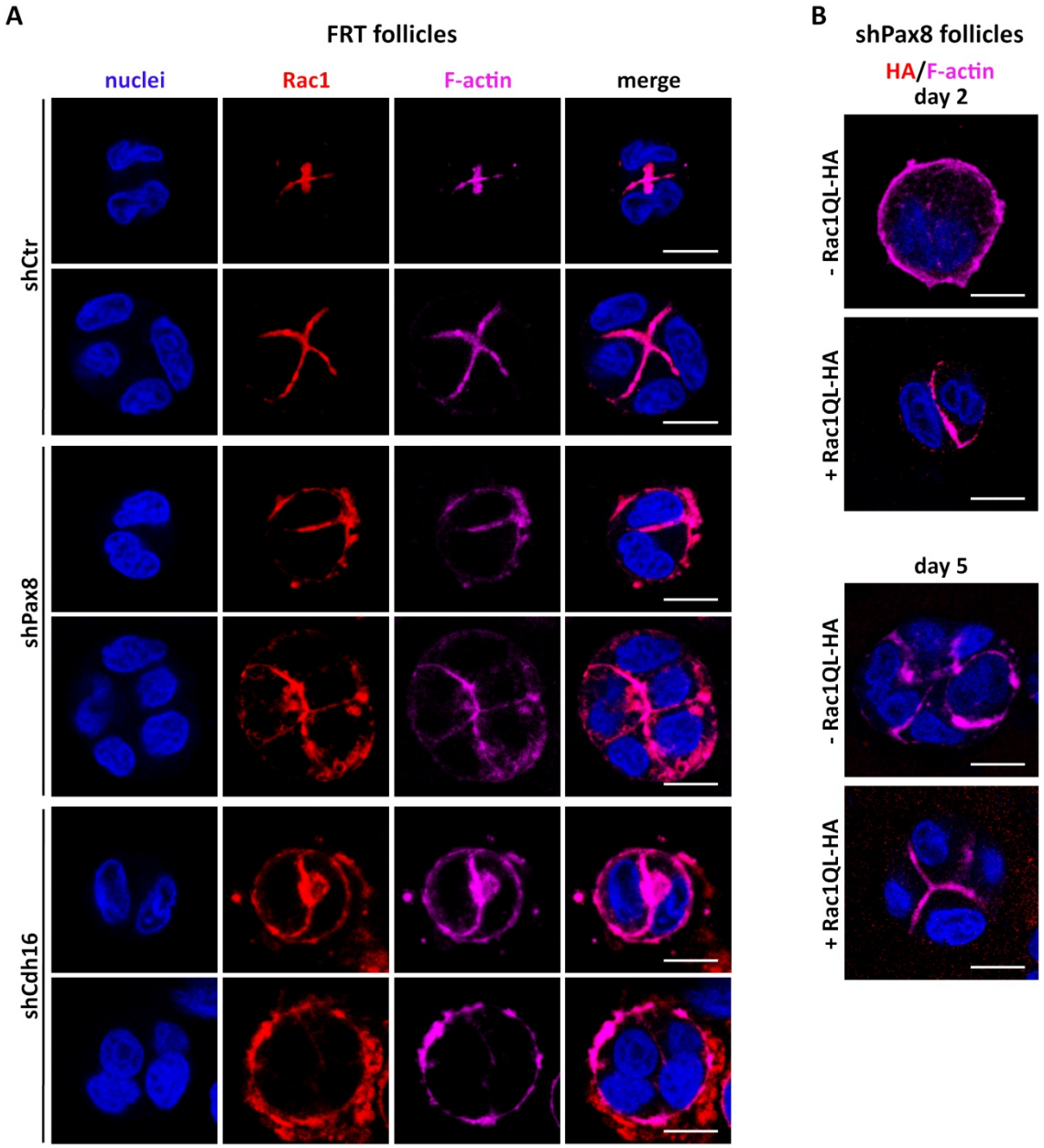

Figure 31. **Rac1 apical localization is necessary for the apical distribution of actin filaments in polarizing follicles.** (A) Rac1 apical localization is disturbed in shPax8 and shCdh16 follicles. Representative single confocal immunofluorescence sections in the middle of FRT control, shPax8 and shCdh16 follicles stained for Rac1 (red) and F-actin (magenta) in order to determine Rac1 localization and its relation with actin cytoskeleton. (B) Apical active Rac1 localization rescues actin filaments polarized distribution in shPax8 follicles. Representative single confocal immunofluorescence sections in the middle of shPax8 FRT follicles with or without exogenous expression of Rac1QL-HA stained for HA (red) and F-actin (magenta). Nuclei are all stained with DAPI (blue). Images are taken with a 63x objective. Scale bar is 10μm.

In 3D environments, activation of Rac1 is sufficient to reorient cyst polarity in cases that it has been inversed (Yu et al., 2005, Monteleon et al., 2012). Preliminary results using shPax8 cells transfected with

the constitutively active Rac1QL-HA expression vector showed that active Rac1 apical expression could restore apical polarity in Pax8 depleted follicles (Fig. 31B). Actin filaments were apically relocalized in the Rac1QL-HA transfected shPax8 follicles and a 42.9% of the follicles formed central lumens with exclusively apical ezrin and upper-lateral ZO-1 localization (data not shown). These results suggest that Rac1 activation should be downregulated upon Pax8 depletion in FRT follicles and GTP-Rac1 pull-down experiments are currently being performed to confirm this hypothesis. Taken together, these data indicate that local activation of Rac1 in the initial zone of cell-cell contact is necessary for correct apical domain polarization during folliculogenesis. Although there is still missing information about the components of Pax8 signaling pathway that leads to follicle polarization we have assigned an important role to Cdh16 in the forming adherens junctions where could interact with the actin cytoskeleton through CRYAB in order to position Rac1 in the first cell-cell junction where active Rac1 would then participate in multiple cell processes that further define the apical domain and finally correct lumen formation.

2. Sodium/iodide Symporter: Basolateral plasma membrane trafficking and endocytic routes

2.1. Identification of NIS basolateral sorting signals.

NIS basolateral plasma membrane localization in thyroid follicular cells is crucial for thyroid hormone synthesis as wells as for radio-iodide therapy in thyroid cancer. The traffic routes involved in NIS basolateral transport have not been identified yet despite of their importance. In the view of this lack of knowledge, we decided to inspect NIS cytosolic tail for potential basolateral sorting signals based on conventional and unconventional motifs reported in literature (Gonzalez and Rodriguez-Boulan, 2009, Janvier et al., 2003, Torres et al., 2011).

Multiple sequence alignment analysis of NIS cytoplasmic C-terminus and intracellular loops revealed leucine and tyrosine-based motifs. In detail, we identified a conserved dileucine motif PGLL ($L^{562}L^{563}$ in human, rat and and other species) followed by a conserved diaromatic motif WW in the beginning of the cytoplasmic domain of the protein ($W^{564}W^{565}$ in human and other species) as shown in figure 32. We also recognized the LVK leucine-based motif preceded by a region of acidic residues similar to the ALVVHP motif of syntaxin 4 demonstrated to be responsible for its basolateral localization depending on clathrin adaptor AP-1B (Torres et al., 2011, Reales et al., 2011). Finally, the last four residues of the cytoplasmic tail presented the highly conserved motif ET[ND]L including a single leucine. Monoleucine motifs with upstream acidic residues have also been reported as basolateral signals in the case of the glycoprotein CD147, however through unknown adaptors (Deora et al., 2004).

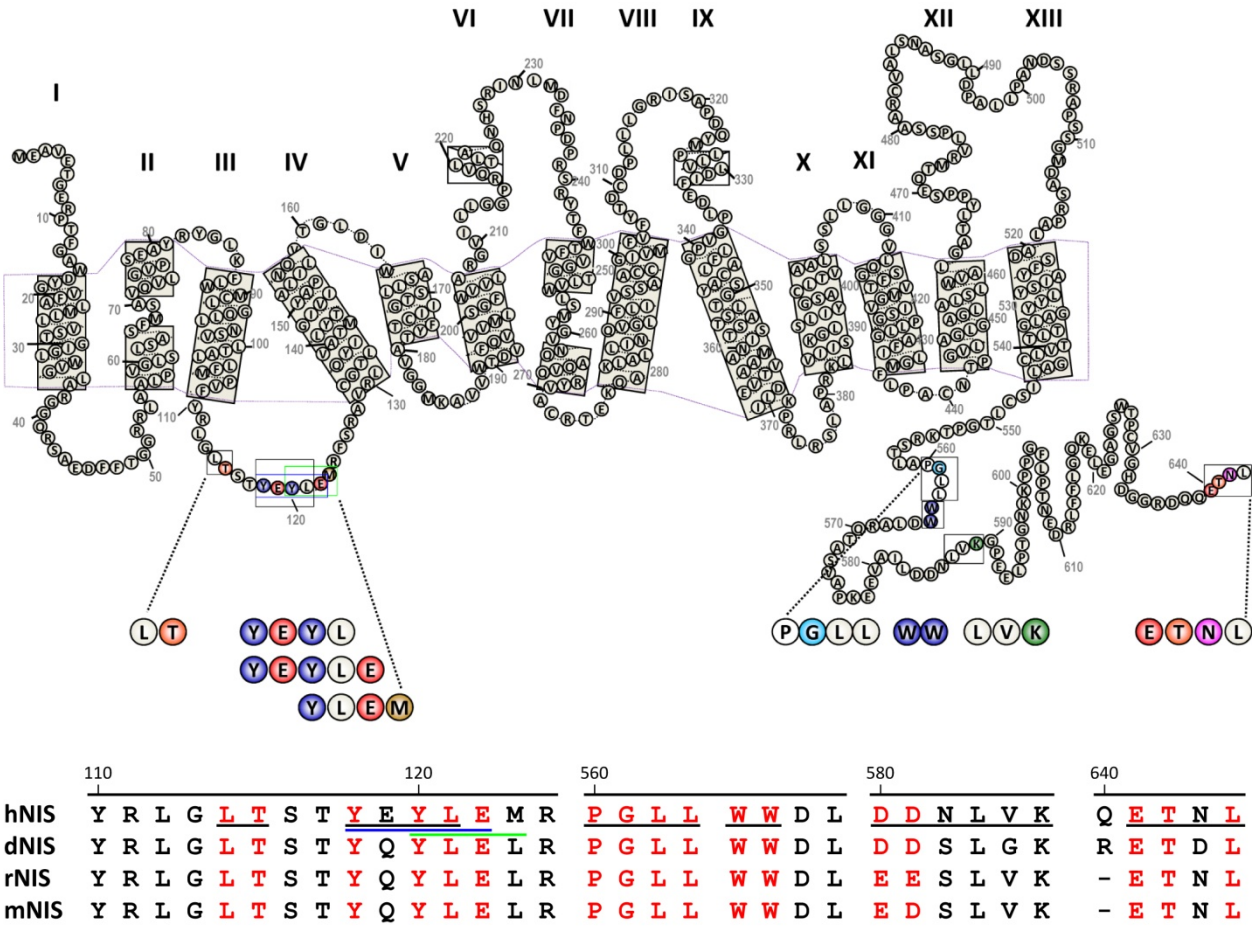

Figure 32. **NIS basolateral sorting signals analysis.** Human NIS topology (kindly provided by Dr. A. De la Vieja) and basolateral sorting signals (black, blue and green boxes) identified in the intracellular loop between III and IV transmembrane domains and NIS C-terminus. The amino acids composing the signals are represented in colours according to polar, non-polar, aromatic, aliphatic and charge common properties. Putative sorting signals (underlined) are conserved (in red) among human, dog, rat and mouse NIS.

Next, we examined the intracellular loops between the transmembrane domains for sorting motifs and we detected a single leucine $L^{114}T^{115}$ motif, a two tyrosine-containing motif ^{118}Y[QE]YL^{121} or/and the ^{118}Y[QE]YLE^{122} and the single tyrosine motif ^{120}YLE[LM]^{123}, all localized in the intracellular region between the III and IV NIS transmembrane domains. Interestingly, the Y[QE]YLE appeared similar to the Yx[FYL][FL]E signal identified in the amyloid precursor protein responsible for its basolateral sorting through its interaction with the μ4 subunit of the AP-4 adaptor protein (Burgos et al., 2010). The YLE[LM] and Y[QE]YL motifs fitted the minimal consensus for YxxØ signals that are known to bind to μ subunits of AP1, 2, 3 complexes (Ohno et al., 1995, Owen and Evans, 1998, Mardones et al., 2013). Together, these results resumed in Table 8, revealed possible mono/dileucine- and tyrosine-based signals in NIS C-terminus and second intracellular loop that could direct its basolateral sorting through interaction with clathrin-dependent and/or independent adaptors such as AP-1 and AP-4 respectively, as well as other unknown adaptors. The presence of the LV dileucine-resembling motif in NIS C-terminus

and more interestingly the YxxØ motif in the intracellular domain, both described to be recognized by the clathrin-associated basolateral sorting proteins AP-1 prompted us to test the role of the well studied adaptor protein complex AP-1 in NIS basolateral trafficking.

Signals localization	Putative signals	Motifs	Adaptors
C-terminus	ET[ND]L	L	Unknown
	PGLL (WW)	LL	AP-1, AP-2
	([DE][DE])xLVK	LV	AP-1B
2nd intracellular loop	LT	L	Unknown
	Y[QE]YL, YLE[LM]	YxxØ	AP-1, AP-2
	Y[QE]YLE	Yx[FYL][FL]E	AP-4

Table 8. Putative NIS basolateral sorting signals and adaptors.

In square brackets are the amino acidic variations among the species, and in parenthesis are amino acids close to the signals.

2.2. NIS exits the *trans*-Golgi network and is delivered to the plasma membrane in clathrin-associated AP-1 vesicles and transferrin receptor positive endosomes.

As NIS basolateral sorting routes have not been characterized yet, at first place we evaluated the subcellular localization of newly synthesized NIS in thyroid follicular cells upon induction of NIS expression by TSH. Confluent PCCl3 follicular cells were maintained in starvation medium for 5 days in order to completely abolish NIS expression as it has a half-life of approximately 3 days in the absence of TSH (Riedel et al., 2001). Cells were then stimulated with TSH for 12 and 24 hours and NIS plasma membrane (PM) and subcellular localization were determined through membrane biotinylation assay and colocalization immunofluorescence, respectively. As it is shown in figure 33, NIS was completely absent from both the plasma membrane and cytosolic extracts (Fig. 33A) or the cell cytoplasm (Fig. 33B) in the absence of TSH. Addition of TSH induced NIS *de novo* protein synthesis that became detectable at the cytosolic fraction at 12 hours of stimulation and needed 24 hours to appear at the membrane fraction (Fig. 33A). Colocalization confocal microscopy at 12 hours of TSH stimulation (Fig. 33B, medium panels of the upper set of images) revealed some NIS at the *trans*-Golgi network by colocalization with the trans-Golgi protein TGN38 (Pearson´s Coefficient Rr=0.22±0.05), also at the perinuclear region and the cell cytoplasm but not yet at the plasma membrane. At 24 hours of stimulation, NIS localized at the plasma membrane and showed a strong perinuclear and cytoplasmic distribution, while its colocalization with the TGN marker was not apreciated (Rr=0.14±0.04) as shown in figure 33B. The high intensity of NIS labeling at a region close to the TGN suggested its association with the recycling endosomes (REs) that can transport cargo from the Golgi to the plasma membrane depending on the clathrin-associated adaptor complex AP-1 (Ang et al., 2004, Gravotta et al., 2007).

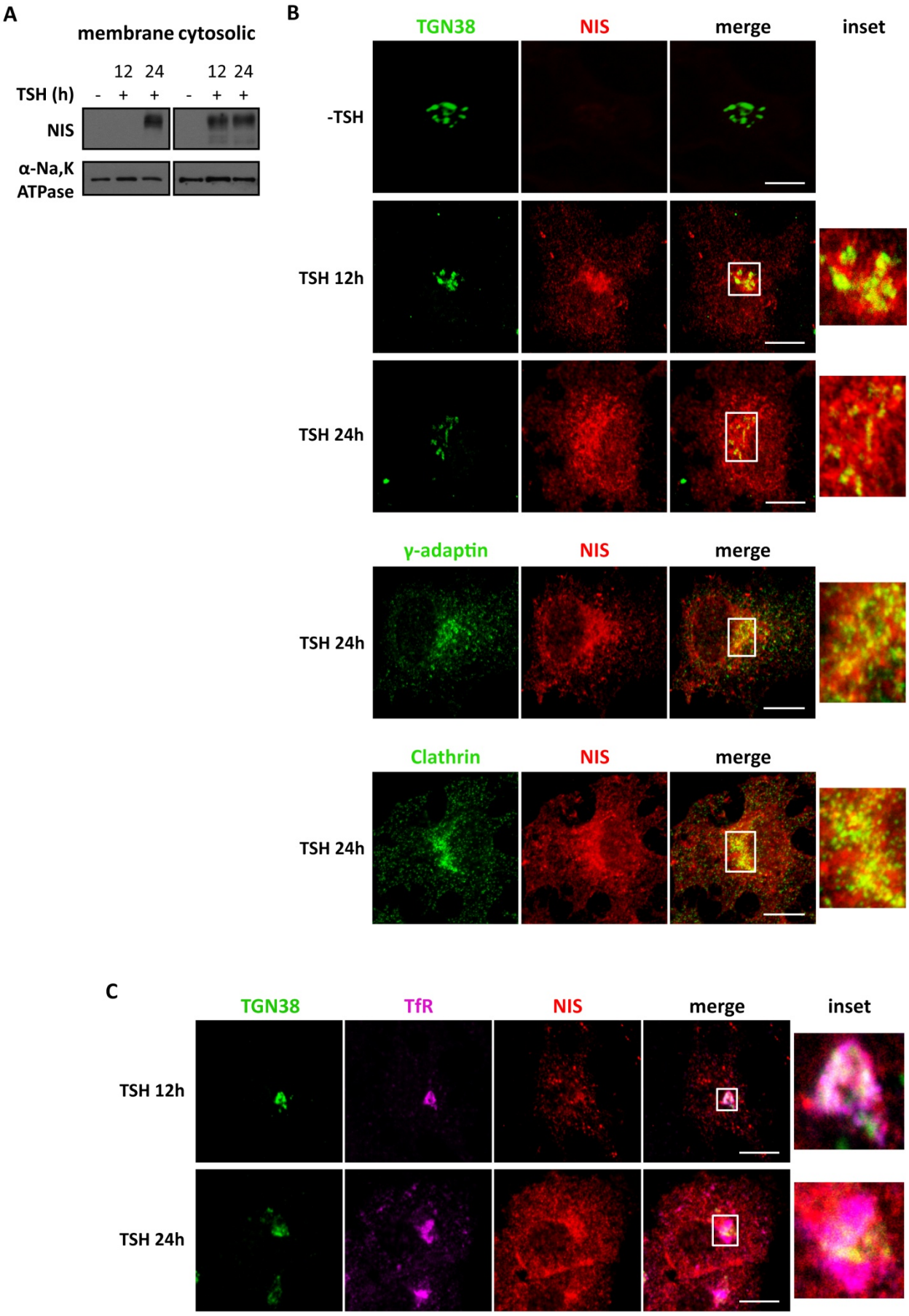
A
membrane cytosolic
12 24 12 24
TSH (h) - + + - + +
NIS
α-Na,K ATPase
B
TGN38
NIS
merge
inset
-TSH
TSH 12h
TSH 24h
γ-adaptin
NIS
merge
TSH 24h
Clathrin
NIS
merge
TSH 24h
C
TGN38
TfR
NIS
merge
inset
TSH 12h
TSH 24h

Figure 33. **Cellular localization of newly synthesized NIS in PCCl3 cells after TSH induction.** A) NIS reaches the plasma membrane at 24 hours after TSH treatment. NIS protein expression was detected by Western-blot in cytosolic and membrane-biotinylated extracts from PCCl3 cells grown in medium without TSH during 5 days and then stimulated with TSH for 0, 12 and 24 hours. The membrane α-NA,K ATPase was used to ensure equal loading. B) NIS localizes at the *trans*-Golgi network at 12 hours of TSH treatment and colocalizes with ɣ-adaptin and clathrin after its exit at 24 hours of treatment. Representative single confocal immunofluorescence sections of PCCl3 cells stained for TGN38 (green, upper panels) and NIS (red) at 12 and 24 hours of TSH treatment, ɣ-adaptin (green, medium panels) and NIS (red), Clathrin (green, lower panels) and NIS (red) in order to determine newly synthesized NIS subcellular localization. Insets of the regions in white boxes are shown. C) NIS colocalizes with transferrin receptor (TfR) at the TGN and the recycling endosomes. Representative single confocal immunofluorescence sections of PCCl3 cells at 12 and 24 hours of TSH stimulation. Cells were stained for TGN38 (green), TfR (magenta) and NIS (red). Scale bar is 10µm.

Double indirect immunofluorescence between NIS and the gamma subunit of the AP-1 clathrin-adaptor complex (ɣ-adaptin) (Fig. 33B medium panels, inset), as well as with clathrin (Fig. 33B bottom panels, inset) showed colocalization at the TGN/RE region (Rr=0.48±0.11 with ɣ-adaptin and Rr=0.41±0.04 with clathrin) and a few colocalization spots at the cytosol at 24 hours of TSH treatment. To further verify NIS localization at REs we performed triple-colocalization between NIS, TGN and REs at 12 and 24 hours of TSH stimulation. We observed an increase in NIS colocalization with the marker of recycling endosomes transferrin receptor (TfR) at 24 hours (0.25±0.08 at 12h *vs.* 0.42±0.07 at 24h) followed by a decrease in the colocalization between TfR and TGN38 (0.78±0.08 at 12h *vs.* 0.49±0.07 at 24h).

These results suggest that NIS exits the *trans*-Golgi compartment and follows a clathrin-dependent biosynthetic pathway towards the plasma membrane of thyroid follicular cells mediated by AP-1 coated vesicles and TfR rich recycling endosomes. Taking in account that γ-adaptin is a common subunit of AP-1A and 1B complexes, and that TfR interacts with both of them at the TGN and the recycling endosomes (Gravotta et al., 2012), we decided to study the role of each clathrin-adaptor variant in NIS sorting.

2.3. Knockdown of the medium subunit of AP-1A adaptor does not affect NIS basolateral membrane localization in MDCK cells.

AP-1A is the ubiquitously expressed form of AP-1 adaptor and controls biosynthetic trafficking from the TGN to the basolateral membrane by interaction between its medium subunit (µ1A) with the cargo proteins through canonical YxxØ and non-canonical motifs (Carvajal-Gonzalez et al., 2012, Gravotta et al., 2012). To determine the role of AP-1A in NIS sorting we knocked down µ1A and we studied the effect on the polarized NIS localization in MDCKhNIS cells. Using confocal microscopy (Fig. 34A) we observed no changes in basolateral NIS localization in fully polarized µ1A-KDhNIS cells compared to the steady-state basolateral NIS localization in polarized control cells. These results were confirmed through quantitative domain-selective biotinylation followed by Western-blot analysis (Fig. 34B) that revealed almost the same amount of NIS in the basolateral (BL) domains of both control (BL, 95%) and µ1A-KDhNIS polarized cells (BL, 96%) and practically no apical (AP) NIS distribution. We also observed that polarized distribution of the endogenous basolateral plasma membrane protein α-Na,K ATPase was not

disturbed by the loss of µ1A (Fig. 34B, 97% in control *vs.* 96% in µ1A-KDhNIS cells). Similarly, the localization of the apical membrane glycoprotein gp135 was affected (Fig. 34A and B, AP 91% in control *vs.* 95% in µ1A-KDhNIS).

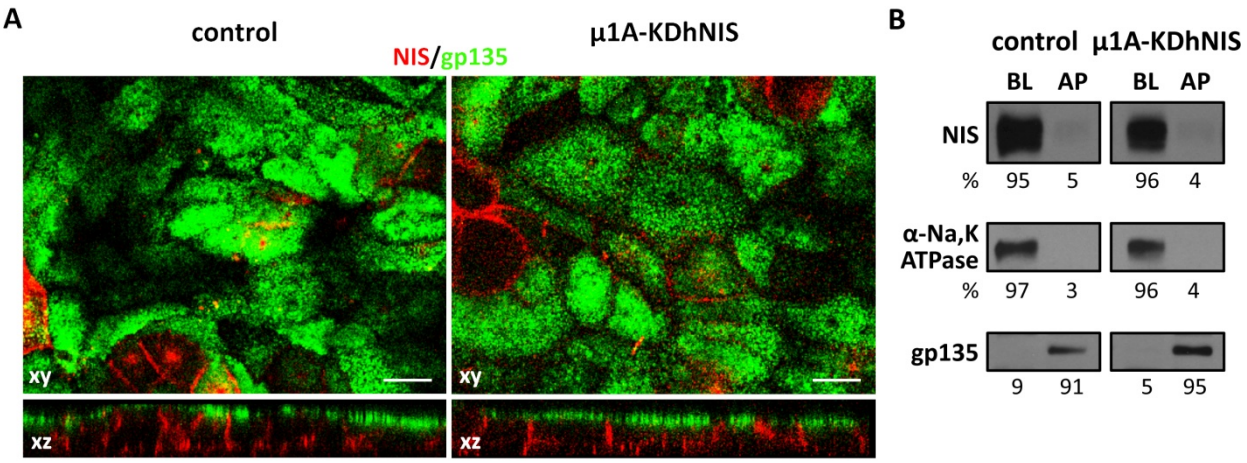

Figure 34. **NIS is basolaterally tageted in the absence of µ1A.** Control and µ1A knockdown (µ1A-KDhNIS) MDCKhNIS cells were plated on polycarbonate filters and analyzed for the polarized distribution of NIS and several endogenous membrane markers by (A) immunofluorescense and (B) domain-selective biotinylation, streptavidin-agarose retrieval and Western-blotting. (A) NIS localizes at the basolateral membrane of control and µ1A-KDhNIS cells. Representative confocal immunofluorescence of apical xy sections from a z-stack and orthogonal xz views stained for NIS (red) and the apical glycoprotein gp135 (green). Scale bar is 10µm. (B) NIS, α-Na,K ATPase and gp135 present correct polarized plasma membrane distribution in control and µ1A-KDhNIS cells. Representative Western-blot analysis and quantification of NIS, α-Na,K ATPase and gp135 proteins in apical (AP) and basolateral (BL) domains as percent of the total surface protein amount (AP+BL).

These results suggested that µ1A is not necessary for NIS basolateral sorting despite the tyrosine-based ^{120}YLEM^{123} motif in its second intracellular loop.

2.4. Knockdown of the medium subunit of AP-1B adaptor missorts NIS at the apical membrane of polarized MDCK cells.

Next, we examined the role of the epithelial specific AP-1 variant AP-1B, demonstrated to sort basolateral proteins in recycling and biosynthetic routes through interaction of its medium subunit µ1B with conventional tyrosine-based and unconventional signals localized on the cytoplasmic tail of the cargo proteins (Gravotta et al., 2012, Carvajal-Gonzalez et al., 2012, Guo et al., 2013). Confocal microscopy of confluent µ1B-knockdown MDCKhNIS cells (µ1B-KDhNIS) revealed a dramatic apical redistribution of NIS that contrasted with its exclusive basolateral localization in MDCKhNIS (Fig. 35A) or control cells (Fig. 34A). Nevertheless, tight junctions (ZO-1) and adherens junctions (β-catenin) morphology and polarized localization were preserved in µ1B-KDhNIS cells as shown in the midcell confocal sections at the lower panels of figure 35A. Quantitative domain-selective biotinylation (Fig. 35B) confirmed that µ1B-KD decreased the steady-state basolateral polarity of NIS at 53% *vs.* 95% in MDCKhNIS and furthermore affected the basolateral distribution of the exogenous expressed transferrin

receptor (TfR 61% *vs.* 86% in MDCKhNIS). Conversely, the endogenous BL α-Na,K ATPase and AP gp135 plasma membrane proteins displayed normal polarity in μ1B-KDhNIS cells in agreement with the observations of Dr. Enrique Boulan group who first generated and studied the μ1B depleted MDCK cell line (Gravotta et al., 2007).

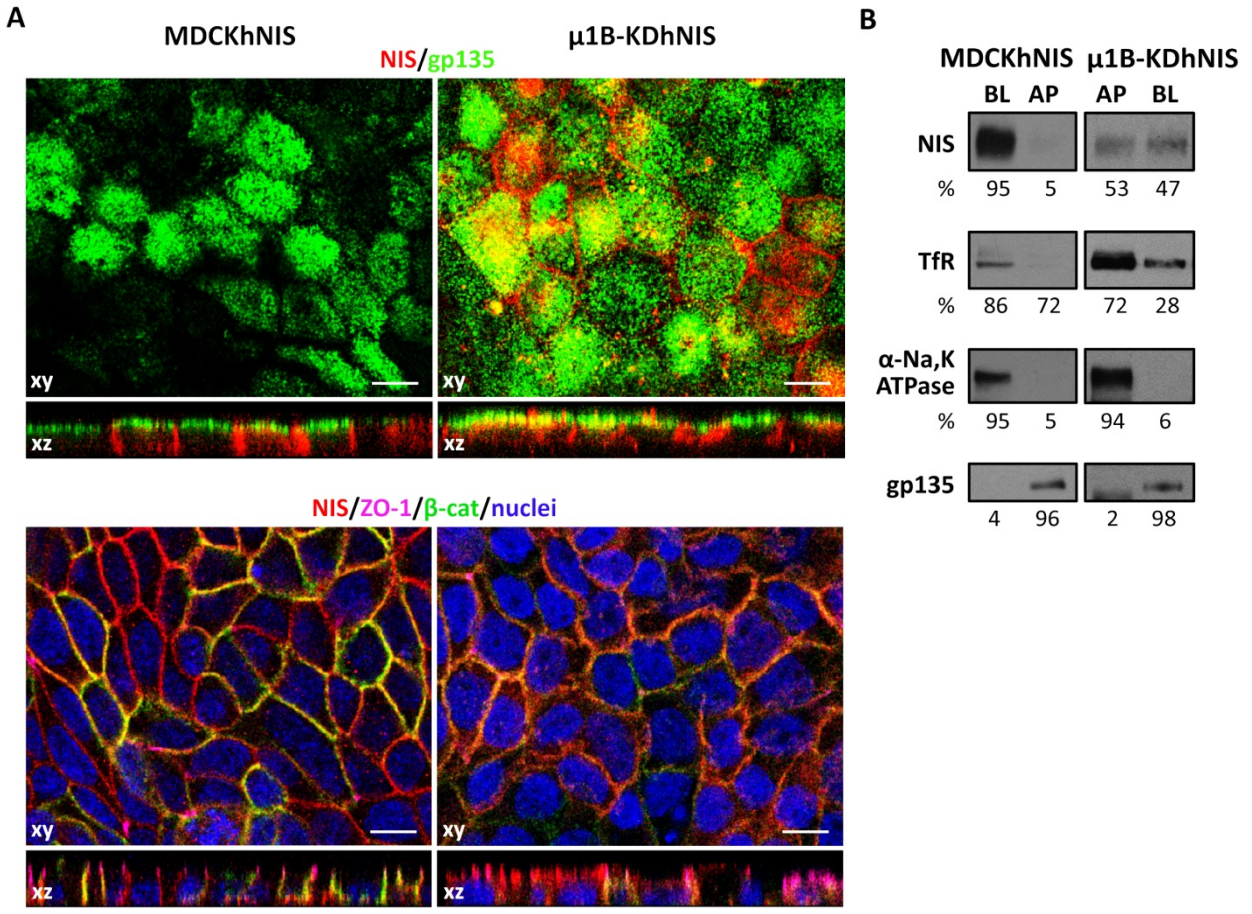

Figure 35. **NIS is apically targeted in the absence of μ1B.** MDCKhNIS and μ1B knockdown-MDCKhNIS cells (μ1B-KDhNIS) were plated on polycarbonate filters and analyzed for the polarized distribution of NIS and several endogenous PM markers by (A) immunofluorescense and (B) domain-selective biotinylation, streptavidin-agarose retrieval and Western-blotting. (A) NIS localizes at the apical membrane in μ1B-KDhNIS cells while membrane polarity is preserved. Representative confocal immunofluorescence of apical xy sections from a z-stack and orthogonal xz views stained for NIS (red) and the apical glycoprotein gp135 (green)(upper panels), NIS (red), tight junctions ZO-1 (magenta) and adherens junction β-catenin (green) (lower panels). Scale bar is 10μm. (B) NIS and TfR show decreased polarity whereas α-Na,K ATPase and gp135 have correct polarized plasma membrane distribution in μ1B-KDhNIS cells. Representative Western-blot analysis and quantification of NIS, TfR, α-Na,K ATPase and gp135 proteins in apical (AP) and basolateral (BL) domains as percent of the total surface protein amount (AP+BL).

Next, to characterize the subcellular compartment where AP-1B sorts NIS we performed triple-labeling for NIS, the μ1B subunit and the TGN in non-polarized MDCK cells. Qualitative and quantitative analysis showed small differences in colocalization between NIS and both the TGN protein marker TGN48 (0.24±0.03) and μ1B (HA, 0.26±0.1). A partial colocalization was also observed between the μ1B positive compartment and the TGN (0.26±0.05), as shown in figure 36.

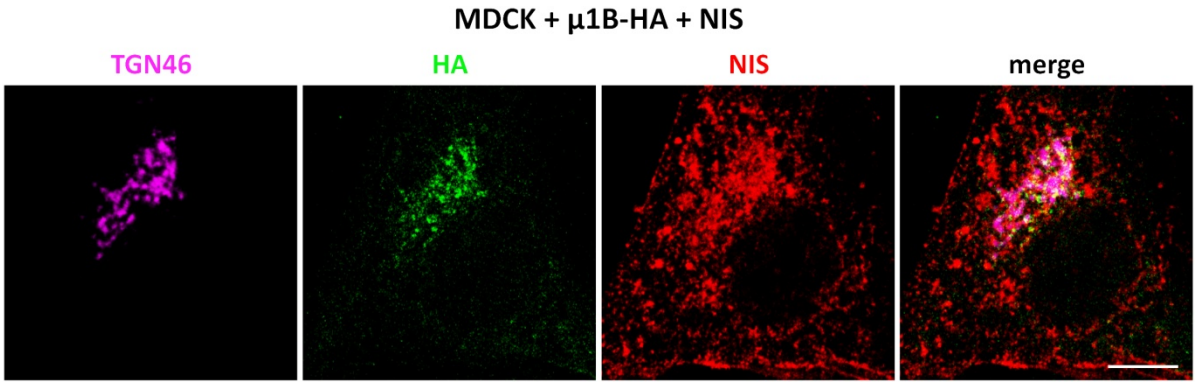

Figure 36. **NIS subcellular localization in MDCK cells.** MDCK cells were transfected with µ1B-HA and NIS expression vectors and proteins colocalization was analyzed by immunofluorescense 48 hours post transfection. Representative single confocal section labeled with TGN46 (magenta), HA (green) and NIS (red). Scale bar is 10µm.

We also wondered if the apically mislocalized NIS was still functional and could transport iodide given that NIS mislocalization has been associated with impaired function in some cases (De la Vieja et al., 2005). To answer this question, we performed a time course ^{125}Iodide uptake assay with MDCKhNIS and µ1B-KDhNIS fully polarized cells. First, we analysed uptake after adding radio-iodide at the basolateral chamber side (Fig. 37A) and we observed that iodide uptake from the basolateral localized NIS was relatively similar in both cells at the beginning, while µ1B-KDhNIS cells had an evident delay in iodide uptake after 30 minutes of incubation that was maintained until the end of the experiment (Fig. 37A). The iodide efflux through the apical plasma membrane in µ1B-KDhNIS cells was slower than in MDCKhNIS cells and this result could be explained by the presence of functional NIS molecules in the apical membrane that would re-uptake iodide from the apical chamber side to the intracellular medium in µ1B-KDhNIS cells. This intracellular iodide increase would consequently slow down iodide uptake from the basolateral side and would explain the delay in basolateral influx observed after 30 min of incubation. When radio-iodide was added at the apical chamber side (Fig. 37B), iodide influx was observed in both cells however slower in µ1B-KDhNIS than in MDCKhNIS cells. At the same time, µ1B depleted cells presented lower basolateral iodide concentration as a result of slower efflux due to the apical delayed influx. These data can be explained if apically localized NIS allows iodide influx and quick efflux back to the apical chamber side leading to radio-iodide apical accumulation and thus the higher radioactivity levels observed. Alltogether, these results clearly demonstrate the presence of a functional apically localized sodium/iodide transporter, NIS.

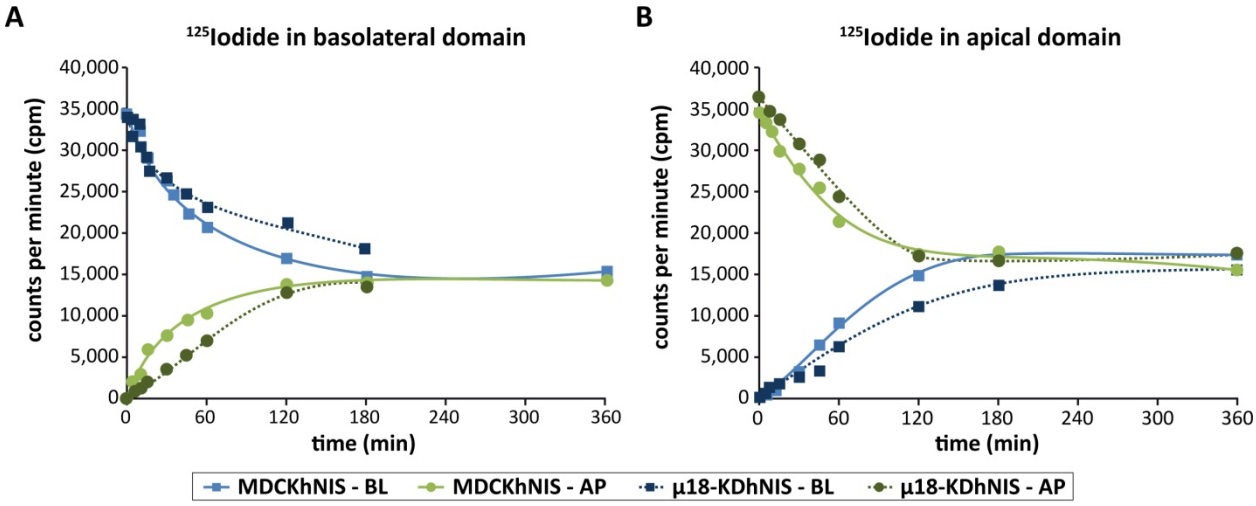

Figure 37. **Apical localzed NIS is functional in μ1B-KDhNIS cells.** Graphs representing NIS activity determined by iodide transport time-course assay in fully polarized parental MDCKhNIS and μ1B-KDhNIS cells. ^{125}Iodide was added to the basolateral or apical chamber sides during 0, 2, 5, 10, 15, 30, 45, 60, 120, 180, 360 minutes (min) and then radioactivity was quantified at both sides as counts per minute (cpm). Measurements are the mean of two replicates.

2.5. Double knockdown of μ1A and μ1B causes a more severe NIS missorting.

According to the above findings, μ1B knockdown causes a substantial loss of NIS polarized membrane localization, whereas μ1A loss does not affect NIS trafficking, suggesting that only AP-1B mediates NIS basolateral sorting**.** However, the group of Dr. Enrique Boulan has demonstrated that AP-1B can compensate for AP-1A function in the case of the TfR and LDL receptor basolateral sorting and membrane targeting in MDCK cells (Gravotta et al., 2012). Therefore, in order to clarify the role of AP-1A in NIS basolateral traffic we generated a double knockdown for both μ1A and μ1B in MDCKhNIS cells (μ1AB-KDhNIS) and then we examined the polarized distribution of NIS and several PM markers by immunofluorescence and domain-selective biotinylation. Orthogonal views of serial z-sections using confocal microscopy revealed strong apical NIS staining and colocalization with the apical gp135 as shown in figure 38A. Quantitative domain-selective biotinylation (Fig. 38B) demonstrated that a 43% of NIS was at the basolateral domain in μ1AB-KDhNIS cells, whereas a 57% was apically mistargeted. Conversely, μ1AB knockdown did not cause any further loss of polarity of the TfR when compared to its BL localization in μ1B-KDhNIS cells (78% *vs.* 72%). Moreover, the polarized distribution of the endogenous basolateral α-Na,K ATPase and the apical gp135 was not impacted by the double knockdown. The more prominent NIS delocalization in μ1AB-KD cells than in μ1B-KD cells indicates that AP-1A complex also participates in NIS basolateral sorting and mediates correct NIS polarized plasma membrane distribution through it medium subunit.

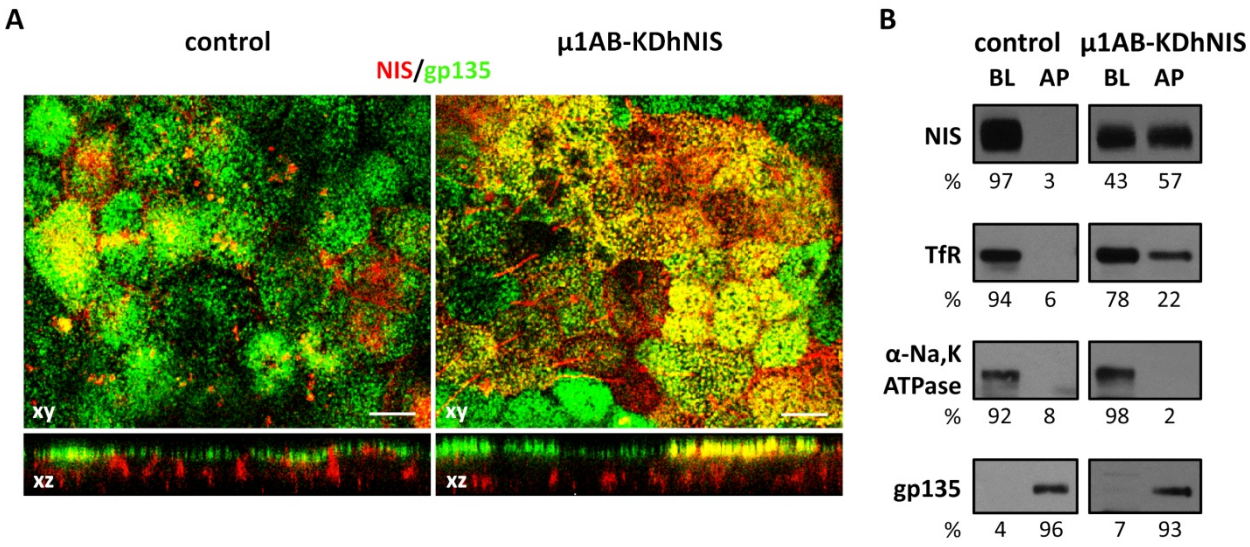

Figure 38. **NIS is apically targeted in the absence of both µ1A and µ1B.** Control and µ1A,1B knockdown (µ1AB-KDhNIS) MDCKhNIS cells were plated on polycarbonate filters and analyzed for the polarized distribution of NIS and several endogenous PM markers by (A) immunofluorescense and (B) domain-selective biotinylation, streptavidin-agarose retrieval and Western-blotting. (A) NIS localizes at the apical membrane in µ1AB-KDhNIS cells. Representative confocal immunofluorescence of apical xy sections from a z-stack and orthogonal xz views stained for NIS (red) and gp135 (green). Scale bar is 10µm. (B) NIS and TfR show decreased polarity whereas α-Na,K ATPase and gp135 have correct polarized plasma membrane distribution in µ1AB-KDhNIS cells. Representative Western-blot analysis and quantification of NIS, TfR, α-Na,K ATPase and gp135 proteins in apical (AP) and basolateral (BL) domains as percent of the total surface protein amount (AP+BL).

Next, we examined the subcellular localization of µ1A and its colocalization with NIS in MDCKhNIS cells transiently transfected with a µ1A expression vector tagged with HA. Few colocalization spots were detected between µ1A and NIS (0.206±0.03) in the *trans*-Golgi compartment shown as white dots in the colocalization inset in figure 39. These results indicate that AP-1A mediates NIS basolateral sorting at the TGN and in combination with the above findings in the double knockdown cells, reveal a clathrin adaptor carrier involved in NIS direct trafficking.

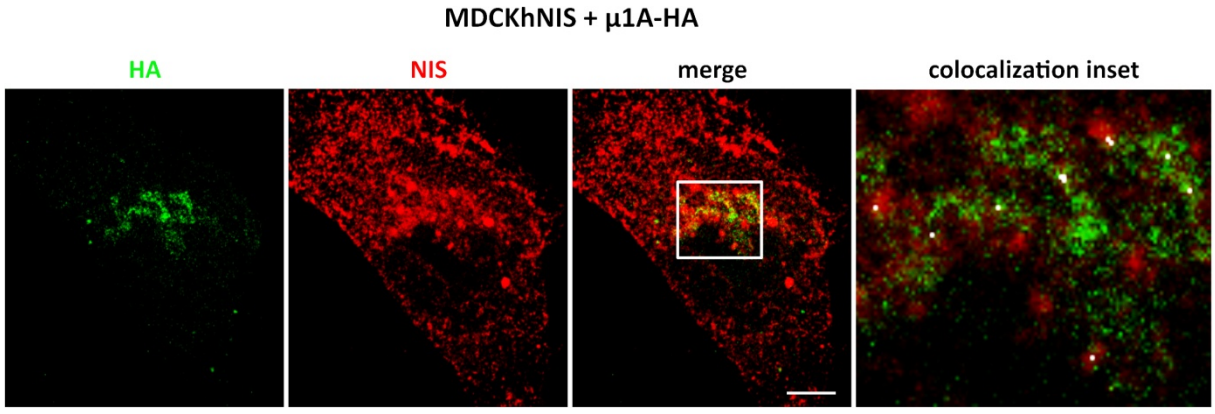

Figure 39. **NIS colocalization with exogenous µ1A in MDCKhNIS cells.** MDCKhNIS cells were transfected with µ1A-HA expression vector and proteins colocalization was analyzed 48 hours post-transfection by immunofluorescense. Representative single confocal section with HA (green) and NIS (red). Scale bar is 10µm. Region of interest in white box is augmented and colocalization points are shown in white dots.

2.6. TSH deprivation induces clathrin-independent NIS internalization and lysosome-mediated degradation.

NIS plasma membrane localization is crucial for the proper gland function, however in poorly differentiated or dedifferentiated thyroid cancers and upon certain stimuli *in vitro*, NIS is internalized from the plasma membrane (Kogai and Brent, 2012). Interestingly, TSH deprivation is also reported to induce NIS internalization in FRTL5 thyroid cells (Riedel et al., 2001). As we have been studying NIS biosynthetic pathway upon TSH stimulation, we also aimed to determine the TSH-dependent NIS internalization pathway in PCCl3 thyroid cells. Analysing NIS cytoplasmic tail and intracellular loops we identified a dileucine motif ^{560}PGLL^{563} and a tyrosine based ^{120}YLE[LM]^{123} motif in the cytoplasmic tail and the second intracellular loop respectively, that could both act as endocytic signals interacting with the clathrin-dependent endocytic (CDE) route. Specifically, AP-2 which is the main endocytic clathrin-associated adaptor, recognizes YxxØ and [DE]xxxL[LI] signals through its µ2 and α-σ2 subunits (Ohno et al., 1995, Doray et al., 2007) and therefore consists in a possible NIS carrier.

To study NIS internalization process, almost confluent PCCl3 follicular cells were initially cultured in starvation medium supplemented with TSH in order to stimulate NIS expression and membrane localization. Next, we removed TSH from the medium and performed time course kinetics followed by biotinylation and Western-blot analysis and we observed that membrane protein levels started to decrease after 24 hours of TSH deprivation as shown in figure 40A. Cells cultured without TSH for 48 hours showed a drastic decrease in both cytosolic and membrane NIS expression and localization (Fig. 40A) also confirmed by immunofluorescence microscopy (data not shown).

Then, to verify if NIS internalization follows a CDE pathway upon TSH deprivation, we colocalized NIS with AP-2, clathrin and transferrin receptor, all of them markers of the clathrin mediated endocytosis. As it can be appreciated in figure 40B, NIS did not colocalize with either of the proteins 24 hours after TSH removal indicating that this pathway is not involved in NIS early events of internalization despite its implication in NIS basolateral sorting.

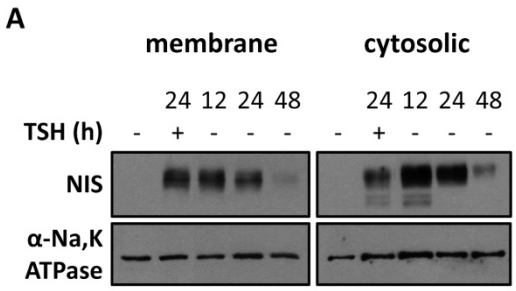

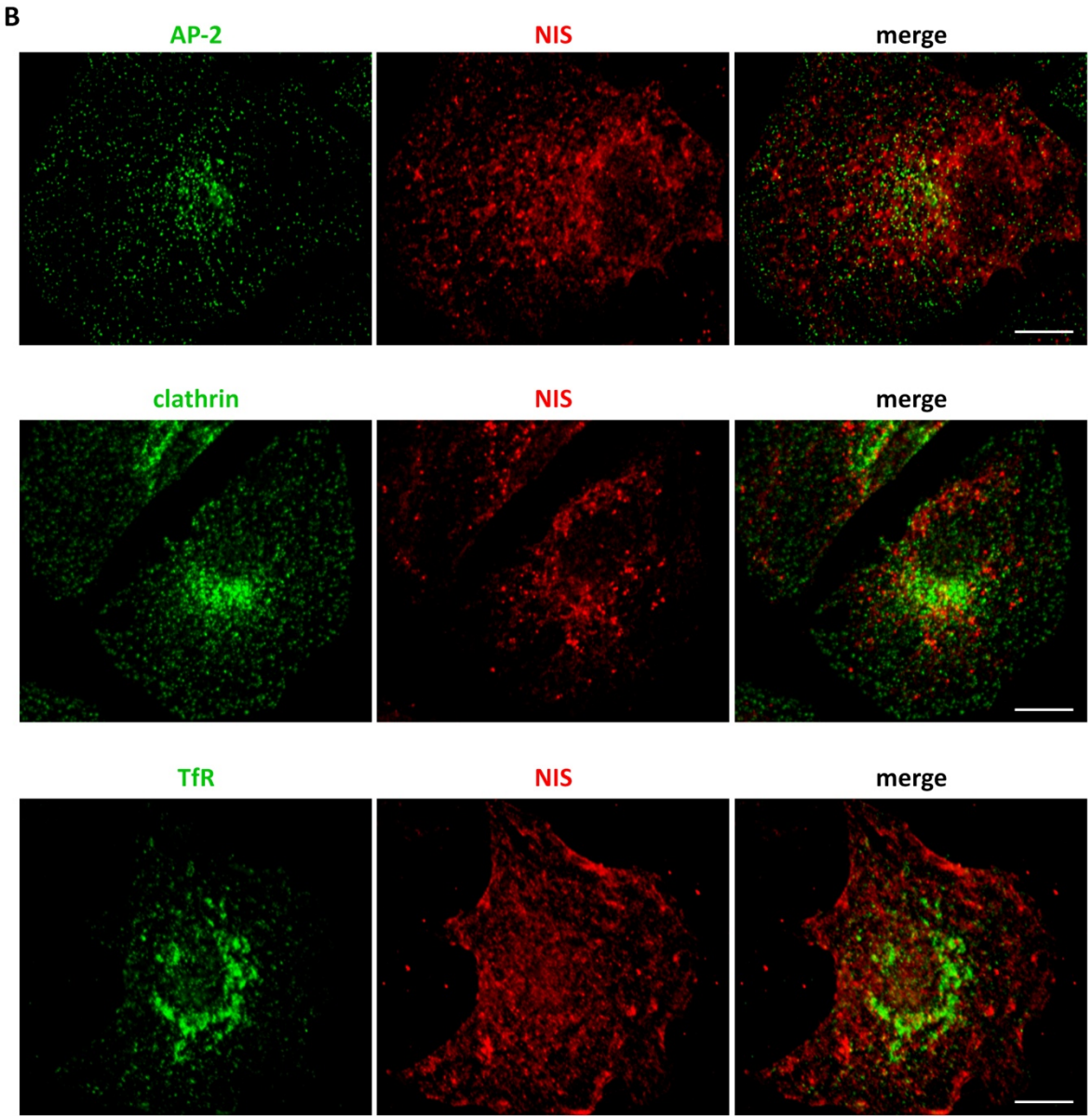

Figure 40. **NIS internalization follows a clathrin-independent pathway.** A) NIS leaves the plasma membrane 24 hours after TSH deprivation. NIS protein expression was detected by Western-blot in total and membrane-biotinylated extracts from PCCl3 cells grown in starvation medium during 5 days and then stimulated with TSH for 24 hours to induce NIS synthesis and plasma membrane targeting. Then TSH was removed for 12, 24 and 48 hours. α-NA,K ATPase was used to ensure equal loading. B) Membrane NIS suffers internalization at 24 hours of TSH deprivation. Representative single confocal immunofluorescence sections of PCCl3 cells stained for AP-2 (green, upper panels), clathrin (green, medium panels), transferrin receptor (green, lower panels) and NIS (red) at 24 hours of TSH removal in order to determine NIS colocalization with markers of clathrin-dependent pathway. Scale bar is 10µm.

Then, to check if the canonical endosome to lysosome pathway is implicated in NIS internalization we performed colocalization assays with early and late endosomal markers after 24 hours of TSH removal. NIS showed no colocalization with the early endosomal marker EEA1 or with the late endosomal marker syntaxin 7 (Stx7) as exhibited in figure 41A, at the upper and medium panels, respectively. Next, we examined NIS lysosome-mediated degradation through colocalization analysis with lysosomal markers as well as by lysosomal inhibition and Western-blot analysis (Fig. 41A lower panels and B).

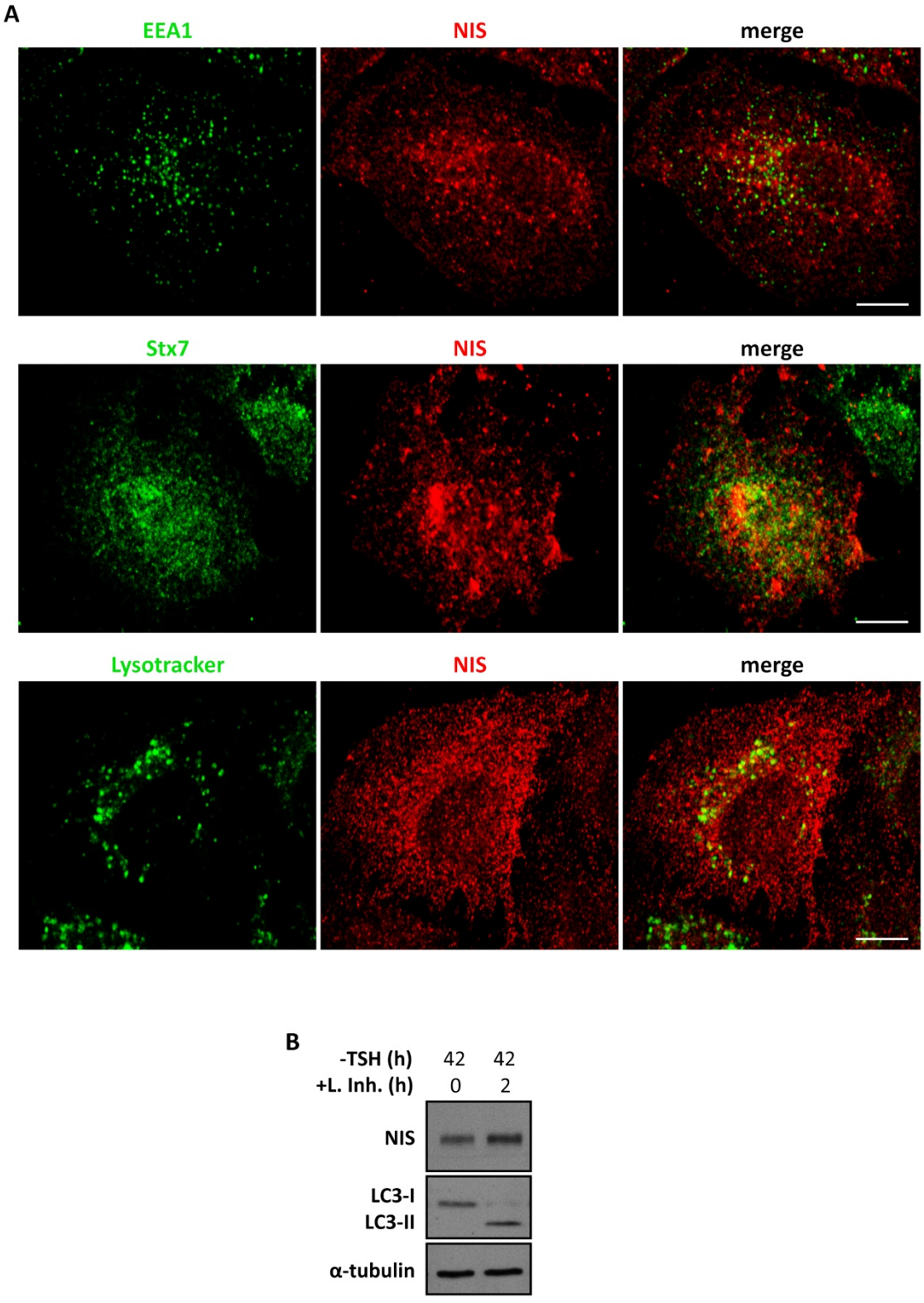

Figure 41. **NIS is degraded in lysosomes after removal of TSH.** A) Subcellular NIS localization in endosomal compartments after 24 hours of TSH deprivation. Representative single confocal immunofluorescence sections of PCCl3 cells stained for early endosomal protein EEA1 (green, upper panels), late endosomal protein syntaxin 7 (Stx7) (green, medium panels), lysosomal dye Lysotracker (green, lower panels) and NIS (red). Scale bar is 10µm. B) NIS accumulates after lysosome inhibition in the absence of TSH. NIS protein expression was detected by Western-blot in total extracts from PCCl3 cells after TSH removal for 42 hours with or without lysosomal inhibition (L. Inh.) for 2 hours. LC3 antibody was used to detect autophagosomes accumulation and thus serves as a lysosome-inhibition positive control. α-tubulin was used to ensure equal loading.

Although, we did not observe colocalization between NIS and the lysosomal dye lysotracker after 24 hours of TSH removal, lysosomal inhibition during 2 hours resulted in accumulation of NIS protein in the absence of TSH for 42 hours (Fig. 41B, upper panel). Lysosomes inhibition was indirectly evaluated through the autophagosomal LC3 protein that correlates with the number of autophagosomes in its lipidated membrane-bound LC3-II form (Tanida et al., 2005). Our results showed that autolysosomal degradation was efficiently inhibited, as the LC3-II protein was accumulated after the addition of lysosome inhibitors (L. Inh.) for 2 hours (Fig. 42B medium panel). Threrefore, we demonstrate that NIS is degraded in the lysosomes due to TSH removal for 42 hours.

Altogether these results indicate that the absence of TSH induces NIS internalization in a clathrin-independent way and lysosome-mediated degradation in rat thyroid follicular cells.

DISCUSSION

1. The follicular structure of the thyroid gland

Thyroid gland, as other epithelial organs, is generated during embryogenesis from groups of non-polarized cells by a combination of processes that induce the acquisition of cell polarity, lumen formation and the subsequent steps required for final gland morphogenesis. Throughout evolution, invertebrates do not produce thyroid hormones and lack a thyroid structure, although they respond to exogenous THs and are able to metabolize them (Eales, 1997). Conversely chordata, which include protochordata and vertebrates, established specific structures where thyroid hormones biosynthesis and storage take place. Endostyle was the first TH-producing organ formed in protochordata that evolved to a folliculated thyroid in the parasitic lamprey, a primitive vertebrate, and this folliculated thyroid structure is common in all vertebrates despite gross anatomic differences. Therefore, it seems that follicular structure is required for hormone synthesis, storage and regulated secretion in vertebrates, whether cell polarity is essential for iodide uptake. Accordingly, mammalian primary thyrocytes that show correct apical-basal polarity *in vitro* fail to synthesize T_3 or T_4 in monolayer, demonstrating that cell polarity is not enough for THs synthesis (Takasu et al., 1992). On the contrary, follicles formed from primary thyrocytes and embryonic stem cells in 3D ECM cultures, show thyroglobulin iodination and THs accumulation in the follicular lumen (Toda and Sugihara, 1990, Antonica et al., 2012). In humans, the physiological role of the gland can be disturbed due to disruption of thyroid hormone biosynthesis (dyshormonogenesis) or by developmental defects including thyroid agenesis or athyreosis, ectopia, hypoplasia and hemiagenesis, described as thyroid dysgenesis (TD). TD is present in 85% of congenital hypothyroidism (CH), a disorder with an incidence of about 1 per 3,500 newborns (De Felice and Di Lauro, 2004). Mutations in thyroid transcription factors have been associated to TD and involved epigenetic mechanisms are still to be elucidated (Fernandez et al., 2015). To illuminate thyroid morphogenesis classical 3D primary cultures (Chambard et al., 1981) and new model systems such as zebrafish (Opitz et al., 2013) or embryonic stem cells (Antonica et al., 2012) are now available.

1.1. *In vitro* thyroid follicle morphogenesis, polarity acquisition and lumen formation

In the present Thesis we established a 3D Matrigel culture system in which isolated mouse thyrocytes and rat FRT cells reorganized to form follicles in a morphological sequence very similar to that which occurs during embryogenesis. When cells are seeded in Matrigel their entire surface comes in contact with the extracellular matrix and in combination with the lack of cell´s basal lamina, cells lose polarity. At that time, primary thyrocytes resemble to the differentiated state of thyroid precursors at the stage of folliculogenesis during thyroid morphogenesis. Next, many small cavities are formed, accumulate and fuse to form a main cavity that could orient the mitotic spindle and cell division axis. This big

intracytoplasmic cavity has been also described in rat and porcine thyrocytes grown in 2D and 3D cultures, and it is considered to develop after possible fusion of Golgi secreted vesicles in order to constitute the apical side of the individual cells (Remy et al., 1980, Toda and Sugihara, 1990). This process seems to be the first step of thyroid follicle reconstruction. Then, single cells undergo cell division or aggregation and linkage with other cells and a follicular structure consisting of two or more cells is reconstructed supporting both theories of single cell and plural cell follicle origin (Toda et al., 1993). At that moment the component thyrocytes regain polarity as two different membrane domains are defined: a surface in contact with the ECM, and a contact site between the apposing cells.

Cell-ECM interaction is mediated by integrins that become fully activated upon engagement of ECM proteins. It is known that thyroid cells synthesize and secrete collagen IV and laminin in order to form basal lamina at the cell side that is not in contact with the neighbour cell (Frohlich et al., 1995). As a consequence, we demonstrate that β1-integrins become activated in the 3D environment and can thus transduce ECM signals involved in the establishment of polarized trafficking machinery, membrane domain identity and 3D follicular organization through still uncharacterized mechanisms in thyroid.

The recruitment of cell adhesion proteins to cell-cell contact site after the first cell division constitute the earliest evidence of cell surface polarization in two-cell follicles. Apical domains are formed when vesicles or vacuolar apical compartments (VACs) transporting apical membrane components (ezrin, Tg) fuse with the cell surface at the cell-cell contact and between sites of maturing tight junctions (TJs). The establishment of the TJs prevents lateral diffusion of proteins and lipids and therefore determines cell polarization.

The presence of filamentous actin delineating VACs and intracellular vesicles (data not shown) as well as its apical localization, where Rac1 is also observed from the early first steps of follicle polarization, suggest that actin cytoskeleton is involved in apical vesicular transport and fusion. Similarly, the subapically localized acetylated microtubules in thyroid follicles, also found enriched in 3D *vs.* 2D MDCK cysts (Quinones et al., 2011), may support apical cargo transport in polarizing follicles through specific motors as it is described in other cell models (Reed et al., 2006). Finally, lumen initiation occurs by apical membrane separation due to apically transported anti-adhesive factors that have been reported in other cell systems (Martin-Belmonte and Mostov, 2008).

Our findings in both cell type follicles support a lumenogenesis mechanism through a hollowing process according to which thyroid cells adhere without luminal space and then vesicles (FRT cells) or VACs (thyrocytes) containing luminal components are exocytosed in a coordinated way to a central luminal region. In FRT cells, vesicle fusion at cell contact site first defines apical membrane and then nascent lumen gradually grows by the constitutive transport and insertion of new membrane components. Conversely, in mouse thyrocytes a primitive apical luminal space is formed after VACs fusion with the

junctional complex and its local resolution leads to consequent coalescence between the VACs of the cells composing the follicle. Central lumen grows bigger through further VACs apical coalescence and this mechanism has been already reported in porcine primary cultures (Remy et al., 1977) and in the neonatal rat folliculogenesis (Nathaniel, 1986). The differences in lumenogenesis between the two cell types could be attributed to the role of TSH that appears to increase the secretion from the Golgi apparatus and enhances intervesicular fusion which promotes the formation of intracellular big vacuoles (Remy et al., 1983). Lack of such apical vacuolar compartments and slow luminal growth in FRT cells could be due to the absence of TSH receptor and therefore, to failure of TSH signalling. Alternative lumen formation mechanisms such as the cavitation that has been reported for grass snake thyroid (Rupik, 2012), may not be exclusive but mutually compensatory in case that one is perturbed, as it has been suggested in MDCK cyst lumenogenesis (Martin-Belmonte et al., 2008). Finally, mature polarized follicles are characterized by a central open lumen rich in thyroglobulin and ezrin-positive microvilli. Lumen expands thanks to ion and water efflux, while mature tight junctions prevent leakage. Apical recruitment of F-actin mediated by phosphorylated ezrin that in turn links to the apical membrane through binding to phosphoinositol-4,5-diphosphate (PIP2) (Fievet et al., 2004) can be generating force for lumen expansion and maintenance apart from supporting microvilli formation.

All these observations together, define thyroid follicle morphogenesis *in vitro*, in a process that could happen also *in vivo* during thyroid organogenesis. Thyroid cell-ECM and cell-cell interaction through β1-integrins signalling, adherens and tight junction initial formation as well as cell cytoskeleton organization contribute to apical-basal cell polarity acquisition. As a consequence, coordinated apical vesicular exocytosis and polarity protein distribution define apical domain and lumen initiation site. Lumen filling and tight junction maturation prevent colloid leakage and guarantee proper thyroid structure and function.

1.2. Pax8 as a regulator of follicle morphogenesis

One of the unsolved questions in thyroid morphogenesis concerns the molecular pathways that are involved in the three dimensional organization of thyroid epithelial cells into follicles. Taking advantage of the fact that FRT cells can undergo polarization into either 2D or 3D cultures, we used microarray analysis and we found several gene sets known to be implicated in 3D epithelial architecture. As most studies of cell polarization have focused on post-translational events implicated in proteins organization and distribution, and little is known about transcriptional events involved in the development of epithelial polarity; we focused on the transcriptional changes that accompany polarization in FRT cells and relate them to key steps in the development of cell polarity. Our findings have uncovered the

transcription factor Pax8 within a complex pattern of regulation of genes that correlated with the formation of structural and functional characteristics of polarized follicles.

According to our results, Pax8 controls the orientation of apical-basal polarity during follicle formation. The apical pole of Pax8 silenced follicles is consistently inverted towards the follicle periphery and this phenotype contrasts with the loss of polarity or multiple lumens formation that is frequently observed when regulation of polarization is disrupted (Martin-Belmonte et al., 2007, Jaffe et al., 2008). It also underscores the independent natures of pole formation and pole orientation. Thus, in Pax8 knockdown cells, the microvillar protein ezrin is redistributed to the outer surface of follicles where presents a continuous or a patchy distribution and forms surface blebs that protrude towards the ECM. Similar basal ezrin localization has been reported in patients with Sjögren´s syndrome characterized by disorganized salivary acini, basal SNARE complex localization and ectopic mucin exocytosis (Barrera et al., 2012).

Polarized cytoskeleton is generally affected as actin filaments appear delocalized at the periphery of the follicles and link to phosphorylated ezrin at the base of the protrusions. As ezrin binds to membranes containing PIP2 simultaneously to F-actin binding, failure in apical membrane enrichment in PIP2 could explain the inverted phenotype. Acetylated microtubules polarized apical distribution is also disrupted showing a diffuse basal cytoplasmic localization. The role of microtubules (MT) cytoskeleton in maintaining thyroid cell polarity and follicular organization through MT-dependent transport of TJ components and VACs has been reported (Yap and Manley, 2001), and make us hypothesize that TJ mistargeting at the lower-lateral plasma membrane could be due to impaired MT polarized organization. Moreover, MT-dependent Golgi positioning towards the basal cell side reveals that intracellular polarity is misoriented too (data not shown).

To initiate a luminal space *de novo* during the development of follicle polarity, apical membrane components must be delivered to the site of lumen initiation between neighboring cells. Pax8-induced polarity inversion observed from the first cell division led to lumen disappearance in mature follicles, consistent with the evidence that apical membrane biogenesis in the determining step that establishes the follicular lumen and hence completes folliculogenesis (Yap et al., 1995b). Phenotypic differences among follicles and between cells of the same follicle related to ezrin or actin localization were due to silencing heterogeneity. Thus, it seems that the inverted apical pole is subject to remodelling in response to restored Pax8 signalling.

This is the first time that a thyroid transcription factor is related to follicular polarity and follicle formation. The fact that FRT cells have lost all the thyroid differentiation markers and thyroid transcription factors except from Pax8, but have maintained the ability to polarize and form three-dimensional follicle like structures, reinforces our findings about the important role Pax8 in cell

polarization and follicle formation and constitute this cell line an ideal model system to study the molecular mechanisms implicated in thyroid folliculogenesis.

1.3. Cdh16 impairs cell cytoskeleton polarized distribution and leads to inversion of cell polarity during follicle morphogenesis

Despite the polarity inversion due to Pax8 loss, cell-cell junctions are formed and basolateral markers of adherens junctions as β-catenin remain concentrated in contact zones between cells. However, cadherin-16 (Cdh16) mRNA and protein levels are dramatically diminished in the absence of Pax8 in primary thyrocytes and FRT cells, confirming the transcriptional regulation of Cdh16 by Pax8 transcription factor previously reported in thyroid cells (Ruiz-Llorente et al., 2012) and in Pax8 KO mice (de Cristofaro et al., 2012). Our microarray results show that Cdh16 is upregulated during thyroid follicle morphogenesis and its important role in 3D MDCK cyst formation has also been demonstrated (Galvez-Santisteban et al., 2012). Interestingly, silencing Cdh16 in FRT cells and primary thyrocytes reveals similar defects in apical domain and cytoskeleton orientation, TJ localization and lumen formation as in Pax8 depleted follicles, suggesting that a Pax8-Cdh16 pathway may be involved in apical domain orientation from the first steps of polarity acquisition. As adherens junctions are apparently unaffected due to other cadherins expression at the cell-cell contact, while cell cytoskeleton is completely delocalized, we suggest that Cdh16 absence from the initial contact site of two-cell follicles is responsible for the incorrect actin and microtubule distribution and consequently for the apical membrane components mistargeting. As cells keep dividing, new contact sites lacking Cdh16 fail to guide and dock apical cargo properly, and the follicles formed present apical domain both in the center and at the periphery of the follicles. This hypothesis is supported by the apical re-localization of actin filaments after Cdh16 exogenous expression in Pax8 depleted cells.

However, a direct interaction between Cdh16 and cytoskeleton remains unclear in thyroid cells, and the lack of β-catenin binding site in Cdh16 cytoplasmic tail (Wendeler et al., 2004) indicates the requirement of a protein linker between Cdh16 and actin filaments. αB-crystallin (CRYAB), a small heat shock protein involved in the stabilization and regulation of cytoskeletal proteins such as actin, vimentin and tubulin, among others (Nicholl and Quinlan, 1994, Wang and Spector, 1996, Arai and Atomi, 1997), is demonstrated to interact with actin filaments linking them to Cdh16 at the basal side of renal collecting ducts (Thedieck et al., 2008). This chaperone is expressed in the thyroid gland and demonstrates a consistent reduction correlated to Cdh16 reduction observed in papillary and follicular thyroid carcinomas as well as to a complete protein abrogation and loss of follicular architecture in anaplastic thyroid carcinomas (Cali et al., 2012). The role of CRYAB as a link between Cdh16 and cortical actin cytoskeleton remains to be demonstrated in polarizing thyroid follicles through co-immunoprecipitation

experiments and confocal colocalization analysis. However, our results reveal a regulatory path that explains the reported reduction in CRYAB expression levels in thyroid tumours and is in agreement with its use as a differentiation marker in thyroid tissues as it is the consequence of Pax8 loss which is the master gene of thyroid differentiation. Interestingly, the expression of Pax8 is significantly decreased in almost 70% of thyroid cancers, along with reduced NIS expression, especially in poorly differentiated thyroid cancers (Puglisi et al., 2000). Nevertheless, Pax8 screening and further correlation between its expression and CRYAB expression in thyroid carcinomas is necessary. Loss of CRYAB could also explain the cytoskeleton rearrangements necessary to the tumour cells in order to lose the differentiated polarized phenotype and suffer the epithelial-mesenchymal transition.

Moreover, the observed up-regulation of Pax8 in Cdh16 depleted cells could be explained as a compensatory mechanism for the cell in an attempt to regain the loss Cdh16 expression and reverse the dedifferentiation and loss of polarity process in case of Pax8 loss. Pax8 increase can also be responsible for the milder phenotype observed, concerning central lumen formation and apical polarity in Cdh16 depleted follicles, as Pax8 downstream targets involved in apical transport such as Rab17, Rab8a, Rab11a and Myo5b would be reinforced in these conditions. Interestingly, mRNA levels of Rab17 and Myo5b genes that are transcriptionaly regulated by Pax8 and upregulated in FRT follicles; are significantly reduced in Pax8 but not in Cdh16 silenced FRT cells (not shown). Both Rab17 and Myo5b - associated with Rab8a and Rab11a are required for apical membrane trafficking and *de novo* lumen formation through apical recycling endosomes and basolateral to apical transcytosis (Rodriguez-Boulan and Macara, 2014). Moreover, mutations in Myo5b are a cause of microvillus inclusion disease, characterized by the failure to form a mature apical membrane and the appearance of large intracellular vacuoles that contain microvilli, mainly in enterocytes (Ruemmele et al., 2010). This data suggests a specific role of Pax8 in apical membrane definition through its targets, whose role in thyroid folliculogenesis need to be elucidated through gain- and loss-of-function experiments.

Altogether, these results led us to postulate a pathway in which deletion of Pax8 inhibits the expression of Cdh16 and of its cytoplasmic partner CRYAB. As a consequence, actin filaments and microtubules distribution and stabilization at the initial cell-cell contact site is impaired and they may no further serve as tracks and docking mediators for apical vesicles and VACs at the apical membrane initiation site. Additional disruption of the apical trafficking machinery due to the transcriptional inhibition of Myo5b, Rab17 and other Pax8 indirect targets involved in polarized apical traffic impair the formation of the apical domain in the centre of the follicle. All the above mentioned events in combination with a wrong extracellular cue would lead to apical domain inversion followed by cytoskeleton components basal accumulation and organization. This transcriptionally regulated set of genes and their interactions correlated with the formation of structural and functional characteristics of polarized follicles could have

great relevance in other organs such as the kidney, in which Pax8 is highly expressed and cadherin-16 is involved in the later stages of tubulogenesis (Thedieck et al., 2005).

1.4. Rac1 role in follicular polarity orientation

In vivo and *in vitro* experiments performed in different cellular models have demonstrated that correct orientation of cell polarity and tissue morphogenesis depend on laminin assembly in the cells basement membrane through activation of β1-integrins outside-inside signalling pathway that in turn activates the cytosplasmic Rho-GTPase Rac1 (O'Brien et al., 2001, Yu et al., 2005, Wu et al., 2009). Inhibition of β1-integrin prevents organization of laminin around the MDCK cysts periphery and leads to inversion of polarity through activation of RhoA-ROCK I-myosin II (Yu et al., 2008). In the present study, we see that β1-integrins are activated in the FRT follicles and that loss of Cdh16 downregulates their expression. To further understand the mechanisms that lead to polarity misorientation in thyroid follicles due to Pax8 depletion and Cdh16 inhibition, we need to examine the localization of β1-integrin and laminin assembly in silenced follicles. Moreover, evaluation of Rac1 and RhoA activity through effectors pull down assays would give us more information about the implication of those paths in inverted follicles due to Pax8-dependent Cdh16 loss and the consequent downregulation of β1-integrin.

Although integrin-ECM engagement leads to Rac1 cytoplasmic activation and correct laminin assembly providing one cue of polarity, active Rac1 localization at the newly formed cell-cell contact provides another cue participating in cadherins transport through actin polymerization and adherens junction assembly. At the nascent AJs, cadherins can further activate Rac1 in order to mark a site for actin assembly at the cell surface, and can also stimulate Cdc42 activation and therefore promote the functionality of the Par/aPKC complex which translocates to apical sites of cell-cell adhesion and determines apical-basal membrane polarity. In our system we observe that exclusive Rac1-GTP localization in the apical domain is necessary in order to establish correct apical-basal polarization in newly polarized two-cell follicles. The apical membrane initiation site is defined by active Rac1 that is further carried to the preapical patch by actin filaments, as vesicles positive for F-actin and Rac1 are visualized first close to the adjacent cells plasma membrane and then integrated in it. Locally activated Rac1 might also recruit IQGAP, enabling it to polarize microtubules at the apical contact region (Fukata et al., 2002). Bigger follicles maintain Rac1 apically following the same localization pattern as actin filaments. Conversely, Rac1 localization in the periphery of the structures in Pax8 and Cdh16 silenced follicles is coupled to actin filaments basal accumulation that in turn leads to basal ezrin activation and the formation of ezrin-rich protrusions probably due to the increased local Rac1 activity. In that way follicle formation is compromised. Exogenous expression of Rac1-GTP is always apically localized and

restores ezrin and actin filaments apical localization, indicating that local activation of Rac1 is essential to polarized cytoskeleton and apical domain definition process.

Taking our findings together with already reported data we propose the following mechanism involved in follicular polarity and lumen formation summarized in figure 42:

When unpolarized follicular thyroid cells expressing Pax8 are surrounded by ECM the epithelial polarity program is correctly executed. First, intracellular vacuoles are formed and accumulate at a specific cell site where fuse with each other (Fig. 42, single cell) in a process that may orient the mitotic spindle and tell the cell in which axis to divide. As soon as the first cell division takes place, β1-integrin (Itgb1) activation from components of the ECM leads to Rac1 cytoplasmic activation and thus laminin secretion and assembly at the basement membrane establishing the axis of apical-basal cell polarity (Fig. 42, unpolarized two-cell follicle). Simultaneous, actin polymerization triggered from active Rac1 mediates cadherins transport at the cell-cell contact zone where establish homophilic junctions between the two cells. Consequently, actin filaments and microtubules transiently link to the intracellular domain of cadherin-16 (Cdh16) through CRYAB, as well as to E-cadherin by α-catenin and dynein complex, respectively (Fig. 42, unpolarized two-cell follicle). In that manner, adherens junction-cell cytoskeleton interaction establishes trafficking paths towards the apical membrane initiation site facilitating the transport and local activation of Rac1, Cdc42 and polarity complex proteins.

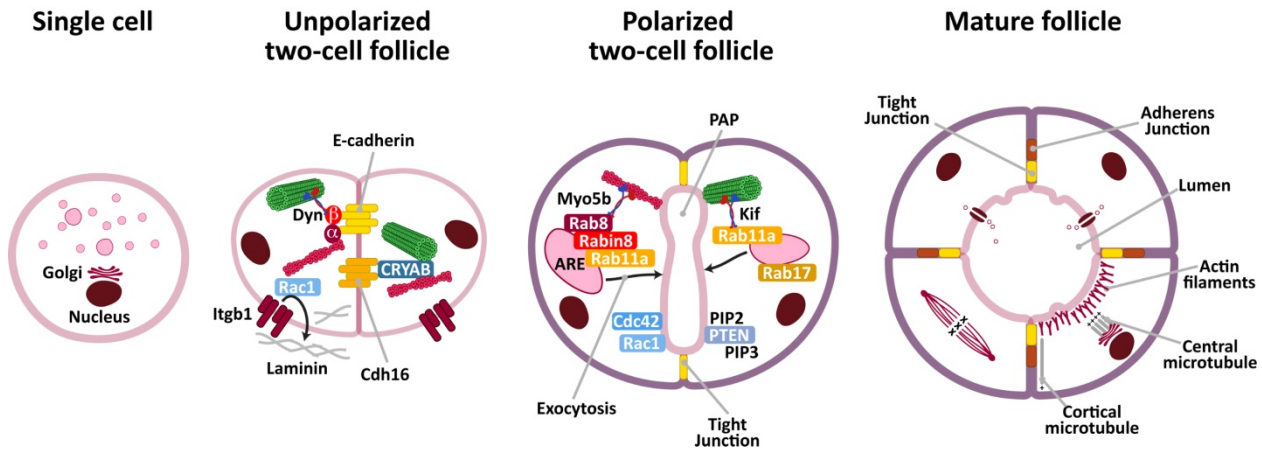

Figure 42. ***In vitro* thyroid follicle morphogenesis mechanisms.** Unpolarized single cells embedded in Matrigel accumulate vacuoles and then divide to form a two-cell follicle with loose cell-cell contacts rich in cadherins. Itgb1 activation leads to Rac1 cytoplasmic activation and basal laminin assembly that establish the axis of cell polarity through cytoskeleton organization. Actin filaments carry Rac1 at the cell-cell contact where promotes further cadherin transport and binding to the cell cytoskeleton. E-cadherin binds to actin filaments and to microtubules through α-catenin (α) and β-catenin (β)-dynein complex (Dyn), respectively. Cdh16 binds to actin filaments and microtubules through CRYAB. In polarizing two-cell follicles, Cdc42, polarity complex and PTEN apical localization determine cell polarity and membrane identity. VACs rich in apical membrane components are transported by Rabs and motor proteins (Myo5b and Kifs) at the apical membrane initiation site where are exocytosed leading to the formation of the preapical patch (PAP) and subsequent lumen initiation. Ion channels and pumps participate in lumen expansion, TJ prevent colloid leakage and a mature follicle is finally formed.

Once Cdc42 localizes at the AMIS coordinates the distribution of polarity complexes in order to define apical-basal membrane polarity. The apical accumulation of PTEN by the Par complex leads to the exclusion of PtdIns(3,4,5)P3 (PIP3) and the apical enrichment of PtdIns(4,5)P2 (PIP2) which is necessary for apical membrane definition. Additionally, Rac1 regulates actin filaments formation and microtubules polarized distribution and concentration at the under-formation apical domain. As a consequence, vesicular transport of apical membrane components mediated by Rabs and facilitated by actin and microtubule motors, is correctly directed towards the apical surface limited by the tight junctions. This process converts AMIS into a preapical patch (PAP) that marks lumen initiation (Fig. 42, polarized two-cell follicle). Vesicular fusion with the membrane and apical domain expands giving place to the preapical patch that will next form the follicular lumen with the help of ion channels and pumps (Fig. 42, mature follicle). Mature lumen presents microvilli rich in ezrin that increase the membrane surface necessary for thyroglobulin iodination and hormone synthesis. Mature tight junctions at the upper-lateral membrane site prevent colloid leakage and guarantee follicle integrity.

In the absence of Pax8, cells lack Cdh16 in the nascent adherens junctions and through a mechanism that we still ignore, Cdh16 loss downregulates Itgb1 expression at the plasma membrane. We hypothesize that this results to an inhibition of signal transduction from the outside-inside signalling pathway that in turn impedes Rac1 cytoplasmic activation and laminin assembly at the basement membrane and therefore inverts apical-basal axis. Due to Rac1 inactive state, actin polymerization and Rac1 transport at the initial contact site through actin filaments are impaired. As a consequence, local Rac1 activation and thus polarized cytoskeleton distribution at that region are further affected. Moreover, the absence of Cdh16 from the cell-cell contact and the additional loss of CRYAB inhibit actin filaments and microtubules to link and get stabilized at the contact site through their interaction with cadherins and they instead follow Rac1 basal distribution. In that manner, although AJ are finally defined, the routes towards the surface between the apposing cells are misoriented and apical protein delivery is also affected due to the suppression of proteins that participate in apical vesicular traffic, such as Rab17, Myo5b and other Pax8 targets. As a consequence apical components are finally delivered at the periphery of the follicle and tight junctions have lower-lateral localization. Finally, lumen fails to get formed and follicles present characteristic microvillar protrusions towards the ECM. It seems probable that changes in PIP2 distribution due to PTEN mislocalization in Pax8 depleted follicles would lead to the rearrangements observed for the proteins evaluated in the current work.

It is well established that transcriptional regulation of the polarity machinery can modify the behavior of epithelial differentiated cells or stem cells and lead to diseases such as epithelial cancer (Moreno-Bueno et al., 2008). In the case of thyroid carcinomas, more than 90% of all the tumors arise from follicular thyroid cells. Although inversion of thyroid follicular polarity has not been reported yet, inversion of

glandular epithelial polarity has been detected in a subset of invasive ductal breast carcinomas, demonstrating that inversion of polarity can also occur *in vivo* during tumorigenesis (Adams et al., 2004).

2. Iodide transport as a determinant of follicular function

Thyroid function depends on the adequate supply of iodide (I^-), an essential constituent of thyroid hormones. I^- is a scarce element in the environment and can be acquired only through the diet. As the reported concentration of free I^- in mammalian plasma is only 50nM to 300nM (Carrasco, 1993), the thyroid evolved an extremely efficient mechanism to actively accumulate I^- from the blood. The nature of I^- conduit was a subject of debate for many decades. At one point, even phospholipids were proposed to act as I^- carriers through complexing anions and making them lipid-soluble (Vilkki, 1962). Ultimately, the molecule responsible for active iodide transport in the thyroid was identified as NIS (Dai et al., 1996), which is located at the basolateral membrane of thyroid epithelial cells. NIS membrane localization and function have been exploited for diagnosis and therapeutic management of benign thyroid diseases and thyroid cancers. To treat hyperactive thyroid states and differentiated thyroid carcinoma, radio-iodide therapy is successfully used thanks to NIS mediated $^{131}I^-$ uptake. Conversely, in the case of congenital hypothyroidism resulting from mutations in *SLCA5A* gene, the specifically referred as iodide transport defect (ITD) is diagnosed by reduced or absent thyroid I^- uptake. Molecular characterization of these mutations found in ITD patients localized in distinct transmembrane segments (TMSs), intracellular helix and loops between TMSs, reveal mostly non-functional although membrane localized protein, as well as immature, intracellular retained NIS (Portulano et al., 2014). Diminished iodide uptake in poorly differentiated or dedifferentiated carcinomas, despite NIS expression or over-expression, revealed intracellular NIS localization (Dohan et al., 2001) pointing out that membrane targeting is crucial for NIS function. Taking in account the great physiological and clinical importance of NIS basolateral localization, we aimed to elucidate the still unknown mechanisms by which NIS is targeted to, retained at, and retrieved from the basolateral plasma membrane.

2.1. NIS plasma membrane sorting mechanisms.

It is well known that functional NIS expression is regulated at both transcriptional and post-translational levels. TSH is its primary regulator in thyroid gland and also demonstrated to participate in NIS post-translational regulation and membrane translocation. The exact sorting mechanisms and the specific basolateral trafficking pathways are still unknown and our results shed some light on these aspects.

Using two different cell models we demonstrate for the first time that NIS is transported towards the plasma membrane in a clathrin-mediated pathway. In thyroid cells *de novo* NIS synthesis induced by TSH is followed by NIS sorting at the TGN and the recycling endosomes (REs) through the AP-1 clathrin

adaptor complex. Interestingly, NIS travels in REs along with the basolateral transmembrane transferrin receptor (TfR), which is already known to interact with the clathrin machinery. To define the components of the trafficking machinery involved in NIS transport to the basolateral surface of polarized epithelial cells we made use of the polarized MDCK cell system knockdown for the μ1A and μ1B subunits. Depletion of μ1B results in apical NIS mislocalization and demonstrates that AP-1B is a key NIS sorting element as its function cannot be fully compensated by AP-1A or other adaptors. Conversely, we found that knockdown of μ1A can mislocalize AP-1B cargo only when μ1B subunit is missing, suggesting that AP-1B can fully compensate the role of AP-1A in agreement with previous studies (Gravotta et al., 2012). NIS mislocalization in the double knockdown is expected to be more prominent in higher *AP1M1* depletion conditions, as the two basolateral proteins used as controls, the Na,K ATPase and TfR, showed either no regulation or slight depolarization in contrast to their demonstrated depolarized levels. Taking in account that the biosynthetic delivery of TfR depends on μ1A in MDCK cells (Gravotta et al., 2012) and that newly synthesized NIS colocalizes with TfR in PCCl3 cells, we suggest that AP-1A is responsible for NIS direct biosynthetic delivery from the TGN, whereas AP-1B controls indirect NIS transport or/and recycling at the common recycling endosomes (CREs) that have the ability to carry both apical and basolateral cargo.

Our findings are in agreement with the generally accepted role of each μ subunit, according to which μ1A and μ1B mediate basolateral sorting predominantly at the *trans*-Golgi network and the recycling endosomes, respectively (Folsch et al., 2003, Cancino et al., 2007). However, a recent publication comes to demonstrate that both proteins largely colocalize with each other and to similar extents with TGN and recycling endosome markers, as well as with basolateral cargos transiting biosynthetic and endocytic-recycling routes (Guo et al., 2013). The authors suggest that the two isoforms differ in their signal-recognition specificity in order to expand the repertoire of signals recognized by AP-1 for sorting a broader range of cargos to the basolateral surface. Our immunofluorescence results showed some extent of colocalization between μ1B and the TGN suggesting that this protein could sort NIS at both TGN and CRE compartments. Moreover, similar degree of colocalization between NIS and both isoforms could further imply a possible NIS interaction with each of them at the TGN through different sorting motifs supporting the recent theory. Both medium subunits of AP-1A and 1B adaptors have been shown to recognize conventional tyrosine-based YxxØ sorting motifs or non-conventional signals in the cytoplasmic tail of the cargo proteins (Carvajal-Gonzalez et al., 2012, Guo et al., 2013). NIS presents two tyrosine-based sorting signals resembling canonical YxxØ motif and one similar to Yx[FYL][FL]E, all of them in the intracellular helix between the third and fourth transmembrane domains. Although this domain is not a common site for sorting motifs, we believe that it is important for correct NIS membrane traffic as a R124H mutation reported in patients with ITD and localized a few amino acids

after the Y-motifs, caused NIS intracellular retention (Paroder et al., 2013). Mutational analysis of the putative tyrosine-based sorting motives followed by steady-state NIS distribution assays will indicate the NIS BL sorting signals. Additionally, to demonstrate a protein-protein interaction between μ1B subunit and NIS we carried out in MDCK cells after exogenous expression of both proteins. Still, we have not been able to demonstrate an interaction and this could be due to either a weak interaction between the proteins or to the small amount of NIS that localizes at the TGN/RE compartment at a specific time point. Nevertheless, we cannot exclude the role of leucine-based motifs localized at NIS cytoplasmic tail in mediating basolateral NIS sorting through their interaction with AP-1 and unknown adaptors.

To date, the contribution of the ubiquitous AP-1A and the epithelial specific AP-1B adaptors to basolateral sorting of thyroid protein markers and their regulation in thyroid cells is unknown. Knowledge of the exact mechanisms and the specific transport carriers in thyroid and in other NIS expressing tissues would lead to new therapeutic approaches to further enhance functional endogenous NIS expression and exogenous NIS introduction via gene transfer expanding application of ^{131}I therapy. However, basolateral NIS targeting cannot be completely explained by the activities of clathrin adaptor complex AP-1A or AP-1B, either singly or together. Although some sorting events are clearly dependent on this class of adaptor, it is clear that other such sorting elements remain to be discovered. The contribution of the clathrin independent AP-4 adaptor to NIS sorting is one candidate due to the presence of Yx[FYL][FL]E signal that has been reported to be implicated in basolateral cargo sorting (Burgos et al., 2010).

Our results together with reported data suggest a novel pathway responsible for NIS basolateral membrane targeting. As shown in figure 43, NIS sorting takes place at the TGN and CREs and is mediated by AP-1A and AP-1B clathrin-adaptors. It is possible that both AP-1A and AP-1B localize at the TGN and that AP-1A is responsible for NIS direct basolateral targeting, whereas AP-1B is implicated in NIS indirect transport and recycling through common recycling endosomes. In that way, thyroid cells may have at least two alternative paths to guarantee effective NIS targeting at the basolateral membrane in order to fulfil its function. Additional adaptors and alternative simultaneous paths implicated in NIS basolateral targeting are possible and remain to be elucidated.

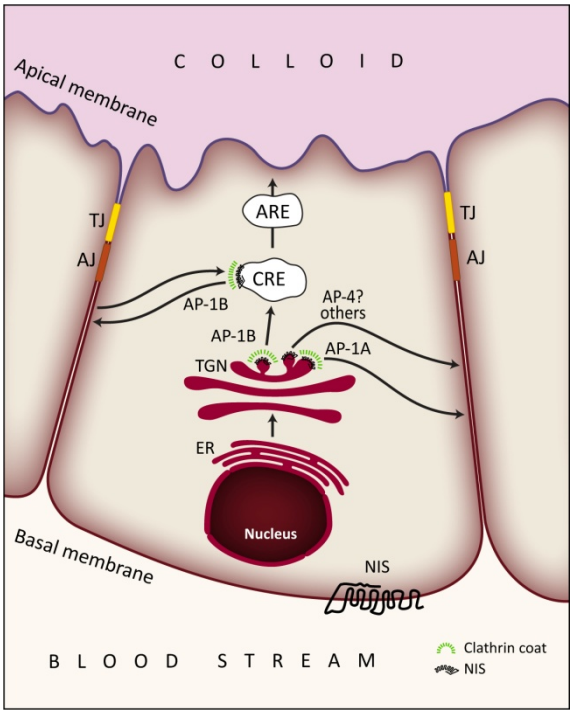

Figure 43. **Possible NIS basolateral sorting pathways in follicular thyroid cells.** AP-1A clathrin adaptor sorts NIS at the TGN in a direct basolateral route. AP-1B clathrin adaptor localized at TGN and CRE sorts NIS in CRE-mediated basolateral biosynthetic and recycling pathways. Alternative adaptors e.g. AP-4, could also sort NIS directly from TGN to the basolateral plasma membrane.

2.2. NIS internalization as a cause of thyroid pathology

NIS internalization has been reported in several *in vivo* and *in vitro* studies after different stimuli and through diverse pathways (Kogai and Brent, 2012). Among them, the absence of TSH is one of the factors that induce NIS internalization and our observations in PCCl3 cells confirm the results reported in FRTL5 cells (Riedel et al., 2001). In order to determine this thyroid-specific NIS endocytic pathway induced by TSH deprivation we performed inmmunofluorescence colocalization experiments with different endocytic markers. Although we were expecting the implication of the clathrin-dependent endocytic pathway, due to the presence of tyrosine- and leucine-based signals in NIS amino acid sequence and the clathrin adaptors involvement in NIS basolateral sorting, we weren´t able to demonstrate such an interaction. These results underline the fact that different biosynthetic, recycling and internalization routes and machineries can be involved in the traffic of the same protein as it was demonstrated in the case of the overlapping tyrosine-based BL sorting signal with the endocytic signal in the neurotrophin receptor p75 that was not recognized by the same clathrin machinery in FRT cells (Lipardi et al., 2002). We could neither detect any interaction between NIS and the components of the classical endosomal route that includes early and late lysosomes and ends up with protein lysosomal degradation. However, lysosomal inhibition resulted in NIS and autophagosomal marker accumulation indicating that after long TSH deprivation NIS is degraded in the lysosomes. Additional endocytic

markers and alternative experimental approaches including inhibition of dynamin-dependent endocytosis may give us useful information about TSH-dependent NIS endocytosis.

Intracellular NIS localization observed in poorly differentiated and dedifferentiated thyroid cancers may be due to failure of NIS translocation to the cell membrane or NIS internalization. Altered NIS trafficking would be the reason for its intracellular retention, whether activation of endocytic mechanisms would explain its internalization. The mechanisms that lead to NIS retrieval and the trafficking paths are largely unknown. Among the factors that induce NIS exclusion is the PTTG-binding factor (PBF), an oncogene that is significantly increased in thyroid cancers. Interestingly, exogenous PBF is predominantly expressed in CD63-positive late endosomes in Cos7 cells where colocalizes with internalized NIS (Smith et al., 2009). Moreover, our laboratory has demonstrated that $BRAF^{V600E}$ mutation in papillary carcinoma impairs NIS targeting at the plasma membrane (Riesco-Eizaguirre et al., 2006) through TGFβ secretion via an autocrine loop (Riesco-Eizaguirre et al., 2009). Willing to determine the traffic mechanisms involved we treated differentiated PCCl3 cells with TGFβ and we have observed a quick loss of NIS membrane steady-state localization indicating an internalization process (data not shown). Identification of NIS endocytic pathway upon TGFβ addition would then open a new field of study on the use of specific inhibitors to block internalization with an important clinical value.

3. Development of a functional thyroid gland

On the whole, the results of this Thesis uncover a new role for Pax8 as one of the main regulators of thyroid gland morphogenesis. Up to now it was mainly considered as the master regulator of the differentiated thyroid phenotype due to the transcriptional activation of *Tg*, *Tpo* and *Slc5a5* genes in thyroid cells. However, proper thyroid differentiation requires a polarized distribution of these thyroid protein markers. We demonstrate that Pax8 determines follicular cell apical-basal polarity orientation, polarized cytoskeleton organization and lumen formation through direct and indirect regulation of genes that are components of adherens junctions, tight junctions and the apical trafficking machinery. Moreover, it is known that Pax8 regulates Wnt4, which is necessary for the maintenance of the epithelial phenotype of thyroid cells, and that also controls proliferation, apoptosis and cancer pathways (Fernandez et al., 2015). For all these reasons, deregulation of Pax8 expression would impair follicular structure, transform polarized epithelial phenotype and spoil differentiated thyroid state including NIS expression and membrane localization leading to a non-functional thyroid gland.

CONCLUSIONS

1. Thyroid follicles acquire apical-basal cell polarity at the first cell division and define the apical membrane at a specific site of the cell-cell contact through exocytosis of apical membrane components leading to lumen formation in a process called hollowing.

2. Pax8 transcription factor regulates thyroid follicle formation through its transcriptional targets that are involved in epithelial polarity programme.

3. Pax8 silencing impairs cytoskeleton organization at the apical membrane initiation site due to the inhibition of cadherin-16 and of its possible cytoplasmic partner and cytoskeleton linker, αB-crystallin.

4. Pax8 silencing downregulates β1-integrins expression through cadherin-16 and misorients Rac1 apical transport mediated by actin filaments. Rac1 apical activation restores apical organization of the filaments, correct apical domain orientation and follicular lumen formation.

5. Sodium/Iodide symporter NIS is transported towards the basolateral plasma membrane in a clathrin-mediated pathway through clathrin adaptor AP-1 and TfR positive vesicles.

6. NIS basolateral sorting takes place at the *trans*-Golgi compartment and the recycling endosomes through the AP-1 clathrin adaptor complexes.

7. The medium subunit of AP-1B adaptor is required for NIS basolateral sorting at the biosynthetic and/or recycling routes. In the absence of μ1B, NIS is apically missorted where is still functional.

8. The medium subunit of AP-1A adaptor participates in NIS direct trafficking from the trans-Golgi to the basolateral membrane, and in its absence AP-1B fully compensates its function.

9. Internalized NIS follows a clathrin independent pathway and is finally degraded in lysosomes.

CONCLUSIONES

1. El folículo tiroideo adquiere la polaridad ápico-basal tras la primera división celular determinando el dominio apical en la zona de contacto entre las dos células a través de exocitosis de componentes de membrana apical que da lugar al lumen mediante un proceso denominado “hollowing”.

2. El factor de transcripción Pax8 regula la formación del folículo tiroideo a través de sus dianas transcripcionales implicadas en la polarización epitelial.

3. El silenciamiento de Pax8 impide la organización del citoesqueleto en el sitio de iniciación de la membrana apical mediante la inhibición de cadherina-16 y de su posible proteína de unión al citoesquleto, cristalina alfa B.

4. El silenciamiento de Pax8 disminuye la expresión de las β1-integrinas a través de cadherina-16 y desorienta el transporte apical de Rac1 mediado por los filamentos de actina. La activación apical de Rac1 es necesaria para la organización apical de los filamentos que da lugar a la correcta orientación del dominio apical y la formación del lumen folicular.

5. El simportador de sodio/yodo, NIS se transporta hacía la membrana basolateral mediante una vía mediada por clatrina a través de vesículas positivas para el adaptador de clatrina AP-1 y el receptor de transferrina.

6. NIS es segregado a nivel del compartimento *trans*-Golgi y de los endosomas de reciclaje por los complejos protéicos de adaptadores de clatrina AP-1.

7. La subunidad mediana del complejo AP-1B es necesaria para el tráfico basolateral de NIS en la ruta de secreción y/o de reciclaje endocítico. En su ausencia, NIS se transporta a la membrana apical donde sigue siendo funcional.

8. La subunidad mediana del complejo AP-1A participa en el transporte directo de NIS del *trans*-Golgi a la membrana basolateral y en su ausencia AP-1B compensa su función.

9. NIS se internaliza por un mecanismo independiente de clatrina y finalmente se degrada en lisosomas.

REFERENCES

ADAMS, C. L., CHEN, Y. T., SMITH, S. J. & NELSON, W. J. 1998. Mechanisms of epithelial cell-cell adhesion and cell compaction revealed by high-resolution tracking of E-cadherin-green fluorescent protein. *J Cell Biol,* 142**,** 1105-19.

ADAMS, S. A., SMITH, M. E., COWLEY, G. P. & CARR, L. A. 2004. Reversal of glandular polarity in the lymphovascular compartment of breast cancer. *J Clin Pathol,* 57**,** 1114-7.

AMBESI-IMPIOMBATO, F. S., PARKS, L. A. & COON, H. G. 1980. Culture of hormone-dependent functional epithelial cells from rat thyroids. *Proc Natl Acad Sci U S A,* 77**,** 3455-9.

ANG, A. L., TAGUCHI, T., FRANCIS, S., FOLSCH, H., MURRELLS, L. J., PYPAERT, M., WARREN, G. & MELLMAN, I. 2004. Recycling endosomes can serve as intermediates during transport from the Golgi to the plasma membrane of MDCK cells. *J Cell Biol,* 167**,** 531-43.

ANTONICA, F., KASPRZYK, D. F., OPITZ, R., IACOVINO, M., LIAO, X. H., DUMITRESCU, A. M., REFETOFF, S., PEREMANS, K., MANTO, M., KYBA, M. & COSTAGLIOLA, S. 2012. Generation of functional thyroid from embryonic stem cells. *Nature,* 491**,** 66-71.

ARAI, H. & ATOMI, Y. 1997. Chaperone activity of alpha B-crystallin suppresses tubulin aggregation through complex formation. *Cell Struct Funct,* 22**,** 539-44.

AZA-BLANC, P., DI LAURO, R. & SANTISTEBAN, P. 1993. Identification of a cis-regulatory element and a thyroid-specific nuclear factor mediating the hormonal regulation of rat thyroid peroxidase promoter activity. *Mol Endocrinol,* 7**,** 1297-306.

BAGNAT, M., CHEUNG, I. D., MOSTOV, K. E. & STAINIER, D. Y. 2007. Genetic control of single lumen formation in the zebrafish gut. *Nat Cell Biol,* 9**,** 954-60.

BARRERA, M. J., SANCHEZ, M., AGUILERA, S., ALLIENDE, C., BAHAMONDES, V., MOLINA, C., QUEST, A. F., URZUA, U., CASTRO, I., GONZALEZ, S., SUNG, H. H., ALBORNOZ, A., HERMOSO, M., LEYTON, C. & GONZALEZ, M. J. 2012. Aberrant localization of fusion receptors involved in regulated exocytosis in salivary glands of Sjogren's syndrome patients is linked to ectopic mucin secretion. *J Autoimmun,* 39**,** 83-92.

BEAU, I., GROYER-PICARD, M. T., DESROCHES, A., CONDAMINE, E., LEPRINCE, J., TOME, J. P., DESSEN, P., VAUDRY, H. & MISRAHI, M. 2004. The basolateral sorting signals of the thyrotropin and luteinizing hormone receptors: an unusual family of signals sharing an unusual distal intracellular localization, but unrelated in their structures. *Mol Endocrinol,* 18**,** 733-46.

BELOUZARD, S., DELCROIX, D. & ROUILLE, Y. 2004. Low levels of expression of leptin receptor at the cell surface result from constitutive endocytosis and intracellular retention in the biosynthetic pathway. *J Biol Chem,* 279**,** 28499-508.

BERNIER-VALENTIN, F., KOSTROUCH, Z., RABILLOUD, R. & ROUSSET, B. 1991. Analysis of the thyroglobulin internalization process using in vitro reconstituted thyroid follicles: evidence for a coated vesicle-dependent endocytic pathway. *Endocrinology,* 129**,** 2194-201.

BERNIER-VALENTIN, F., TROUTTET-MASSON, S., RABILLOUD, R., SELMI-RUBY, S. & ROUSSET, B. 2006. Three-dimensional organization of thyroid cells into follicle structures is a pivotal factor in the control of sodium/iodide symporter expression. *Endocrinology,* 147**,** 2035-42.

BIECHE, I., RUFFET, E., ZWEIBAUM, A., VILDE, F., LIDEREAU, R. & FRANC, B. 1997. MUC1 mucin gene, transcripts, and protein in adenomas and papillary carcinomas of the thyroid. *Thyroid,* 7**,** 725-31.

BIZHANOVA, A., CHEW, T. L., KHUON, S. & KOPP, P. 2011. Analysis of cellular localization and function of carboxy-terminal mutants of pendrin. *Cell Physiol Biochem,* 28**,** 423-34.

BOELAERT, K., SMITH, V. E., STRATFORD, A. L., KOGAI, T., TANNAHILL, L. A., WATKINSON, J. C., EGGO, M. C., FRANKLYN, J. A. & MCCABE, C. J. 2007. PTTG and PBF repress the human sodium iodide symporter. *Oncogene,* 26**,** 4344-56.

BOLTE, S. & CORDELIERES, F. P. 2006. A guided tour into subcellular colocalization analysis in light microscopy. *J Microsc,* 224**,** 213-32.

BONIFACINO, J. S. 2014. Adaptor proteins involved in polarized sorting. *J Cell Biol,* 204**,** 7-17.

BONIFACINO, J. S. & TRAUB, L. M. 2003. Signals for sorting of transmembrane proteins to endosomes and lysosomes. *Annu Rev Biochem,* 72**,** 395-447.

BONILHA, V. L., RAYBORN, M. E., SAOTOME, I., MCCLATCHEY, A. I. & HOLLYFIELD, J. G. 2006. Microvilli defects in retinas of ezrin knockout mice. *Exp Eye Res,* 82**,** 720-9.

BOTTA, R., LISI, S., PINCHERA, A., TADDEI, A. R., FAUSTO, A. M., GIORGI, F. & MARINO, M. 2011. Binding, uptake, and degradation of internalized thyroglobulin in cultured thyroid and non-thyroid cells. *J Endocrinol Invest,* 34**,** 515-20.

BRADFORD, M. M. 1976. A rapid and sensitive method for the quantitation of microgram quantities of protein utilizing the principle of protein-dye binding. *Anal Biochem,* 72**,** 248-54.

BRAVO, S. B., GARCIA-RENDUELES, M. E., GARCIA-RENDUELES, A. R., RODRIGUES, J. S., PEREZ-ROMERO, S., GARCIA-LAVANDEIRA, M., SUAREZ-FARINA, M., BARREIRO, F., CZARNOCKA, B., SENRA, A., LAREU, M. V., RODRIGUEZ-GARCIA, J., CAMESELLE-TEIJEIRO, J. & ALVAREZ, C. V. 2013. Humanized medium (h7H) allows long-term primary follicular thyroid cultures from human normal thyroid, benign neoplasm, and cancer. *J Clin Endocrinol Metab,* 98**,** 2431-41.

BRYANT, D. M., DATTA, A., RODRIGUEZ-FRATICELLI, A. E., PERANEN, J., MARTIN-BELMONTE, F. & MOSTOV, K. E. 2010. A molecular network for de novo generation of the apical surface and lumen. *Nat Cell Biol,* 12**,** 1035-45.

BRYANT, D. M. & MOSTOV, K. E. 2008. From cells to organs: building polarized tissue. *Nat Rev Mol Cell Biol,* 9**,** 887-901.

BURGOS, P. V., MARDONES, G. A., ROJAS, A. L., DASILVA, L. L., PRABHU, Y., HURLEY, J. H. & BONIFACINO, J. S. 2010. Sorting of the Alzheimer's disease amyloid precursor protein mediated by the AP-4 complex. *Dev Cell,* 18**,** 425-36.

CALI, G., GENTILE, F., MOGAVERO, S., PALLANTE, P., NITSCH, R., CIANCIA, G., FERRARO, A., FUSCO, A. & NITSCH, L. 2012. CDH16/Ksp-cadherin is expressed in the developing thyroid gland and is strongly down-regulated in thyroid carcinomas. *Endocrinology,* 153**,** 522-34.

CALI, G., RETTA, S. F., NEGRI, R., DAMIANO, I., GENTILE, R., TARONE, G., NITSCH, L. & GARBI, C. 1998. Beta1B integrin interferes with matrix assembly but not with confluent monolayer polarity, and alters some morphogenetic properties of FRT epithelial cells. *Eur J Cell Biol,* 75**,** 107-17.

CALI, G., ZANNINI, M., RUBINI, P., TACCHETTI, C., D'ANDREA, B., AFFUSO, A., WINTERMANTEL, T., BOUSSADIA, O., TERRACCIANO, D., SILBERSCHMIDT, D., AMENDOLA, E., DE FELICE, M., SCHUTZ, G., KEMLER, R., DI LAURO, R. & NITSCH, L. 2007. Conditional inactivation of the E-cadherin gene in thyroid follicular cells affects gland development but does not impair junction formation. *Endocrinology,* 148**,** 2737-46.

CANCINO, J., TORREALBA, C., SOZA, A., YUSEFF, M. I., GRAVOTTA, D., HENKLEIN, P., RODRIGUEZ-BOULAN, E. & GONZALEZ, A. 2007. Antibody to AP1B adaptor blocks biosynthetic and recycling routes of basolateral proteins at recycling endosomes. *Mol Biol Cell,* 18**,** 4872-84.

CARRASCO, N. 1993. Iodide transport in the thyroid gland. *Biochim Biophys Acta,* 1154**,** 65-82.

CARVAJAL-GONZALEZ, J. M., GRAVOTTA, D., MATTERA, R., DIAZ, F., PEREZ BAY, A., ROMAN, A. C., SCHREINER, R. P., THUENAUER, R., BONIFACINO, J. S. & RODRIGUEZ-BOULAN, E. 2012. Basolateral sorting of the coxsackie and adenovirus receptor through interaction of a canonical YXXPhi motif with the clathrin adaptors AP-1A and AP-1B. *Proc Natl Acad Sci U S A,* 109**,** 3820-5.

CIVITAREALE, D., LONIGRO, R., SINCLAIR, A. J. & DI LAURO, R. 1989. A thyroid-specific nuclear protein essential for tissue-specific expression of the thyroglobulin promoter. *EMBO J,* 8**,** 2537-42.

COLOGNATO, H., WINKELMANN, D. A. & YURCHENCO, P. D. 1999. Laminin polymerization induces a receptor-cytoskeleton network. *J Cell Biol,* 145**,** 619-31.

COSTAMAGNA, E., GARCIA, B. & SANTISTEBAN, P. 2004. The functional interaction between the paired domain transcription factor Pax8 and Smad3 is involved in transforming growth factor-beta repression of the sodium/iodide symporter gene. *J Biol Chem,* 279**,** 3439-46.

CROIZET-BERGER, K., DAUMERIE, C., COUVREUR, M., COURTOY, P. J. & VAN DEN HOVE, M. F. 2002. The endocytic catalysts, Rab5a and Rab7, are tandem regulators of thyroid hormone production. *Proc Natl Acad Sci U S A,* 99**,** 8277-82.

CHAMBARD, M., GABRION, J. & MAUCHAMP, J. 1981. Influence of collagen gel on the orientation of epithelial cell polarity: follicle formation from isolated thyroid cells and from preformed monolayers. *J Cell Biol,* 91**,** 157-66.

CHEN, C. A. & OKAYAMA, H. 1988. Calcium phosphate-mediated gene transfer: a highly efficient transfection system for stably transforming cells with plasmid DNA. *Biotechniques,* 6**,** 632-8.

CHRISTOPHE-HOBERTUS, C., LEFORT, A., LIBERT, F. & CHRISTOPHE, D. 2012. Functional inactivation of thyroid transcription factor-1 in PCCl3 thyroid cells. *Mol Cell Endocrinol,* 358**,** 36-45.

DAI, G., LEVY, O. & CARRASCO, N. 1996. Cloning and characterization of the thyroid iodide transporter. *Nature,* 379**,** 458-60.

DAMANTE, G., TELL, G. & DI LAURO, R. 2001. A unique combination of transcription factors controls differentiation of thyroid cells. *Prog Nucleic Acid Res Mol Biol,* 66**,** 307-56.

DATTA, A., BRYANT, D. M. & MOSTOV, K. E. 2011. Molecular regulation of lumen morphogenesis. *Curr Biol,* 21**,** R126-36.

DE CRISTOFARO, T., DI PALMA, T., FICHERA, I., LUCCI, V., PARRILLO, L., DE FELICE, M. & ZANNINI, M. 2012. An essential role for Pax8 in the transcriptional regulation of cadherin-16 in thyroid cells. *Mol Endocrinol,* 26**,** 67-78.

DE FELICE, M. & DI LAURO, R. 2004. Thyroid development and its disorders: genetics and molecular mechanisms. *Endocr Rev,* 25**,** 722-46.

DE FELICE, M. & DI LAURO, R. 2011. Minireview: Intrinsic and extrinsic factors in thyroid gland development: an update. *Endocrinology,* 152**,** 2948-56.

DE LA VIEJA, A., GINTER, C. S. & CARRASCO, N. 2005. Molecular analysis of a congenital iodide transport defect: G543E impairs maturation and trafficking of the Na+/I- symporter. *Mol Endocrinol,* 19**,** 2847-58.

DE MARCO, M. C., MARTIN-BELMONTE, F., KREMER, L., ALBAR, J. P., CORREAS, I., VAERMAN, J. P., MARAZUELA, M., BYRNE, J. A. & ALONSO, M. A. 2002. MAL2, a novel raft protein of the MAL family, is an essential component of the machinery for transcytosis in hepatoma HepG2 cells. *J Cell Biol,* 159**,** 37-44.

DEBNATH, J., MUTHUSWAMY, S. K. & BRUGGE, J. S. 2003. Morphogenesis and oncogenesis of MCF-10A mammary epithelial acini grown in three-dimensional basement membrane cultures. *Methods,* 30**,** 256-68.

DEBORDE, S., PERRET, E., GRAVOTTA, D., DEORA, A., SALVAREZZA, S., SCHREINER, R. & RODRIGUEZ-BOULAN, E. 2008. Clathrin is a key regulator of basolateral polarity. *Nature,* 452**,** 719-23.

DEGROOT, L. J. & NIEPOMNISZCZE, H. 1977. Biosynthesis of thyroid hormone: basic and clinical aspects. *Metabolism,* 26**,** 665-718.

DEL POZO, M. A., ALDERSON, N. B., KIOSSES, W. B., CHIANG, H. H., ANDERSON, R. G. & SCHWARTZ, M. A. 2004. Integrins regulate Rac targeting by internalization of membrane domains. *Science,* 303**,** 839-42.

DEORA, A. A., GRAVOTTA, D., KREITZER, G., HU, J., BOK, D. & RODRIGUEZ-BOULAN, E. 2004. The basolateral targeting signal of CD147 (EMMPRIN) consists of a single leucine and is not recognized by retinal pigment epithelium. *Mol Biol Cell,* 15**,** 4148-65.

DI COSMO, C., LIAO, X. H., DUMITRESCU, A. M., PHILP, N. J., WEISS, R. E. & REFETOFF, S. 2010. Mice deficient in MCT8 reveal a mechanism regulating thyroid hormone secretion. *J Clin Invest,* 120**,** 3377-88.

DI PALMA, T., ZAMPELLA, E., FILIPPONE, M. G., MACCHIA, P. E., RIS-STALPERS, C., DE VROEDE, M. & ZANNINI, M. 2010. Characterization of a novel loss-of-function mutation of PAX8 associated with congenital hypothyroidism. *Clin Endocrinol (Oxf),* 73**,** 808-14.

DOHAN, O., BALOCH, Z., BANREVI, Z., LIVOLSI, V. & CARRASCO, N. 2001. Rapid communication: predominant intracellular overexpression of the Na(+)/I(-) symporter (NIS) in a large sampling of thyroid cancer cases. *J Clin Endocrinol Metab,* 86**,** 2697-700.

DOHAN, O., DE LA VIEJA, A., PARODER, V., RIEDEL, C., ARTANI, M., REED, M., GINTER, C. S. & CARRASCO, N. 2003. The sodium/iodide Symporter (NIS): characterization, regulation, and medical significance. *Endocr Rev,* 24**,** 48-77.

DONOSO, M., CANCINO, J., LEE, J., VAN KERKHOF, P., RETAMAL, C., BU, G., GONZALEZ, A., CACERES, A. & MARZOLO, M. P. 2009. Polarized traffic of LRP1 involves AP1B and SNX17 operating on Y-dependent sorting motifs in different pathways. *Mol Biol Cell,* 20**,** 481-97.

DORAY, B., LEE, I., KNISELY, J., BU, G. & KORNFELD, S. 2007. The gamma/sigma1 and alpha/sigma2 hemicomplexes of clathrin adaptors AP-1 and AP-2 harbor the dileucine recognition site. *Mol Biol Cell,* 18**,** 1887-96.

DUMONT, J. E., MAENHAUT, C., PIRSON, I., BAPTIST, M. & ROGER, P. P. 1991. Growth factors controlling the thyroid gland. *Baillieres Clin Endocrinol Metab,* 5**,** 727-54.

DUNN, A. D., CRUTCHFIELD, H. E. & DUNN, J. T. 1991. Proteolytic processing of thyroglobulin by extracts of thyroid lysosomes. *Endocrinology,* 128**,** 3073-80.

EALES, J. G. 1997. Iodine metabolism and thyroid-related functions in organisms lacking thyroid follicles: are thyroid hormones also vitamins? *Proc Soc Exp Biol Med,* 214**,** 302-17.

EHRLICH, J. S., HANSEN, M. D. & NELSON, W. J. 2002. Spatio-temporal regulation of Rac1 localization and lamellipodia dynamics during epithelial cell-cell adhesion. *Dev Cell,* 3**,** 259-70.

ENDO, T., KANESHIGE, M., NAKAZATO, M., OHMORI, M., HARII, N. & ONAYA, T. 1997. Thyroid transcription factor-1 activates the promoter activity of rat thyroid Na+/I- symporter gene. *Mol Endocrinol,* 11**,** 1747-55.

FAGMAN, H., ANDERSSON, L. & NILSSON, M. 2006. The developing mouse thyroid: embryonic vessel contacts and parenchymal growth pattern during specification, budding, migration, and lobulation. *Developmental dynamics : an official publication of the American Association of Anatomists,* 235**,** 444-55.

FAGMAN, H., GRANDE, M., EDSBAGGE, J., SEMB, H. & NILSSON, M. 2003. Expression of classical cadherins in thyroid development: maintenance of an epithelial phenotype throughout organogenesis. *Endocrinology,* 144**,** 3618-24.

FAGMAN, H. & NILSSON, M. 2010. Morphogenesis of the thyroid gland. *Mol Cell Endocrinol,* 323**,** 35-54.

FAYADAT, L., NICCOLI-SIRE, P., LANET, J. & FRANC, J. L. 1998. Human thyroperoxidase is largely retained and rapidly degraded in the endoplasmic reticulum. Its N-glycans are required for folding and intracellular trafficking. *Endocrinology,* 139**,** 4277-85.

FAYET, G., HOVSEPIAN, S., DICKSON, J. G. & LISSITZKY, S. 1982. Reorganization of porcine thyroid cells into functional follicles in a chemically defined, serum- and thyrotropin-free medium. *J Cell Biol,* 93**,** 479-88.

FEHON, R. G., MCCLATCHEY, A. I. & BRETSCHER, A. 2010. Organizing the cell cortex: the role of ERM proteins. *Nat Rev Mol Cell Biol,* 11**,** 276-87.

FERNANDEZ, L. P., LOPEZ-MARQUEZ, A., MARTINEZ, A. M., GOMEZ-LOPEZ, G. & SANTISTEBAN, P. 2013. New insights into FoxE1 functions: identification of direct FoxE1 targets in thyroid cells. *PLoS One,* 8**,** e62849.

FERNANDEZ, L. P., LOPEZ-MARQUEZ, A. & SANTISTEBAN, P. 2015. Thyroid transcription factors in development, differentiation and disease. *Nat Rev Endocrinol,* 11**,** 29-42.

FERRARI, A., VELIGODSKIY, A., BERGE, U., LUCAS, M. S. & KROSCHEWSKI, R. 2008. ROCK-mediated contractility, tight junctions and channels contribute to the conversion of a preapical patch into apical surface during isochoric lumen initiation. *J Cell Sci,* 121**,** 3649-63.

FIEDLER, K. & SIMONS, K. 1996. Characterization of VIP36, an animal lectin homologous to leguminous lectins. *J Cell Sci,* 109 (Pt 1)**,** 271-6.

FIEVET, B. T., GAUTREAU, A., ROY, C., DEL MAESTRO, L., MANGEAT, P., LOUVARD, D. & ARPIN, M. 2004. Phosphoinositide binding and phosphorylation act sequentially in the activation mechanism of ezrin. *J Cell Biol,* 164**,** 653-9.

FOLSCH, H. 2008. Regulation of membrane trafficking in polarized epithelial cells. *Curr Opin Cell Biol,* 20**,** 208-13.

FOLSCH, H., MATTILA, P. E. & WEISZ, O. A. 2009. Taking the scenic route: biosynthetic traffic to the plasma membrane in polarized epithelial cells. *Traffic,* 10**,** 972-81.

FOLSCH, H., PYPAERT, M., MADAY, S., PELLETIER, L. & MELLMAN, I. 2003. The AP-1A and AP-1B clathrin adaptor complexes define biochemically and functionally distinct membrane domains. *J Cell Biol,* 163**,** 351-62.

FOLSCH, H., PYPAERT, M., SCHU, P. & MELLMAN, I. 2001. Distribution and function of AP-1 clathrin adaptor complexes in polarized epithelial cells. *J Cell Biol,* 152**,** 595-606.

FONG, P. 2011. Thyroid iodide efflux: a team effort? *J Physiol,* 589**,** 5929-39.

FRANCIS-LANG, H., PRICE, M., POLYCARPOU-SCHWARZ, M. & DI LAURO, R. 1992. Cell-type-specific expression of the rat thyroperoxidase promoter indicates common mechanisms for thyroid-specific gene expression. *Mol Cell Biol,* 12**,** 576-88.

FROHLICH, E., WAHL, R. & REUTTER, K. 1995. Basal lamina formation by porcine thyroid cells grown in collagen- and laminin-deficient medium. *Histochem J,* 27**,** 602-8.

FUJITA, H. 1975. Fine structure of the thyroid gland. *Int Rev Cytol,* 40**,** 197-280.

FUKATA, M., WATANABE, T., NORITAKE, J., NAKAGAWA, M., YAMAGA, M., KURODA, S., MATSUURA, Y., IWAMATSU, A., PEREZ, F. & KAIBUCHI, K. 2002. Rac1 and Cdc42 capture microtubules through IQGAP1 and CLIP-170. *Cell,* 109**,** 873-85.

FUSCO, A., BERLINGIERI, M. T., DI FIORE, P. P., PORTELLA, G., GRIECO, M. & VECCHIO, G. 1987. One- and two-step transformations of rat thyroid epithelial cells by retroviral oncogenes. *Mol Cell Biol,* 7**,** 3365-70.

GALVEZ-SANTISTEBAN, M., RODRIGUEZ-FRATICELLI, A. E., BRYANT, D. M., VERGARAJAUREGUI, S., YASUDA, T., BANON-RODRIGUEZ, I., BERNASCONE, I., DATTA, A., SPIVAK, N., YOUNG, K., SLIM, C. L., BRAKEMAN, P. R., FUKUDA, M., MOSTOV, K. E. & MARTIN-BELMONTE, F. 2012. Synaptotagmin-like proteins control the formation of a single apical membrane domain in epithelial cells. *Nat Cell Biol,* 14**,** 838-49.

GARBI, C., MASCIA, A. & NITSCH, L. 1987. Cell polarity and morphogenetic properties of Fischer rat thyroid cells (FRT) cultured in suspension or embedded in different gels. *Cell Mol Biol,* 33**,** 293-305.

GARBI, C., NITSCH, L. & WOLLMAN, S. H. 1984. Embedding in a collagen gel stabilizes the polarity of epithelial cells in thyroid follicles in suspension culture. *Exp Cell Res,* 151**,** 458-65.

GARBI, C., ZURZOLO, C., BIFULCO, M. & NITSCH, L. 1988. Synthesis of extracellular matrix glycoproteins by a differentiated thyroid epithelial cell line. *J Cell Physiol,* 135**,** 39-46.

GARCIA, B. & SANTISTEBAN, P. 2002. PI3K is involved in the IGF-I inhibition of TSH-induced sodium/iodide symporter gene expression. *Mol Endocrinol,* 16**,** 342-52.

GAVARD, J., LAMBERT, M., GROSHEVA, I., MARTHIENS, V., IRINOPOULOU, T., RIOU, J. F., BERSHADSKY, A. & MEGE, R. M. 2004. Lamellipodium extension and cadherin adhesion: two cell responses to cadherin activation relying on distinct signalling pathways. *J Cell Sci,* 117**,** 257-70.

GIULIETTI, A., OVERBERGH, L., VALCKX, D., DECALLONNE, B., BOUILLON, R. & MATHIEU, C. 2001. An overview of real-time quantitative PCR: applications to quantify cytokine gene expression. *Methods,* 25**,** 386-401.

GONZALEZ, A. & RODRIGUEZ-BOULAN, E. 2009. Clathrin and AP1B: key roles in basolateral trafficking through trans-endosomal routes. *FEBS Lett,* 583**,** 3784-95.

GRAPIN-BOTTON, A. & MELTON, D. A. 2000. Endoderm development: from patterning to organogenesis. *Trends Genet,* 16**,** 124-30.

GRAVOTTA, D., CARVAJAL-GONZALEZ, J. M., MATTERA, R., DEBORDE, S., BANFELDER, J. R., BONIFACINO, J. S. & RODRIGUEZ-BOULAN, E. 2012. The clathrin adaptor AP-1A mediates basolateral polarity. *Dev Cell,* 22**,** 811-23.

GRAVOTTA, D., DEORA, A., PERRET, E., OYANADEL, C., SOZA, A., SCHREINER, R., GONZALEZ, A. & RODRIGUEZ-BOULAN, E. 2007. AP1B sorts basolateral proteins in recycling and biosynthetic routes of MDCK cells. *Proc Natl Acad Sci U S A,* 104**,** 1564-9.

GUO, X., MATTERA, R., REN, X., CHEN, Y., RETAMAL, C., GONZALEZ, A. & BONIFACINO, J. S. 2013. The adaptor protein-1 mu1B subunit expands the repertoire of basolateral sorting signal recognition in epithelial cells. *Dev Cell,* 27**,** 353-66.

HAO, Y., DU, Q., CHEN, X., ZHENG, Z., BALSBAUGH, J. L., MAITRA, S., SHABANOWITZ, J., HUNT, D. F. & MACARA, I. G. 2010. Par3 controls epithelial spindle orientation by aPKC-mediated phosphorylation of apical Pins. *Curr Biol,* 20**,** 1809-18.

HILFER, S. R. 1964. Follicle Formation in the Embryonic Chick Thyroid. I. Early Morphogenesis. *J Morphol,* 115**,** 135-51.

HILFER, S. R. 1979. Follicle formation in the embryonic chick thyroid. III. Initiation of follicle formation. *Tissue Cell,* 11**,** 727-40.

IMJETI, N. S., LEBRETON, S., PALADINO, S., DE LA FUENTE, E., GONZALEZ, A. & ZURZOLO, C. 2011. N-Glycosylation instead of cholesterol mediates oligomerization and apical sorting of GPI-APs in FRT cells. *Mol Biol Cell,* 22**,** 4621-34.

IVANOV, A. I., HOPKINS, A. M., BROWN, G. T., GERNER-SMIDT, K., BABBIN, B. A., PARKOS, C. A. & NUSRAT, A. 2008. Myosin II regulates the shape of three-dimensional intestinal epithelial cysts. *J Cell Sci,* 121**,** 1803-14.

JAFFE, A. B., KAJI, N., DURGAN, J. & HALL, A. 2008. Cdc42 controls spindle orientation to position the apical surface during epithelial morphogenesis. *J Cell Biol,* 183**,** 625-33.

JANVIER, K., KATO, Y., BOEHM, M., ROSE, J. R., MARTINA, J. A., KIM, B. Y., VENKATESAN, S. & BONIFACINO, J. S. 2003. Recognition of dileucine-based sorting signals from HIV-1 Nef and LIMP-II by the AP-1 gamma-sigma1 and AP-3 delta-sigma3 hemicomplexes. *J Cell Biol,* 163**,** 1281-90.

JEKER, L. T., HEJAZI, M., BUREK, C. L., ROSE, N. R. & CATUREGLI, P. 1999. Mouse thyroid primary culture. *Biochem Biophys Res Commun,* 257**,** 511-5.

KAMEDA, Y., NISHIMAKI, T., CHISAKA, O., ISEKI, S. & SUCOV, H. M. 2007. Expression of the epithelial marker E-cadherin by thyroid C cells and their precursors during murine development. *J Histochem Cytochem,* 55**,** 1075-88.

KAMINSKY, S. M., LEVY, O., SALVADOR, C., DAI, G. & CARRASCO, N. 1994. Na(+)-I- symport activity is present in membrane vesicles from thyrotropin-deprived non-I(-)-transporting cultured thyroid cells. *Proc Natl Acad Sci U S A,* 91**,** 3789-93.

KIM, S. H., LI, Z. & SACKS, D. B. 2000. E-cadherin-mediated cell-cell attachment activates Cdc42. *J Biol Chem,* 275**,** 36999-7005.

KIM, S. K. 1997. Polarized signaling: basolateral receptor localization in epithelial cells by PDZ-containing proteins. *Curr Opin Cell Biol,* 9**,** 853-9.

KIMURA, S., WARD, J. M. & MINOO, P. 1999. Thyroid-specific enhancer-binding protein/thyroid transcription factor 1 is not required for the initial specification of the thyroid and lung primordia. *Biochimie,* 81**,** 321-7.

KNAUF, J. A. & FAGIN, J. A. 2009. Role of MAPK pathway oncoproteins in thyroid cancer pathogenesis and as drug targets. *Curr Opin Cell Biol,* 21**,** 296-303.

KOGAI, T. & BRENT, G. A. 2012. The sodium iodide symporter (NIS): regulation and approaches to targeting for cancer therapeutics. *Pharmacol Ther,* 135**,** 355-70.

KOGAI, T., CURCIO, F., HYMAN, S., CORNFORD, E. M., BRENT, G. A. & HERSHMAN, J. M. 2000. Induction of follicle formation in long-term cultured normal human thyroid cells treated with thyrotropin stimulates iodide uptake but not sodium/iodide symporter messenger RNA and protein expression. *J Endocrinol,* 167**,** 125-35.

KOGAI, T., ENDO, T., SAITO, T., MIYAZAKI, A., KAWAGUCHI, A. & ONAYA, T. 1997. Regulation by thyroid-stimulating hormone of sodium/iodide symporter gene expression and protein levels in FRTL-5 cells. *Endocrinology,* 138**,** 2227-32.

KOGAI, T., TAKI, K. & BRENT, G. A. 2006. Enhancement of sodium/iodide symporter expression in thyroid and breast cancer. *Endocr Relat Cancer,* 13**,** 797-826.

KOVACS, E. M., GOODWIN, M., ALI, R. G., PATERSON, A. D. & YAP, A. S. 2002. Cadherin-directed actin assembly: E-cadherin physically associates with the Arp2/3 complex to direct actin assembly in nascent adhesive contacts. *Curr Biol,* 12**,** 379-82.

KRENDEL, M. F. & BONDER, E. M. 1999. Analysis of actin filament bundle dynamics during contact formation in live epithelial cells. *Cell Motil Cytoskeleton,* 43**,** 296-309.

KUSAKABE, T., KAWAGUCHI, A., HOSHI, N., KAWAGUCHI, R., HOSHI, S. & KIMURA, S. 2006. Thyroid-specific enhancer-binding protein/NKX2.1 is required for the maintenance of ordered architecture and function of the differentiated thyroid. *Molecular endocrinology,* 20**,** 1796-809.

LAEMMLI, U. K. 1970. Cleavage of structural proteins during the assembly of the head of bacteriophage T4. *Nature,* 227**,** 680-5.

LE DOUARIN, N. M., BRITO, J. M. & CREUZET, S. 2007. Role of the neural crest in face and brain development. *Brain Res Rev,* 55**,** 237-47.

LEVY, O., DE LA VIEJA, A., GINTER, C. S., RIEDEL, C., DAI, G. & CARRASCO, N. 1998. N-linked glycosylation of the thyroid Na+/I- symporter (NIS). Implications for its secondary structure model. *J Biol Chem,* 273**,** 22657-63.

LI, C., HAO, M., CAO, Z., DING, W., GRAVES-DEAL, R., HU, J., PISTON, D. W. & COFFEY, R. J. 2007. Naked2 acts as a cargo recognition and targeting protein to ensure proper delivery and fusion of TGF-alpha containing exocytic vesicles at the lower lateral membrane of polarized MDCK cells. *Mol Biol Cell,* 18**,** 3081-93.

LI, C. & NAREN, A. P. 2010. CFTR chloride channel in the apical compartments: spatiotemporal coupling to its interacting partners. *Integr Biol (Camb),* 2**,** 161-77.

LI, Q., LAU, A., MORRIS, T. J., GUO, L., FORDYCE, C. B. & STANLEY, E. F. 2004. A syntaxin 1, Galpha(o), and N-type calcium channel complex at a presynaptic nerve terminal: analysis by quantitative immunocolocalization. *J Neurosci,* 24**,** 4070-81.

LIPARDI, C., NITSCH, L. & ZURZOLO, C. 1999. Mechanisms of apical protein sorting in polarized thyroid epithelial cells. *Biochimie,* 81**,** 347-53.

LIPARDI, C., RUGGIANO, G., PERRONE, L., PALADINO, S., MONLAUZEUR, L., NITSCH, L., LE BIVIC, A. & ZURZOLO, C. 2002. Differential recognition of a tyrosine-dependent signal in the basolateral and endocytic pathways of thyroid epithelial cells. *Endocrinology,* 143**,** 1291-301.

LUCIANO, L., THIELE, J. & REALE, E. 1979. Development of follicles and of occluding junctions between the follicular cells of the thyroid gland. A thin-section and freeze-fracture study in the fetal rat. *J Ultrastruct Res,* 66**,** 164-81.

MACCHIA, P. E., LAPI, P., KRUDE, H., PIRRO, M. T., MISSERO, C., CHIOVATO, L., SOUABNI, A., BASERGA, M., TASSI, V., PINCHERA, A., FENZI, G., GRUTERS, A., BUSSLINGER, M. & DI LAURO, R. 1998. PAX8 mutations associated with congenital hypothyroidism caused by thyroid dysgenesis. *Nat Genet,* 19**,** 83-6.

MADRID, R., ARANDA, J. F., RODRIGUEZ-FRATICELLI, A. E., VENTIMIGLIA, L., ANDRES-DELGADO, L., SHEHATA, M., FANAYAN, S., SHAHHEYDARI, H., GOMEZ, S., JIMENEZ, A., MARTIN-BELMONTE, F., BYRNE, J. A. & ALONSO, M. A. 2010. The formin INF2 regulates basolateral-to-apical transcytosis and lumen formation in association with Cdc42 and MAL2. *Dev Cell,* 18**,** 814-27.

MAILLEUX, A. A., OVERHOLTZER, M. & BRUGGE, J. S. 2008. Lumen formation during mammary epithelial morphogenesis: insights from in vitro and in vivo models. *Cell Cycle,* 7**,** 57-62.

MALACOMBE, M., CERIDONO, M., CALCO, V., CHASSEROT-GOLAZ, S., MCPHERSON, P. S., BADER, M. F. & GASMAN, S. 2006. Intersectin-1L nucleotide exchange factor regulates secretory granule exocytosis by activating Cdc42. *EMBO J,* 25**,** 3494-503.

MANSOURI, A., CHOWDHURY, K. & GRUSS, P. 1998. Follicular cells of the thyroid gland require Pax8 gene function. *Nature genetics,* 19**,** 87-90.

MARAZUELA, M., MARTIN-BELMONTE, F., GARCIA-LOPEZ, M. A., ARANDA, J. F., DE MARCO, M. C. & ALONSO, M. A. 2004. Expression and distribution of MAL2, an essential element of the machinery for basolateral-to-apical transcytosis, in human thyroid epithelial cells. *Endocrinology,* 145**,** 1011-6.

MARDONES, G. A., BURGOS, P. V., LIN, Y., KLOER, D. P., MAGADAN, J. G., HURLEY, J. H. & BONIFACINO, J. S. 2013. Structural basis for the recognition of tyrosine-based sorting signals by the mu3A subunit of the AP-3 adaptor complex. *J Biol Chem,* 288**,** 9563-71.

MARIANS, R. C., NG, L., BLAIR, H. C., UNGER, P., GRAVES, P. N. & DAVIES, T. F. 2002. Defining thyrotropin-dependent and -independent steps of thyroid hormone synthesis by using thyrotropin receptor-null mice. *Proc Natl Acad Sci U S A,* 99**,** 15776-81.

MARINO, M. & MCCLUSKEY, R. T. 2000. Role of thyroglobulin endocytic pathways in the control of thyroid hormone release. *Am J Physiol Cell Physiol,* 279**,** C1295-306.

MARTIN-BELMONTE, F., ALONSO, M. A., ZHANG, X. & ARVAN, P. 2000a. Thyroglobulin is selected as luminal protein cargo for apical transport via detergent-resistant membranes in epithelial cells. *J Biol Chem,* 275**,** 41074-81.

MARTIN-BELMONTE, F., GASSAMA, A., DATTA, A., YU, W., RESCHER, U., GERKE, V. & MOSTOV, K. 2007. PTEN-mediated apical segregation of phosphoinositides controls epithelial morphogenesis through Cdc42. *Cell,* 128**,** 383-97.

MARTIN-BELMONTE, F., KREMER, L., ALBAR, J. P., MARAZUELA, M. & ALONSO, M. A. 1998. Expression of the MAL gene in the thyroid: the MAL proteolipid, a component of glycolipid-enriched membranes, is apically distributed in thyroid follicles. *Endocrinology,* 139**,** 2077-84.

MARTIN-BELMONTE, F. & MOSTOV, K. 2008. Regulation of cell polarity during epithelial morphogenesis. *Curr Opin Cell Biol,* 20**,** 227-34.

MARTIN-BELMONTE, F., PUERTOLLANO, R., MILLAN, J. & ALONSO, M. A. 2000b. The MAL proteolipid is necessary for the overall apical delivery of membrane proteins in the polarized epithelial Madin-Darby canine kidney and fischer rat thyroid cell lines. *Mol Biol Cell,* 11**,** 2033-45.

MARTIN-BELMONTE, F., YU, W., RODRIGUEZ-FRATICELLI, A. E., EWALD, A. J., WERB, Z., ALONSO, M. A. & MOSTOV, K. 2008. Cell-polarity dynamics controls the mechanism of lumen formation in epithelial morphogenesis. *Curr Biol,* 18**,** 507-13.

MAUCHAMP, J., MIRRIONE, A., ALQUIER, C. & ANDRE, F. 1998. Follicle-like structure and polarized monolayer: role of the extracellular matrix on thyroid cell organization in primary culture. *Biol Cell,* 90**,** 369-80.

MELLMAN, I. & NELSON, W. J. 2008. Coordinated protein sorting, targeting and distribution in polarized cells. *Nat Rev Mol Cell Biol,* 9**,** 833-45.

MONTELEON, C. L., SEDGWICK, A., HARTSELL, A., DAI, M., WHITTINGTON, C., VOYTIK-HARBIN, S. & D'SOUZA-SCHOREY, C. 2012. Establishing epithelial glandular polarity: interlinked roles for ARF6, Rac1, and the matrix microenvironment. *Mol Biol Cell,* 23**,** 4495-505.

MONTESANO, R., SCHALLER, G. & ORCI, L. 1991. Induction of epithelial tubular morphogenesis in vitro by fibroblast-derived soluble factors. *Cell,* 66**,** 697-711.

MORENO-BUENO, G., PORTILLO, F. & CANO, A. 2008. Transcriptional regulation of cell polarity in EMT and cancer. *Oncogene,* 27**,** 6958-69.

MORENO, J. C., KLOOTWIJK, W., VAN TOOR, H., PINTO, G., D'ALESSANDRO, M., LEGER, A., GOUDIE, D., POLAK, M., GRUTERS, A. & VISSER, T. J. 2008. Mutations in the iodotyrosine deiodinase gene and hypothyroidism. *N Engl J Med,* 358**,** 1811-8.

NAKAYAMA, M., GOTO, T. M., SUGIMOTO, M., NISHIMURA, T., SHINAGAWA, T., OHNO, S., AMANO, M. & KAIBUCHI, K. 2008. Rho-kinase phosphorylates PAR-3 and disrupts PAR complex formation. *Dev Cell,* 14**,** 205-15.

NARUMI, S., YOSHIDA, A., MUROYA, K., ASAKURA, Y., ADACHI, M., FUKUZAWA, R., KAMEYAMA, K. & HASEGAWA, T. 2011. PAX8 mutation disturbing thyroid follicular growth: a case report. *J Clin Endocrinol Metab,* 96**,** E2039-44.

NATHANIEL, D. R. 1986. Folliculogenesis in the neonatal thyroid gland of the rat. *J Ultrastruct Mol Struct Res,* 95**,** 29-37.

NICHOLL, I. D. & QUINLAN, R. A. 1994. Chaperone activity of alpha-crystallins modulates intermediate filament assembly. *EMBO J,* 13**,** 945-53.

NITSCH, L., TACCHETTI, C., TRAMONTANO, D. & AMBESI-IMPIOMBATO, F. S. 1984. Suspension culture reveals a morphogenetic property of a thyroid epithelial cell line. *Exp Cell Res,* 152**,** 22-30.

NITSCH, L. & WOLLMAN, S. H. 1980. Suspension culture of separated follicles consisting of differentiated thyroid epithelial cells. *Proc Natl Acad Sci U S A,* 77**,** 472-6.

O'BRIEN, L. E., JOU, T. S., POLLACK, A. L., ZHANG, Q., HANSEN, S. H., YURCHENCO, P. & MOSTOV, K. E. 2001. Rac1 orientates epithelial apical polarity through effects on basolateral laminin assembly. *Nat Cell Biol,* 3**,** 831-8.

OHNO, H., STEWART, J., FOURNIER, M. C., BOSSHART, H., RHEE, I., MIYATAKE, S., SAITO, T., GALLUSSER, A., KIRCHHAUSEN, T. & BONIFACINO, J. S. 1995. Interaction of tyrosine-based sorting signals with clathrin-associated proteins. *Science,* 269**,** 1872-5.

OHNO, M., ZANNINI, M., LEVY, O., CARRASCO, N. & DI LAURO, R. 1999. The paired-domain transcription factor Pax8 binds to the upstream enhancer of the rat sodium/iodide symporter gene and participates in both thyroid-specific and cyclic-AMP-dependent transcription. *Mol Cell Biol,* 19**,** 2051-60.

OHYE, H. & SUGAWARA, M. 2010. Dual oxidase, hydrogen peroxide and thyroid diseases. *Exp Biol Med (Maywood),* 235**,** 424-33.

OPITZ, R., ANTONICA, F. & COSTAGLIOLA, S. 2013. New model systems to illuminate thyroid organogenesis. Part I: an update on the zebrafish toolbox. *Eur Thyroid J,* 2**,** 229-42.

OWEN, D. J., COLLINS, B. M. & EVANS, P. R. 2004. Adaptors for clathrin coats: structure and function. *Annu Rev Cell Dev Biol,* 20**,** 153-91.

OWEN, D. J. & EVANS, P. R. 1998. A structural explanation for the recognition of tyrosine-based endocytotic signals. *Science,* 282**,** 1327-32.

PARLATO, R., ROSICA, A., RODRIGUEZ-MALLON, A., AFFUSO, A., POSTIGLIONE, M. P., ARRA, C., MANSOURI, A., KIMURA, S., DI LAURO, R. & DE FELICE, M. 2004. An integrated regulatory network controlling survival and migration in thyroid organogenesis. *Dev Biol,* 276**,** 464-75.

PARODER, V., NICOLA, J. P., GINTER, C. S. & CARRASCO, N. 2013. The iodide-transport-defect-causing mutation R124H: a delta-amino group at position 124 is critical for maturation and trafficking of the Na+/I- symporter. *J Cell Sci,* 126**,** 3305-13.

PARTON, R. G., PRYDZ, K., BOMSEL, M., SIMONS, K. & GRIFFITHS, G. 1989. Meeting of the apical and basolateral endocytic pathways of the Madin-Darby canine kidney cell in late endosomes. *J Cell Biol,* 109**,** 3259-72.

PELLIZZARI, L., D'ELIA, A., RUSTIGHI, A., MANFIOLETTI, G., TELL, G. & DAMANTE, G. 2000. Expression and function of the homeodomain-containing protein Hex in thyroid cells. *Nucleic Acids Res,* 28**,** 2503-11.

PESCE, L., BIZHANOVA, A., CARABALLO, J. C., WESTPHAL, W., BUTTI, M. L., COMELLAS, A. & KOPP, P. 2012. TSH regulates pendrin membrane abundance and enhances iodide efflux in thyroid cells. *Endocrinology,* 153**,** 512-21.

PORTULANO, C., PARODER-BELENITSKY, M. & CARRASCO, N. 2014. The Na+/I- symporter (NIS): mechanism and medical impact. *Endocr Rev,* 35**,** 106-49.

POSTIGLIONE, M. P., PARLATO, R., RODRIGUEZ-MALLON, A., ROSICA, A., MITHBAOKAR, P., MARESCA, M., MARIANS, R. C., DAVIES, T. F., ZANNINI, M. S., DE FELICE, M. & DI LAURO, R. 2002. Role of the thyroid-stimulating hormone receptor signaling in development and differentiation of the thyroid gland. *Proc Natl Acad Sci U S A,* 99**,** 15462-7.

PRABAKARAN, D., AHIMA, R. S., HARNEY, J. W., BERRY, M. J., LARSEN, P. R. & ARVAN, P. 1999. Polarized targeting of epithelial cell proteins in thyrocytes and MDCK cells. *J Cell Sci,* 112 (Pt 8)**,** 1247-56.

PUGLISI, F., CESSELLI, D., DAMANTE, G., PELLIZZARI, L., BELTRAMI, C. A. & DI LORETO, C. 2000. Expression of Pax-8, p53 and bcl-2 in human benign and malignant thyroid diseases. *Anticancer Res,* 20**,** 311-6.

QUINONES, G. B., DANOWSKI, B. A., DEVARAJ, A., SINGH, V. & LIGON, L. A. 2011. The posttranslational modification of tubulin undergoes a switch from detyrosination to acetylation as epithelial cells become polarized. *Mol Biol Cell,* 22**,** 1045-57.

REALES, E., SHARMA, N., LOW, S. H., FOLSCH, H. & WEIMBS, T. 2011. Basolateral sorting of syntaxin 4 is dependent on its N-terminal domain and the AP1B clathrin adaptor, and required for the epithelial cell polarity. *PLoS One,* 6**,** e21181.

REED, N. A., CAI, D., BLASIUS, T. L., JIH, G. T., MEYHOFER, E., GAERTIG, J. & VERHEY, K. J. 2006. Microtubule acetylation promotes kinesin-1 binding and transport. *Curr Biol,* 16**,** 2166-72.

REMY, L., MICHEL-BECHET, M., ATHOUEL-HAON, A. M., MAGRE, S., CATALDO, C. & JOST, A. 1980. Development of the thyroid gland in the rat fetus in vivo. An ultrastructural and radioautographic study. *Arch Anat Microsc Morphol Exp,* 69**,** 91-108.

REMY, L., MICHEL-BECHET, M., CATALDO, C., BOTTINI, J., HOVSEPIAN, S. & FAYET, G. 1977. The role of intracellular lumina in thyroid cells for follicle morphogenesis in vitro. *J Ultrastruct Res,* 61**,** 243-53.

REMY, L., PENEL, C., RUA, S., MAZZELLA, E. & MICHEL-BECHET, M. 1983. Thyrotropin effects on vesicle transfer and thyroid follicle morphogenesis: a stereological study in the rat. *Biol Cell,* 49**,** 145-52.

RIEDEL, C., LEVY, O. & CARRASCO, N. 2001. Post-transcriptional regulation of the sodium/iodide symporter by thyrotropin. *J Biol Chem,* 276**,** 21458-63.

RIESCO-EIZAGUIRRE, G., GUTIERREZ-MARTINEZ, P., GARCIA-CABEZAS, M. A., NISTAL, M. & SANTISTEBAN, P. 2006. The oncogene BRAF V600E is associated with a high risk of recurrence and less differentiated papillary thyroid carcinoma due to the impairment of Na+/I- targeting to the membrane. *Endocr Relat Cancer,* 13**,** 257-69.

RIESCO-EIZAGUIRRE, G., RODRIGUEZ, I., DE LA VIEJA, A., COSTAMAGNA, E., CARRASCO, N., NISTAL, M. & SANTISTEBAN, P. 2009. The BRAFV600E oncogene induces transforming growth factor beta secretion leading to sodium iodide symporter repression and increased malignancy in thyroid cancer. *Cancer Res,* 69**,** 8317-25.

RODRIGUEZ-BOULAN, E. & MACARA, I. G. 2014. Organization and execution of the epithelial polarity programme. *Nat Rev Mol Cell Biol,* 15**,** 225-42.

RODRIGUEZ-FRATICELLI, A. E., GALVEZ-SANTISTEBAN, M. & MARTIN-BELMONTE, F. 2011. Divide and polarize: recent advances in the molecular mechanism regulating epithelial tubulogenesis. *Curr Opin Cell Biol,* 23**,** 638-46.

ROLAND, J. T., BRYANT, D. M., DATTA, A., ITZEN, A., MOSTOV, K. E. & GOLDENRING, J. R. 2011. Rab GTPase-Myo5B complexes control membrane recycling and epithelial polarization. *Proc Natl Acad Sci U S A,* 108**,** 2789-94.

RUEMMELE, F. M., MULLER, T., SCHIEFERMEIER, N., EBNER, H. L., LECHNER, S., PFALLER, K., THONI, C. E., GOULET, O., LACAILLE, F., SCHMITZ, J., COLOMB, V., SAUVAT, F., REVILLON, Y., CANIONI, D., BROUSSE, N., DE SAINT-BASILE, G., LEFEBVRE, J., HEINZ-ERIAN, P., ENNINGER, A., UTERMANN, G., HESS, M. W., JANECKE, A. R. & HUBER, L. A. 2010. Loss-of-function of MYO5B is the main cause of microvillus inclusion disease: 15 novel mutations and a CaCo-2 RNAi cell model. *Hum Mutat,* 31**,** 544-51.

RUIZ-LLORENTE, S., CARRILLO SANTA DE PAU, E., SASTRE-PERONA, A., MONTERO-CONDE, C., GOMEZ-LOPEZ, G., FAGIN, J. A., VALENCIA, A., PISANO, D. G. & SANTISTEBAN, P. 2012. Genome-wide analysis of Pax8 binding provides new insights into thyroid functions. *BMC Genomics,* 13**,** 147.

RUPIK, W. 2012. Hollowing or cavitation during follicular lumen formation in the differentiating thyroid of grass snake Natrix natrix L. (Lepidosauria, Serpentes) embryos? An ultrastructural study. *Zoology (Jena),* 115**,** 389-97.

SABHARANJAK, S., SHARMA, P., PARTON, R. G. & MAYOR, S. 2002. GPI-anchored proteins are delivered to recycling endosomes via a distinct cdc42-regulated, clathrin-independent pinocytic pathway. *Dev Cell,* 2**,** 411-23.

SAITO, T., ENDO, T., KAWAGUCHI, A., IKEDA, M., NAKAZATO, M., KOGAI, T. & ONAYA, T. 1997. Increased expression of the Na+/I- symporter in cultured human thyroid cells exposed to thyrotropin and in Graves' thyroid tissue. *J Clin Endocrinol Metab,* 82**,** 3331-6.

SANTISTEBAN, P., ACEBRON, A., POLYCARPOU-SCHWARZ, M. & DI LAURO, R. 1992. Insulin and insulin-like growth factor I regulate a thyroid-specific nuclear protein that binds to the thyroglobulin promoter. *Mol Endocrinol,* 6**,** 1310-7.

SARNATARO, D., NITSCH, L., HUNZIKER, W. & ZURZOLO, C. 2000. Detergent insoluble microdomains are not involved in transcytosis of polymeric Ig receptor in FRT and MDCK cells. *Traffic,* 1**,** 794-802.

SASTRE-PERONA, A. & SANTISTEBAN, P. 2014. Wnt-independent role of betacatenin in thyroid cell proliferation and differentiation. *Mol Endocrinol***,** me20131377.

SCHONTEICH, E., WILSON, G. M., BURDEN, J., HOPKINS, C. R., ANDERSON, K., GOLDENRING, J. R. & PREKERIS, R. 2008. The Rip11/Rab11-FIP5 and kinesin II complex regulates endocytic protein recycling. *J Cell Sci,* 121**,** 3824-33.

SHEPARD, T. H. 1967. Onset of function in the human fetal thyroid: biochemical and radioautographic studies from organ culture. *J Clin Endocrinol Metab,* 27**,** 945-58.

SHEPARD, T. H. 1968. Development of the human fetal thyroid. *Gen Comp Endocrinol,* 10**,** 174-81.

SINGH, S. P., MCDONALD, D., HOPE, T. J. & PRABHAKAR, B. S. 2004. Upon thyrotropin binding the thyrotropin receptor is internalized and localized to endosome. *Endocrinology,* 145**,** 1003-10.

SMITH, V. E., READ, M. L., TURNELL, A. S., WATKINS, R. J., WATKINSON, J. C., LEWY, G. D., FONG, J. C., JAMES, S. R., EGGO, M. C., BOELAERT, K., FRANKLYN, J. A. & MCCABE, C. J. 2009. A novel mechanism of sodium iodide symporter repression in differentiated thyroid cancer. *J Cell Sci,* 122**,** 3393-402.

STRATFORD, A. L., BOELAERT, K., TANNAHILL, L. A., KIM, D. S., WARFIELD, A., EGGO, M. C., GITTOES, N. J., YOUNG, L. S., FRANKLYN, J. A. & MCCABE, C. J. 2005. Pituitary tumor transforming gene binding factor: a novel transforming gene in thyroid tumorigenesis. *J Clin Endocrinol Metab,* 90**,** 4341-9.

STRILIC, B., KUCERA, T., EGLINGER, J., HUGHES, M. R., MCNAGNY, K. M., TSUKITA, S., DEJANA, E., FERRARA, N. & LAMMERT, E. 2009. The molecular basis of vascular lumen formation in the developing mouse aorta. *Dev Cell,* 17**,** 505-15.

SUBRAMANIAN, A., TAMAYO, P., MOOTHA, V. K., MUKHERJEE, S., EBERT, B. L., GILLETTE, M. A., PAULOVICH, A., POMEROY, S. L., GOLUB, T. R., LANDER, E. S. & MESIROV, J. P. 2005. Gene set enrichment analysis: a knowledge-based approach for interpreting genome-wide expression profiles. *Proc Natl Acad Sci U S A,* 102**,** 15545-50.

SZINNAI, G., LACROIX, L., CARRE, A., GUIMIOT, F., TALBOT, M., MARTINOVIC, J., DELEZOIDE, A. L., VEKEMANS, M., MICHIELS, S., CAILLOU, B., SCHLUMBERGER, M., BIDART, J. M. & POLAK, M. 2007. Sodium/iodide symporter (NIS) gene expression is the limiting step for the onset of thyroid function in the human fetus. *J Clin Endocrinol Metab,* 92**,** 70-6.

TACHIBANA, K., NAKANISHI, H., MANDAI, K., OZAKI, K., IKEDA, W., YAMAMOTO, Y., NAGAFUCHI, A., TSUKITA, S. & TAKAI, Y. 2000. Two cell adhesion molecules, nectin and cadherin, interact through their cytoplasmic domain-associated proteins. *J Cell Biol,* 150**,** 1161-76.

TAKASU, N., OHNO, S., KOMIYA, I. & YAMADA, T. 1992. Requirements of follicle structure for thyroid hormone synthesis; cytoskeletons and iodine metabolism in polarized monolayer cells on collagen gel and in double layered, follicle-forming cells. *Endocrinology,* 131**,** 1143-8.

TANIDA, I., MINEMATSU-IKEGUCHI, N., UENO, T. & KOMINAMI, E. 2005. Lysosomal turnover, but not a cellular level, of endogenous LC3 is a marker for autophagy. *Autophagy,* 1**,** 84-91.

THEDIECK, C., KALBACHER, H., KRATZER, U., LAMMERS, R., STEVANOVIC, S. & KLEIN, G. 2008. alpha B-crystallin is a cytoplasmic interaction partner of the kidney-specific cadherin-16. *J Mol Biol,* 378**,** 145-53.

THEDIECK, C., KUCZYK, M., KLINGEL, K., STEIERT, I., MULLER, C. A. & KLEIN, G. 2005. Expression of Ksp-cadherin during kidney development and in renal cell carcinoma. *Br J Cancer,* 92**,** 2010-7.

TODA, S., AOKI, S., UCHIHASHI, K., MATSUNOBU, A., YAMAMOTO, M., OOTANI, A., YAMASAKI, F., KOIKE, E. & SUGIHARA, H. 2011. Culture models for studying thyroid biology and disorders. *ISRN Endocrinol,* 2011**,** 275782.

TODA, S., MATSUMURA, S., YONEMITSU, N., FUJITANI, N., TERAYAMA, K., FUNATSUMARU, S. & SUGIHARA, H. 1995. Effects of various types of extracellular matrices on adhesion, proliferation, differentiation, and c-fos protein expression of porcine thyroid follicle cells. *Cell Struct Funct,* 20**,** 345-54.

TODA, S. & SUGIHARA, H. 1990. Reconstruction of thyroid follicles from isolated porcine follicle cells in three-dimensional collagen gel culture. *Endocrinology,* 126**,** 2027-34.

TODA, S., YONEMITSU, N., HIKICHI, Y., SUGIHARA, H. & KOIKE, N. 1992. Differentiation of human thyroid follicle cells from normal subjects and Basedow's disease in three-dimensional collagen gel culture. *Pathol Res Pract,* 188**,** 874-82.

TODA, S., YONEMITSU, N., MINAMI, Y. & SUGIHARA, H. 1993. Plural cells organize thyroid follicles through aggregation and linkage in collagen gel culture of porcine follicle cells. *Endocrinology,* 133**,** 914-20.

TORRES, J., FUNK, H. M., ZEGERS, M. M. & TER BEEST, M. B. 2011. The syntaxin 4 N terminus regulates its basolateral targeting by munc18c-dependent and -independent mechanisms. *J Biol Chem,* 286**,** 10834-46.

TOWBIN, H., STAEHELIN, T. & GORDON, J. 1979. Electrophoretic transfer of proteins from polyacrylamide gels to nitrocellulose sheets: procedure and some applications. *Proc Natl Acad Sci U S A,* 76**,** 4350-4.

TVEIT, H., AKSLEN, L. K., FAGERENG, G. L., TRANULIS, M. A. & PRYDZ, K. 2009. A secretory Golgi bypass route to the apical surface domain of epithelial MDCK cells. *Traffic,* 10**,** 1685-95.

VADYSIRISACK, D. D., CHEN, E. S., ZHANG, Z., TSAI, M. D., CHANG, G. D. & JHIANG, S. M. 2007. Identification of in vivo phosphorylation sites and their functional significance in the sodium iodide symporter. *J Biol Chem,* 282**,** 36820-8.

VALENTICH, J. D. 1981. Morphological similarities between the dog kidney cell line MDCK and the mammalian cortical collecting tubule. *Ann N Y Acad Sci,* 372**,** 384-405.

VAN DEN HOVE, M. F., CROIZET-BERGER, K., JOURET, F., GUGGINO, S. E., GUGGINO, W. B., DEVUYST, O. & COURTOY, P. J. 2006. The loss of the chloride channel, ClC-5, delays apical iodide efflux and induces a euthyroid goiter in the mouse thyroid gland. *Endocrinology,* 147**,** 1287-96.

VASIOUKHIN, V., BAUER, C., YIN, M. & FUCHS, E. 2000. Directed actin polymerization is the driving force for epithelial cell-cell adhesion. *Cell,* 100**,** 209-19.

VASSART, G. & DUMONT, J. E. 1992. The thyrotropin receptor and the regulation of thyrocyte function and growth. *Endocr Rev,* 13**,** 596-611.

VEGA-SALAS, D. E., SALAS, P. J. & RODRIGUEZ-BOULAN, E. 1987. Modulation of the expression of an apical plasma membrane protein of Madin-Darby canine kidney epithelial cells: cell-cell interactions control the appearance of a novel intracellular storage compartment. *J Cell Biol,* 104**,** 1249-59.

VILKKI, P. 1962. An iodide-complexing phospholipid. *Arch Biochem Biophys,* 97**,** 425-7.

VISWANATHA, R., OHOUO, P. Y., SMOLKA, M. B. & BRETSCHER, A. 2012. Local phosphocycling mediated by LOK/SLK restricts ezrin function to the apical aspect of epithelial cells. *J Cell Biol,* 199**,** 969-84.

VITALE, M., ILLARIO, M., DI MATOLA, T., CASAMASSIMA, A., FENZI, G. & ROSSI, G. 1997. Integrin binding to immobilized collagen and fibronectin stimulates the proliferation of human thyroid cells in culture. *Endocrinology,* 138**,** 1642-8.

WANG, K. & SPECTOR, A. 1996. alpha-crystallin stabilizes actin filaments and prevents cytochalasin-induced depolymerization in a phosphorylation-dependent manner. *Eur J Biochem,* 242**,** 56-66.

WEISS, S. J., PHILP, N. J., AMBESI-IMPIOMBATO, F. S. & GROLLMAN, E. F. 1984. Thyrotropin-stimulated iodide transport mediated by adenosine 3',5'-monophosphate and dependent on protein synthesis. *Endocrinology,* 114**,** 1099-107.

WEISZ, O. A. & RODRIGUEZ-BOULAN, E. 2009. Apical trafficking in epithelial cells: signals, clusters and motors. *J Cell Sci,* 122**,** 4253-66.

WENDELER, M. W., PRAUS, M., JUNG, R., HECKING, M., METZIG, C. & GESSNER, R. 2004. Ksp-cadherin is a functional cell-cell adhesion molecule related to LI-cadherin. *Exp Cell Res,* 294**,** 345-55.

WU, W., KITAMURA, S., TRUONG, D. M., RIEG, T., VALLON, V., SAKURAI, H., BUSH, K. T., VERA, D. R., ROSS, R. S. & NIGAM, S. K. 2009. Beta1-integrin is required for kidney collecting duct morphogenesis and maintenance of renal function. *Am J Physiol Renal Physiol,* 297**,** F210-7.

YAMASHITA, K., FUJITA, H., KITAJIMA, K. & NISHII, Y. 1989. Inter- and intracellular luminal formation in porcine thyroid tissues cultured in a collagen substrate. *Arch Histol Cytol,* 52**,** 109-14.

YAP, A. S. & MANLEY, S. W. 2001. Microtubule integrity is essential for apical polarization and epithelial morphogenesis in the thyroid. *Cell Motil Cytoskeleton,* 48**,** 201-12.

YAP, A. S., STEVENSON, B. R., ABEL, K. C., CRAGOE, E. J., JR. & MANLEY, S. W. 1995a. Microtubule integrity is necessary for the epithelial barrier function of cultured thyroid cell monolayers. *Exp Cell Res,* 218**,** 540-50.

YAP, A. S., STEVENSON, B. R., ARMSTRONG, J. W., KEAST, J. R. & MANLEY, S. W. 1994. Thyroid epithelial morphogenesis in vitro: a role for bumetanide-sensitive Cl- secretion during follicular lumen development. *Exp Cell Res,* 213**,** 319-26.

YAP, A. S., STEVENSON, B. R., KEAST, J. R. & MANLEY, S. W. 1995b. Cadherin-mediated adhesion and apical membrane assembly define distinct steps during thyroid epithelial polarization and lumen formation. *Endocrinology,* 136**,** 4672-80.

YOSHIDA, A., HISATOME, I., TANIGUCHI, S., SASAKI, N., YAMAMOTO, Y., MIAKE, J., FUKUI, H., SHIMIZU, H., OKAMURA, T., OKURA, T., IGAWA, O., SHIGEMASA, C., GREEN, E. D., KOHN, L. D. & SUZUKI, K. 2004. Mechanism of iodide/chloride exchange by pendrin. *Endocrinology,* 145**,** 4301-8.

YU, W., DATTA, A., LEROY, P., O'BRIEN, L. E., MAK, G., JOU, T. S., MATLIN, K. S., MOSTOV, K. E. & ZEGERS, M. M. 2005. Beta1-integrin orients epithelial polarity via Rac1 and laminin. *Mol Biol Cell,* 16**,** 433-45.

YU, W., SHEWAN, A. M., BRAKEMAN, P., EASTBURN, D. J., DATTA, A., BRYANT, D. M., FAN, Q. W., WEISS, W. A., ZEGERS, M. M. & MOSTOV, K. E. 2008. Involvement of RhoA, ROCK I and myosin II in inverted orientation of epithelial polarity. *EMBO Rep,* 9**,** 923-9.

ZANNINI, M., FRANCIS-LANG, H., PLACHOV, D. & DI LAURO, R. 1992. Pax-8, a paired domain-containing protein, binds to a sequence overlapping the recognition site of a homeodomain and activates transcription from two thyroid-specific promoters. *Mol Cell Biol,* 12**,** 4230-41.

ZHANG, J., PIONTEK, J., WOLBURG, H., PIEHL, C., LISS, M., OTTEN, C., CHRIST, A., WILLNOW, T. E., BLASIG, I. E. & ABDELILAH-SEYFRIED, S. 2010. Establishment of a neuroepithelial barrier by Claudin5a is essential for zebrafish brain ventricular lumen expansion. *Proc Natl Acad Sci U S A,* 107**,** 1425-30.

ZHANG, X. & ARVAN, P. 2000. Cell type-dependent differences in thyroid peroxidase cell surface expression. *J Biol Chem,* 275**,** 31946-53.

ZOVEIN, A. C., LUQUE, A., TURLO, K. A., HOFMANN, J. J., YEE, K. M., BECKER, M. S., FASSLER, R., MELLMAN, I., LANE, T. F. & IRUELA-ARISPE, M. L. 2010. Beta1 integrin establishes endothelial cell polarity and arteriolar lumen formation via a Par3-dependent mechanism. *Dev Cell,* 18**,** 39-51.

ZUCKIER, L. S., DOHAN, O., LI, Y., CHANG, C. J., CARRASCO, N. & DADACHOVA, E. 2004. Kinetics of perrhenate uptake and comparative biodistribution of perrhenate, pertechnetate, and iodide by NaI symporter-expressing tissues in vivo. *J Nucl Med,* 45**,** 500-7.

ZURZOLO, C., LE BIVIC, A., QUARONI, A., NITSCH, L. & RODRIGUEZ-BOULAN, E. 1992. Modulation of transcytotic and direct targeting pathways in a polarized thyroid cell line. *EMBO J,* 11**,** 2337-44.

Annex I. Upregulated and downregulated genes in 3D *vs.* 2D conditions with FDR<0.01

The 4,520 differentially expressed genes are shown at the following link:

http://www2.iib.uam.es/psantisteban_lab/Annex I/public

Genes are divided in upregulated (in red) and downregulated genes (in green). Each group is organized in alphabetical order.

Annex II. Differentially expressed 3D *vs.* 2D genes involved in 3D epithelial morphogenesis

PROBE	RANK IN GENE LIST	RUNNING ES	CORE ENRICHMENT
MYO6	44	0.08931867	Yes
MAL2	168	0.14219373	Yes
OCLN	207	0.19538449	Yes
ANXA2	300	0.23854335	Yes
MUC1	388	0.27745292	Yes
CDX2	524	0.30937484	Yes
ATP1A1	623	0.33982655	Yes
MYO5B	1021	0.34613547	Yes
KIF3B	1173	0.3629028	Yes
DNMBP	1436	0.37039143	Yes
PODXL	1454	0.39041376	Yes
SLC9A1	1491	0.40904102	Yes
CTNND1	1508	0.42856377	Yes
VAMP7	1607	0.44273275	Yes
RAB11A	1787	0.45088592	Yes
ITGB1	1805	0.4673355	Yes
PKD2	1844	0.48240492	Yes
CTNNB1	2014	0.48941106	Yes
KIF16B	2023	0.5047213	Yes
RAB11B	2256	0.5066626	Yes
PTEN	2270	0.51989156	Yes
CTBP1	2550	0.5176798	No
SEC23A	3538	0.4741681	No
VAMP3	3711	0.47246453	No
CDC42	3808	0.47443005	No
SYTL4	3930	0.474803	No
GSK3B	4209	0.4663166	No
CLDN2	6076	0.37207398	No

STX2	6290	0.36347046	No
STK10	6695	0.34439024	No
ITSN2	7834	0.28586957	No
EZR	8269	0.26347417	No
CLDN6	8336	0.2601232	No
RHOA	10970	0.12581608	No
CLDN15	11914	0.08038011	No
CLDN5	13129	0.022281768	No
SLC9A2	14392	-0.036591113	No
ARL3	14549	-0.037714537	No
CDH1	15532	-0.07978422	No
RAB25	15890	-0.0883888	No
RDX	16267	-0.09670524	No
STK11	16355	-0.08963487	No
CRB3	17243	-0.11845504	No
RAC1	17311	-0.10400048	No
KIFC3	17327	-0.086626865	No
KIF5B	17738	-0.08551516	No
STX4	18093	-0.07702719	No
STX3	18201	-0.053893846	No
MSN	18440	-0.03287656	No
GPSM2	18651	-0.005566172	No
CLDN4	18664	0.03233531	No

Annex III. Differentially expressed 3D *vs.* 2D genes related to epithelial tubulogenesis

PROBE	RANK IN GENE LIST	RUNNING ES	CORE ENRICHMENT
MAL2	168	0.23329626	Yes
OCLN	207	0.45658264	Yes
MYO5B	1021	0.52443856	Yes
KIF3B	1173	0.61712325	Yes
PODXL	1454	0.68796235	Yes
SLC9A1	1491	0.7697963	Yes
RAB11A	1787	0.82578033	Yes
CDC42	3808	0.74939066	No
CLDN2	6076	0.6430653	No
CLDN15	11914	0.35489893	No
SLC9A2	14392	0.25389084	No

Annex IV. Differentially expressed 3D *vs.* 2D genes involved in 3D MDCK cyst formation

PROBE	RANK IN GENE LIST	RUNNING ES	CORE ENRICHMENT
MUC20	24	0.09495156	Yes
SMTNL2	33	0.18161516	Yes
S100A4	45	0.26119244	Yes
TSPAN8	121	0.31743023	Yes
VPS37D	325	0.34795815	Yes
SEC62	560	0.3689606	Yes
TMEM205	619	0.39731917	Yes
DIRC2	631	0.42788714	Yes
DAK	981	0.43398643	Yes
IFT172	1233	0.44184977	Yes
FUZ	1282	0.4596484	Yes
ICK	1596	0.4604112	Yes
HINT2	1620	0.47610232	Yes
PIK3R2	1696	0.48840606	Yes
PKIG	1824	0.496939	Yes
SNX4	1899	0.5077163	Yes
S100A5	2130	0.5089261	Yes
FXYD2	2163	0.5202525	Yes
IP6K2	2290	0.5258312	Yes
PCM1	2828	0.50733465	No
GNB5	2870	0.51440954	No
AQP5	2951	0.5190811	No
S100A13	3028	0.5236646	No
VAMP1	3155	0.5251342	No
SNX17	3488	0.5148295	No
IFT74	3520	0.5201237	No
FYCO1	3554	0.5252174	No
DYSF	3680	0.52516645	No
PIK3R1	3818	0.52413994	No
ARHGAP24	3916	0.52497613	No
STX1B	4837	0.48123497	No
UNC5C	5193	0.46634755	No
HHAT	5667	0.44468147	No
PTPLAD2	6754	0.38981366	No
CASC4	6909	0.38328078	No
IHH	7223	0.36816546	No
AXIN2	7626	0.34802464	No
DLG2	7635	0.3483765	No
EFCAB1	8007	0.32944775	No
FGFR4	8905	0.2832295	No
HECW2	10475	0.20342168	No
ANKRD28	10693	0.19414747	No

NGEF	11059	0.17751418	No
SEC14L3	11582	0.15320373	No
IGFBP6	12240	0.1224611	No
FBLIM1	12254	0.12523855	No
FRZB	12341	0.12431347	No
ADRBK2	12708	0.10922486	No
FABP1	13114	0.09254857	No
MYO18A	13199	0.09265964	No
TGFBR3	13651	0.07416869	No
ARL3	14549	0.033650134	No
SNX5	14720	0.031243023	No
EFCAB10	14775	0.03495073	No
RAB10	15196	0.020312551	No
SYT13	15454	0.014683788	No
WBSCR16	15511	0.019633237	No
STARD10	15559	0.025144652	No
CADM1	16823	-0.028002769	No
VAPB	17498	-0.04545562	No
FARP1	17647	-0.034182813	No
KIF5B	17738	-0.019126713	No
SNX2	17747	2,84E+03	No
MYADM	18035	0.008343054	No
BST2	18184	0.02563233	No
SYNGR1	18559	0.037823353	No

Annex V. Genes upregulated in 3D follicles and downregulated in Pax8 silenced cells (siPax8)

GeneSymbol	logFC_3D	logFC_siPax8	FDR_3D	adj.P.Val_siPax8
Tgm2	4,47	-0,16	1,06E-13	3,50E-03
Dynlrb2	2,26	-0,59	5,81E-11	2,27E-05
Ephx1	1,83	-0,25	8,61E-11	7,35E-03
Sh3kbp1	1,81	-0,33	3,31E-10	7,12E-04
Acaa2	1,24	-0,34	6,58E-09	1,29E-04
Nid2	1,17	-0,16	4,06E-09	8,03E-03
Folr1	1,05	-0,32	1,63E-08	2,44E-04
Fgfr2	1,04	-0,35	6,69E-08	3,96E-04
Cacybp	1,01	-0,25	1,30E-07	6,65E-05
Rab17	1,01	-0,31	2,04E-07	1,76E-05
Map7	0,97	-0,24	4,31E-08	5,05E-03
Pemt	0,96	-0,33	8,47E-08	5,96E-05
Nme3	0,95	-0,35	2,86E-07	5,12E-03
Sptbn2	0,93	-0,72	1,53E-07	1,01E-06

Gcnt1	0,92	-0,34	5,60E-08	1,25E-03
Ocln	0,92	-0,26	1,33E-07	5,77E-03
Pbld	0,85	-0,31	8,21E-07	4,24E-03
Oat	0,84	-0,61	3,21E-08	1,16E-06
Pdzk1ip1	0,81	-0,56	4,72E-07	2,49E-06
St6gal1	0,77	-0,17	1,02E-06	1,93E-03
Cbs	0,76	-0,24	1,78E-07	1,55E-03
Mlph	0,75	-0,45	2,63E-07	1,24E-05
Rbm4b	0,75	-0,72	1,43E-06	1,36E-06
Synj2	0,70	-0,34	1,81E-07	7,49E-04
Mocos	0,68	-0,27	2,21E-07	1,61E-03
Cyb5r1	0,65	-0,26	3,17E-03	2,22E-03
Calr	0,60	-0,26	6,61E-05	1,24E-03
RT1-Db1	0,54	-0,31	2,50E-06	1,97E-04
Enpp1	0,50	-0,39	9,80E-06	3,59E-03
Gne	0,50	-0,16	4,13E-06	2,88E-03
Spg20	0,50	-0,30	8,24E-06	3,53E-03
Ndufv3	0,50	-0,19	8,32E-06	2,85E-03
Syt5	0,48	-0,74	1,73E-05	1,19E-03
Mllt3	0,48	-0,26	2,41E-05	2,32E-03
Rhpn2	0,48	-0,41	2,80E-05	4,68E-04
Acp6	0,48	-0,25	5,69E-06	8,94E-03
Myo5b	0,47	-0,46	4,54E-05	2,28E-06
Parp1	0,46	-0,17	1,58E-04	5,93E-03
Cdh16	0,46	-0,32	2,40E-05	3,83E-03
Cxxc5	0,46	-0,25	1,08E-05	4,12E-03
Klf5	0,42	-0,27	5,55E-04	1,62E-04
Per2	0,42	-0,22	2,84E-05	1,77E-03
Brwd3	0,41	-0,17	4,30E-04	3,01E-03
G0s2	0,41	-0,39	2,26E-04	2,57E-04
Ift172	0,40	-0,10	4,02E-05	9,47E-03
Hspa14	0,40	-0,21	5,74E-04	8,47E-03
Becn1	0,40	-0,11	6,93E-04	6,39E-03
Atp11b	0,39	-0,28	6,47E-03	3,65E-03
Cd74	0,38	-0,30	1,23E-04	2,99E-05
Ccs	0,37	-0,19	1,74E-04	6,22E-03
Tmem98	0,34	-0,24	2,67E-04	3,94E-03
Zbtb1	0,33	-0,17	8,46E-04	3,37E-03
Hmgn3	0,33	-0,18	5,09E-04	1,32E-03
Abcg3l1	0,32	-0,25	4,44E-04	4,12E-03
Ppp2r1b	0,32	-0,25	2,88E-03	2,25E-04
Grtp1	0,31	-0,12	1,43E-03	2,23E-03
Kcnk1	0,30	-0,35	4,72E-04	2,27E-03
Fas	0,29	-0,23	8,45E-04	6,11E-03
Dab2ip	0,28	-0,42	7,18E-03	2,73E-04
Tnfrsf14	0,28	-0,16	8,73E-04	5,21E-03

Galk2	0,27	-0,19	4,97E-03	4,43E-03
Cask	0,26	-0,17	3,06E-03	5,71E-03
Slc25a10	0,26	-0,20	7,38E-03	9,13E-05
Serpinb5	0,26	-0,56	4,34E-03	1,64E-05
Mycn	0,25	-0,38	7,15E-03	3,84E-04
Mpg	0,25	-0,19	4,38E-03	8,79E-03
Atp10d	0,24	-0,22	7,34E-03	9,34E-04
Rasd1	0,23	-0,43	9,63E-03	7,85E-04
Fzd3	0,23	-0,35	5,13E-03	7,44E-05
Hdhd2	0,22	-0,16	4,79E-03	2,56E-03
Nedd4l	0,22	-0,25	8,76E-03	3,60E-03